THE COOLING OF SPENT CARBON ANODES IN THE ALUMINIUM SMELTING INDUSTRY

A THESIS PRESENTED IN PARTIAL FULFILMENT
OF THE REQUIREMENTS FOR
THE DEGREE OF MASTER OF SCIENCE IN
MATHEMATICS AT
MASSEY UNIVERSITY

Matthew Cole

March 1996

Abstract

As part of the New Zealand Aluminium Smelters (NZAS) upgrade, a hot butt cleaning system has been proposed, this would remove the bath from anodes as they are removed from the cells. It is expected that the time to cool for hot cleaned anodes would be significantly less than for current method of allowing the butts to cool before the bath is removed.

In this project a mathematical model of the cooling process of both the clean and dirty anodes is developed. This model will aid in the investigation of the hot butt cleaning system by showing the difference in cooling times between the clean and dirty anodes.

The temperature profiles within both clean and dirty anodes is calculated for one-, two- and three-dimensional models. Temperature changes in the anodes with time are also compared to experimental data.

Acknowledgments

Many people have helped me in during the writing of this thesis. In particular I would like to acknowledge the following people:

Professor Robert McKibbin for his guidance and supervision over the last year.

I thank New Zealand Aluminium Smelters (NZAS) for their support. Thank you to John Carran and Rob Wallace for your ideas and assistance.

Graeme and Rowena my parents for all their support and encouragement, for being there when I need you and letting me borrow the car when needed.

My brother Richard for all the email messages and helping out with the drawing of the diagrams. My brother Nicholas, sister Louise and brother-in-law Murray.

My flatmates who have helped me over the last year, especially Phillip and Nigel for being good mates.

Associate Professor Dean Halford and colleagues of the Mathematics Department for your encouragement and support. Professor Graeme Wake for suggesting I apply for the scholarship and do a Masters.

The other graduate assistants for your encouragement and advice, especially Mark Johnston for all help with the computers.

All my friends at Christian Community Church for your guidance and prayers, especially Hugh and Donna McGarvey and the homegroup.

Nomenclature

All constants and variables used in this thesis are defined when first used. Commonly used notation is summarized here.

a, b, c, d, e, f, g	diffusivity coefficients $[m^2/s]$
A	surface area $[m^2]$
A, B, C, D	defined variables
A_h	horizontal downward facing surface area $[m^2]$
Bi	Biot number $[-]$
c	heat capacity $[kJ/kgK]$
c_1, c_2, c_3	defined constant
D	diameter of sphere $[m]$
E_g	energy generated in a system $[J]$
E_{in}	energy transferred into a system $[J]$
E_{out}	energy transferred out of a system $[J]$
E_s	energy stored in a system $[J]$
$F(x), G(t)$	defined function
Fo	Fourier number $[-]$
g	gravitional acceleration $[m/s^2]$
h	heat transfer coefficient $[W/m^2K]$
h_c	convection heat transfer coefficient $[W/m^2K]$

h_r	radiation heat transfer coefficient $[W/m^2K]$
H	height $[m]$
H	characteristic length $[m]$
H	dimensionless heat transfer coeffecient $[-]$
k	thermal conductivity $[W/mK]$
k_x	thermal conductivity in x-direction $[W/mK]$
k_y	thermal conductivity in y-direction $[W/mK]$
k_z	thermal conductivity in z-direction $[W/mK]$
L	length $[m]$
L_m	longest linear dimension $[m]$
L_x	x dimension $[m]$
L_y	y dimension $[m]$
L_z	z dimension $[m]$
Nu	Nusselt Number $[-]$
$\bar{P}$	mean horizontal perimeter $[m]$
Pr	Prandtl Number $[-]$
q	rate of heat transfer $[kW]$
q_c	rate of convection heat transfer $[kW]$
q_r	rate of radiation heat transfer $[kW]$
q''	rate of heat transfer $[kW]$
$q_1, q_2, q_3, q_4, q_5, q_6$	rate of heat transfer from specific direction $[kW]$
Ra_H	Rayleigh Number $[-]$
Re	Reynolds Number $[-]$
t	time $[s]$

t_o	time normalisation constant $[s]$
$\bar{t}$	normalised time $[-]$
T	temperature $[K]$
T_i	initial temperature $[K]$
T_o	temperature normalisation constant $[K]$
T_s	surface temperature of anode $[K]$
T_∞	ambient temperature $[K]$
$\bar{T}$	normalised temperature $[-]$
U_∞	air speed $[m/s^2]$
v_o	length normalisation constant $[m]$
V	volume of body $[m^3]$
x, y, z	spatial coordinate
x_o	length normalisation constant $[m]$
$\bar{x}, \bar{y}, \bar{y}$	normalised spatial coordinate $[-]$
$X(x), Y(y), Z(z)$	defined function
z_f	thickness of body $[m]$

Greek

α	thermal diffusivity $[m^2/s]$
β	coefficient of thermal volumetric expansion $[K^{-1}]$
δ	ratio of timesteps to grid size squared $[s/m^2]$
Δt	size of timestep $[s]$
Δx	distance between mesh points in x-direction $[m]$
Δy	distance between mesh points in y-direction $[m]$
Δz	distance between mesh points in z-direction $[m]$
ϵ	emissivity $[-]$

λ, μ, ν	defined variables
μ_s	viscosity of air at surface temperature $[kg/sm]$
μ_∞	viscosity of air at ambient temperature $[kg/sm]$
ν	kinematic viscosity $[m^2/s]$
ρ	density $[kg/m^3]$
σ	Stefan-Boltzmann Constant $[W/m^2K^4]$

Subscripts

b	bath
c	carbon
i	grid points
j	grid points
k	grid points
s	steel

Superscripts

m	timesteps

Contents

List of Figures

List of Tables

Chapter 1

Introduction

1.1 Background

The smelting of aluminium converts bauxite into aluminium, this process consumes carbon anodes within the cells. These anodes hang in the cells as shown in Figure 1.1. Known as the Hall-Heroult process, the smelting of aluminium can be represented by the following equation

$$2Al_20_3 + 3C \rightarrow 4Al + 3CO_2$$

The spent anodes or butts are removed from the cells at a temperature of approximately 950 $^{\circ}C$. The removed butts are placed on pallets for up to six hours before being hung on a conveyor for transport to the anode cleaning station. If the anodes have a temperature in excess of 400 $^{\circ}C$ when they reach the cleaning station further cooling must take place until they can be processed. The cleaning station removes bath, a by-product of the smelting process.

The spent anodes can vary in size and shape but a standard spent anode is shown on the right hand side in Figure 1.2; also shown is a new anode. The bath cover can be seen sitting on top of the carbon.

As part of the NZAS upgrade a hot anode cleaning system is being considered. This would remove the bath from the anodes while they are still hot. This has several advantages. Firstly hot bath is softer and easier to remove and secondly, the cooling time of the spent anodes is expected to be reduced since unremoved bath insulates the spent anode.

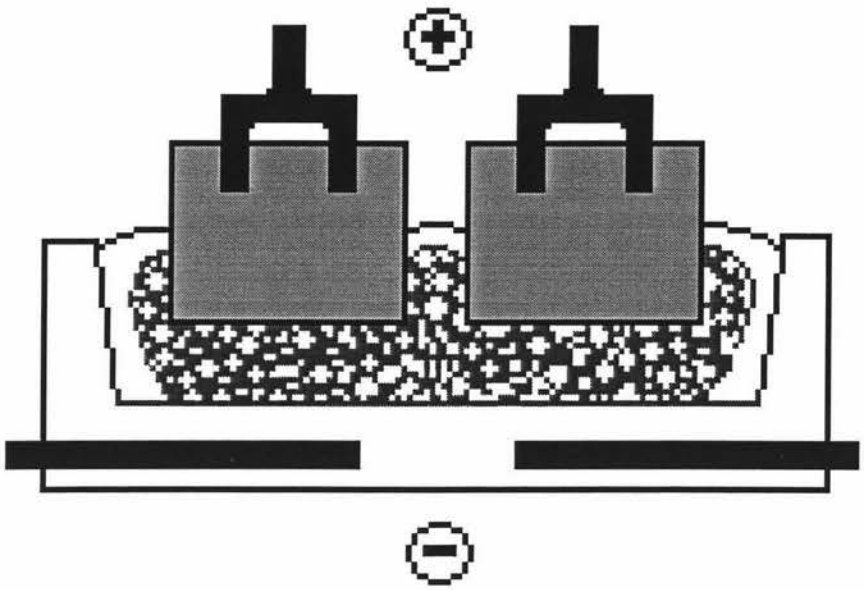

Figure 1.1: Schematic of smelting cell

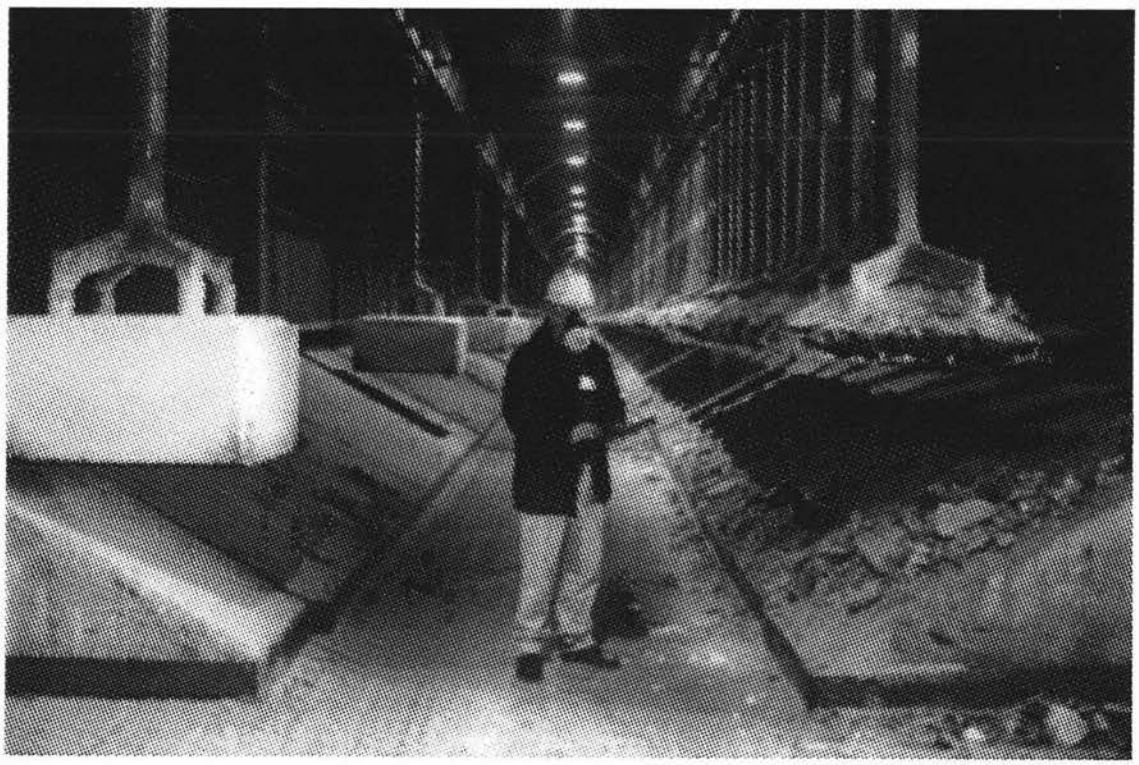

Figure 1.2: Spent anode and new anode in cooling gallery

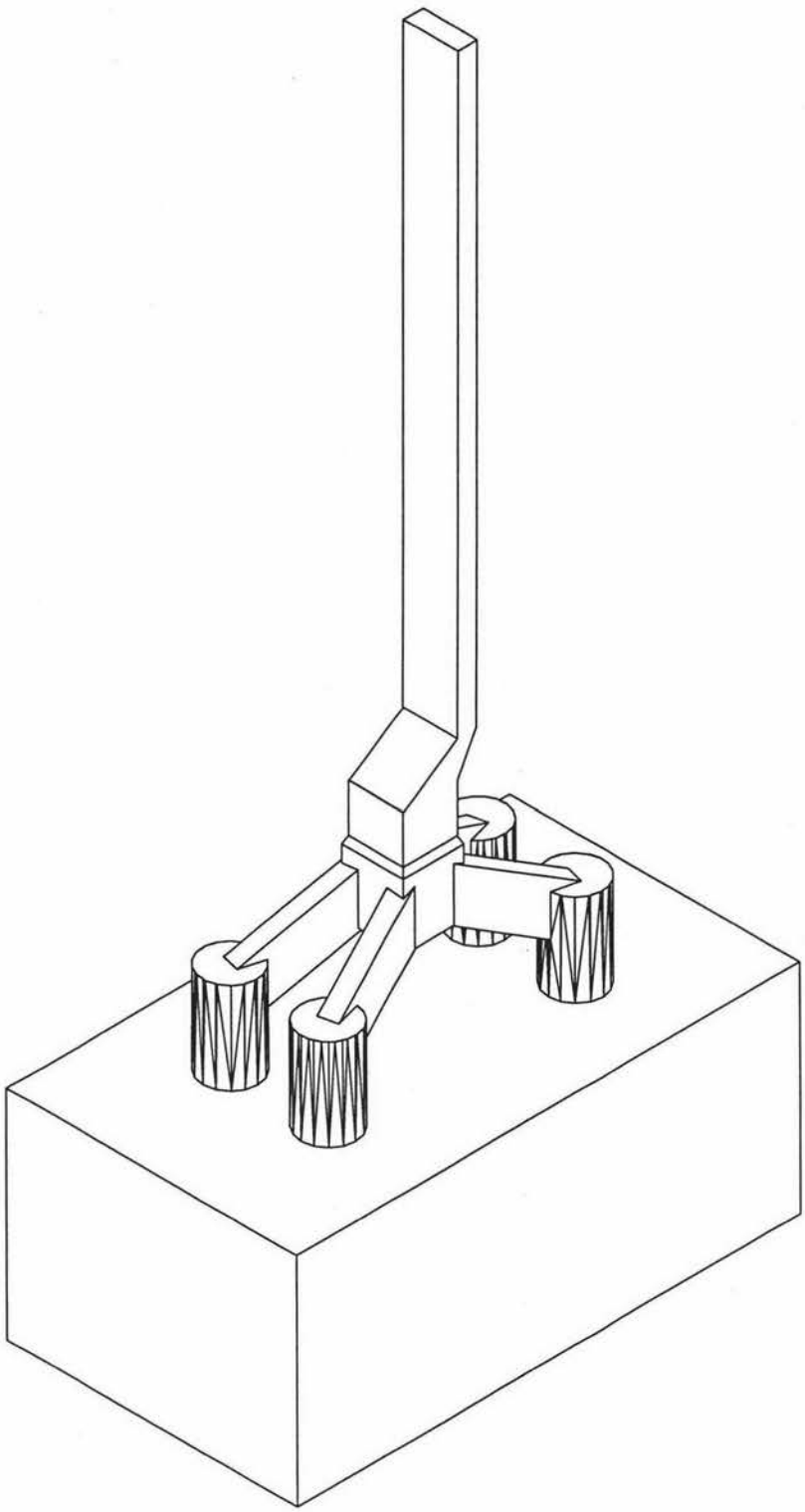

Figure 1.3: A new anode with assembly yoke

1.2 Outline

This work develops a mathematical model of the cooling process which takes place for anodes with a bath cover and those with the bath cover removed. The input variables within the model include the physical and thermal properties of the materials which make up the anodes. Other important factors are the air temperature, the initial temperature of the anodes and the air movement around the anodes. The size and shape of the anodes is also another important consideration. The effect of other anodes cooling nearby may also be significant.

In Chapter 2 the rate of heat transfer from the anode to the surrounding environment due to convection and radiation is investigated. It is shown that radiation heat transfer is the significant mode of heat transfer for cooling anodes, especially at high temperatures.

The rates of heat transfer calculated in Chapter 2 are used in Chapter 3 to develop a lumped system model. In this model the anode is treated as being of uniform temperature at any given time.

In Chapter 4 the heat equation which describes heat conduction within the anode is developed for one-, two- and three-dimensions. The boundary conditions for the heat equation are found using the assumption that heat is removed only by radiation.

By simplifying the radiation boundary conditions, an approximate solution can be found analytically using the method of separation of variables. This is done for one-, two- and three-dimensions in Chapter 5. The analytic solution only allows simple-shaped regions.

In Chapters 6, 7 and 8 the mathematical problem is solved numerically using an explicit finite difference method for one-, two- and three-dimensions respectively. This allows more complicatedly shaped regions and the possibility of several materials with different thermodynamic properties within the anode model.

Chapter 2

Modes of Heat Transfer for a Cooling Anode

A cooling anode is a solid object in which heat is transferred within the anode by conduction; at the surface heat is lost from the anode due to both convection and radiation. If the butt is considered to be at a uniform temperature throughout at any given time, this simple model allows the radiation and convection heat transfer rates to be compared.

In this chapter both radiation and convection heat transfer rates are calculated for an anode at various temperatures.

2.1 Convection

Convection is the process by which thermal energy is transferred between a solid and a fluid flowing past it. There are two types of convection: natural or free convection and forced convection. In natural convection fluid movement is due to the buoyancy effect felt by the relatively warmer regions of flow. Forced convection occurs when another entity pushes the fluid past the surface.

The rate of heat transfer due to convection between the surface and the fluid may be given by

$$q_c = hA(T_s - T_\infty) \tag{2.1}$$

where h is the heat transfer coefficient, T_s is the surface temperature of the object, and T_∞ is the fluid temperature away from the surface which is of area A.

2.1.1 Natural Convection

For natural convection the value of h depends on the orientation of the surface i.e. if the surface is vertical or horizontal. Also the convection from a surface facing upward is different from the convection from a surface facing down. The heat transfer from a three-dimensional arbitrarily-shaped body due to natural convection can be found by using the method described in [3]. A characteristic length H can be defined as

$$H = (z_f \bar{P}^2)^{1/3}$$

where z_f is the thickness of the body and $\bar{P}$ is the mean horizontal perimeter of the body. The Rayleigh number based on H can be defined as

$$Ra_H = \frac{g\beta}{\nu\alpha} H^3 (T_s - T_\infty)$$

where $g\beta/\nu\alpha$ is known for air. The Rayleigh number can be used to find the Nusselt number

$$Nu_{\sqrt{A}} = \left\{ \left[(\bar{C}_l Ra_H^{1/4})^m + (\hat{C}_t Ra_H^{1/3})^m \right]^{n/m} + (Nu_{c\sqrt{A}})^n \right\}^{1/n} \tag{2.2}$$

where $\bar{C}_l = 0.515$ and $Nu_{c\sqrt{A}} = 3.51$ are approximately constant. $\hat{C}_t$ is given by

$$\bar{C}_t = \left(0.098 - 0.065 \frac{A_h}{A} + 0.008 \frac{z_f \bar{P}}{A} \right) \frac{\sqrt{A}}{H}$$

where A is the surface area and A_h is the horizontal downward-facing surface area of the body. The exponents n and m in Equation (2.2) are estimated by

$$m = 2.5 + 12 e^{-13|\hat{C}_t Ra_H^{1/12} - 0.5|}$$

and

$$n = \left(1.26 - \frac{2 - \sqrt{A}/L_m}{9\sqrt{1 - 4.79 V^{2/3}/A}}, 1 \right)_{\max}$$

where V is the volume of the body and L_m is the longest linear dimension. The heat transfer coefficient is

$$h_c = Nu_H \frac{k}{H}$$

and the heat transfer rate is found from Equation (2.1).

The rate of heat transfer for an anode which is $0.2\,m$ high by $1.4\,m$ long and $0.8\,m$ wide and a sphere of diameter $1.0\,m$ which has the same surface area are given in Table 2.1.

Table 2.1: Natural Convection Heat Transfer Rates for rectangular anode and sphere (kW)

temperature $^{\circ}C$	Sphere	Cuboid
50	0.26	0.03
150	1.57	0.52
250	3.19	1.51
350	4.66	2.64
450	6.18	3.93
550	7.91	5.53
650	9.79	7.34
750	11.79	9.32
850	13.59	11.10
950	14.87	12.24

2.1.2 Forced Convection

The heat transfer due to forced convection is also found from Equation (2.1) but the heat transfer coefficient depends on the velocity of the air movement around the butt. In the smelter there is no forced air movement around the butts except for any drafts due to outside wind. This makes any analysis of forced convection around butts difficult as the air speed and direction are both unknown. Also the shape of the butts means the movement of air around them is difficult to predict.

To get an idea of the amount of heat lost due to forced convection the heat transfer from a sphere was calculated. This was compared to the heat loss due to natural convection and radiation from a sphere. The heat transfer coefficient is found from the Nusselt number

$$\bar{Nu}_D = 2 + (0.4Re_D^{1/2} + 0.06Re_D^{2/3})Pr^{0.4}\left(\frac{\mu_\infty}{\mu_s}\right)$$

where Pr (the Prandtl number) is approximately 0.7 for air, μ_∞ is the viscosity of air at the ambient temperature (kg/ms) and μ_s is the viscosity of air at the surface temperature (kg/ms). Re_D is the Reynolds number given by

$$Re_D = \frac{U_\infty D}{\nu}$$

where U_∞ is the air speed (m/s), D is the diameter of the sphere (m) and ν is the kinematic viscosity (m^2/s). The heat transfer coefficient is given by

$$h = \frac{Nu\ k}{D}$$

Using Equation (2.1),

$$q_c = hA(T_s - T_\infty)$$

gives the rate of heat transfer from a sphere at temperature T_s due to forced convection.

The rates of heat transfer due to forced convection from a sphere with a diameter of $1.0\,m$ for various surface temperatures and air speeds are shown in Table 2.2.

2.2 Radiation

Thermal radiation is the stream of electromagnetic radiation emitted by a material entity (solid body, pool of liquid, cloud of reacting gaseous mixture) on account of its finite absolute temperature [1]. If each surface of the anode is treated as if it is surrounded by a much larger surface the heat exchange between the surface and its surroundings is given by

$$q_r = \epsilon\sigma A(T_s^4 - T_\infty^4) \tag{2.3}$$

where ϵ is the emissivity of the surface, $\sigma = 5.67 \times 10^{-8}\,W/m^2K^4$ is the Stefan-Boltzmann constant, T_s and T_∞ are surface and ambient temperatures respectively and A is the surface area.

It can be seen from Equation (2.3) that the rate of heat transfer due to radiation does not depend on the orientation or shape of the surface. This means that for a body of given surface area the rate of heat transfer due to radiation does not depend on shape or orientation. The heat transfer rates for a sphere and butt of the same surface area is the same.

The rates of heat transfer due to radiation from a sphere with a diameter of $1\,m$ for various surface temperatures is shown in Table 2.2.

2.3 Summary

Heat is lost from the butt by both convection and radiation. Due to the difficulty in calculating forced convection for an anode shaped body, the convection from a sphere was used. Table 2.1 shows that for natural convection this is a reasonable

Table 2.2: Heat Transfer Rates for sphere (kW)

	Convection				Radiation
	Natural	Forced			
Air Speed (m/s)	0	5	10	20	
Temperature ($^{\circ}C$)					
50	0.26	0.61	0.95	1.50	0.50
150	1.57	2.56	4.01	6.30	3.51
250	3.19	4.41	6.90	10.85	9.61
350	4.66	6.16	9.63	15.11	20.41
450	6.18	7.88	12.30	19.28	37.88
550	7.91	9.63	15.00	23.50	64.32
650	9.79	11.58	18.02	28.21	102.36
750	11.79	13.53	21.04	32.91	154.99
850	13.59	15.85	24.64	38.51	225.55
950	14.87	18.87	29.32	45.80	317.70

approximation. Table 2.2 shows that for temperatures above $350\,^{\circ}C$ heat transfer due to radiation is the most significant. As the air speed increases the rate of heat transfer due to forced convection also increases however even with an air speed of $20\,m/s$ (that is about $40\,knots$) this is still significantly less than the heat loss due to radiation. This means initially the model will include only heat loss due to radiation.

Chapter 3

Lumped System Model

If the anodes are considered to be of uniform temperature throughout at any given time, the heat transfer rates, q, calculated in Chapter 2 can be used to model the cooling rate of the anode. This is called the lumped system transient model.

3.1 Heat Transfer in a System

This is done by looking at the energy terms affecting the system. In this case the system is the entire anode, with energy transfer into the system (E_{in}), energy transfer out of the system (E_{out}), energy generated within the system (E_g) and energy storage within the system (E_s). The first law of thermodynamics states that these must be conserved which gives the following equation for the energy balance

$$E_{in} + E_g = E_{out} + E_s \tag{3.1}$$

For a cooling anode E_{in} and E_g equal zero and $E_{out} = q$. Equation (reflubalance1) can then be written as

$$E_s = -q \tag{3.2}$$

The heat transfer rate out of the anode, q is given by

$$q = \epsilon\sigma A(T^4 - T_\infty^4) \tag{3.3}$$

The change in the energy stored in the anode is proportional to the change in temperature, this is given by

$$E_s = \rho c V \frac{dT}{dt} \tag{3.4}$$

where ρ is the density (kg/m^3), c is the specific heat capacity (kJ/kgK) and V is the volume of the anode. Substituting Equation (3.3) and Equation (3.4) into Equation (3.2) gives

$$\rho cV\frac{dT}{dt} = -\epsilon\sigma A(T^4 - T_\infty^4)$$

3.2 Numerical Solution

If the rate of heat transfer q is calculated using the same methods as in Chapter 2 the change in temperature can be calculated using a forward finite difference scheme in time:

$$\rho cV\frac{T^{m+1} - T^m}{\Delta t} = -\epsilon\sigma A\left[(T^m)^4 - T_\infty^4\right]$$

which can be rearranged to give

$$T^{m+1} = T^m - \Delta t\frac{\epsilon\sigma A}{\rho cV}\left[(T^m)^4 - T_\infty^4\right]$$

If the anode has the following thermal and physical properties

Length $= L = 1.4\,m$	Width $= W = 0.8\,m$
Height $= H = 0.2\,m$	Density $= \rho = 1580\,kg/m^3$
Heat Capacity $= c = 1670\,kJ/kgK$	Emissivity $= 0.8$
Initial Temperature $= T_i = 1112\,K$	Ambient Temperature $= T_\infty = 293\,K$

and if $\Delta t = 10\,s$ the solution can be seen in Figure 3.1. This figure also shows the temperature profiles of the data collected in [9].

3.3 Summary

The temperature throughout the anode is of course not uniform at any given time. It would be expected that the outside of the anode would cool down more quickly than the interior. The temperature calculated from the lumped system model would be expected to be lower than the average of the actual temperature distribution since it assumes the interior temperature is the same as the surface temperatures. This can be seen by the fact that the temperature for the lumped system model is significantly lower than the lower quartile temperature for the data supplied.

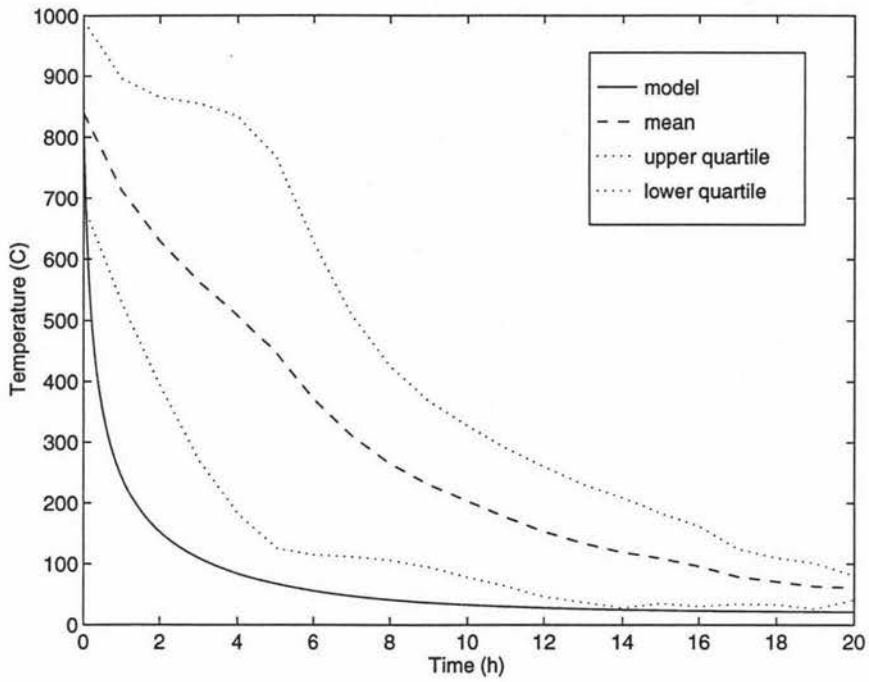

Figure 3.1: Cooling curve for lumped system model compared with measured data

If the butt is made up of several different materials (e.g carbon, bath and steel) a lumped system model would be inadequate. The thermal properties would be different for the different materials, leading to temperature variation within the butt.

In the next chapters the fact that the temperature is not uniform throughout the anode is included in the model. This leads to the heat equations developed in Chapter 4. These are then solved to give the temperature distribution throughout the anode.

Chapter 4

Heat Equation

To find the differential equations that describe heat transfer due to conduction within a solid, energy balances and rate equations are used. The energy balance is found in the same way as in Chapter 3 but in this case the system is a small part of the anode.

4.1 Formulation of the Heat Equation

The energy transfer into the system (E_{in}), the energy transfer out of the system (E_{out}), energy generated within the system (E_g) and energy storage within the system (E_s). The first law of thermodynamics states that these must be conserved which gives the following equation for the energy balance

$$E_{in} + E_g = E_{out} + E_s$$

The energy transfer into and out of the system is given by the rate of heat flow by conduction through a surface of area A given by

$$q = -kA\frac{\partial T}{\partial x} \tag{4.1}$$

Thermal energy storage in a solid occurs when the temperature increases (or decreases) with time. The equation describing this is

$$E_s = \rho V c\frac{\partial T}{\partial t} \tag{4.2}$$

where it has been assumed that ρ, V and c are constant. The term $\rho V c$ is known as the thermal capacitance of the solid. In the problem being considered it is assumed

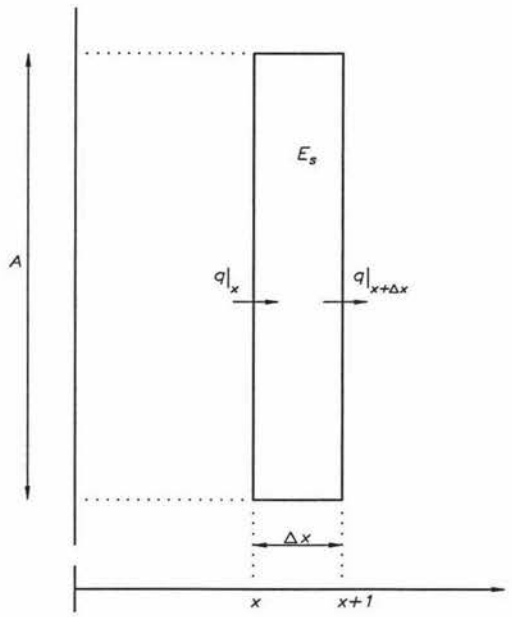

Figure 4.1: Important energy terms for a plane-wall system

that there is no energy generated in the system. The one-dimensional form of the heat equation describes the flow of energy in a plane wall, where the temperature varies only in the x-direction. A system of length Δx is defined in the x direction with cross sectional area A normal to the x direction, see Figure 4.1.

The energy balance equation can be written as

$$q|_{x+\Delta x} + E_s = q|_x$$

Where

$$q|_x = -\,kA\frac{\partial T}{\partial x}\bigg|_x$$

$$q|_{x+\Delta x} = -\,kA\frac{\partial T}{\partial x}\bigg|_{x+\Delta x}$$

and

$$E_s = \rho A \Delta x c \frac{\partial T}{\partial t}$$

Substituting into the energy balance equation gives

$$-\,kA\frac{\partial T}{\partial x}\bigg|_{x+\Delta x} + \rho A \Delta x c \frac{\partial T}{\partial t} = -\,kA\frac{\partial T}{\partial x}\bigg|_x$$

This can be rearranged to give

$$\rho Ac\frac{\partial T}{\partial t} = \frac{kA\frac{\partial T}{\partial x}\Big|_{x+\Delta x} - kA\frac{\partial T}{\partial x}\Big|_{x}}{\Delta x}$$

As $\Delta x \to 0$ this becomes

$$\rho Ac\frac{\partial T}{\partial t} = \frac{\partial}{\partial x}\left(kA\frac{\partial T}{\partial x}\right)$$

A is constant; if k is also constant then this can be written as

$$\rho c\frac{\partial T}{\partial t} = k\frac{\partial^2 T}{\partial x^2}$$

The thermal diffusivity α is defined as $\alpha = k/\rho c$ so this equation can be written as

$$\frac{\partial T}{\partial t} = \alpha\frac{\partial^2 T}{\partial x^2} \tag{4.3}$$

This is known as the one-dimensional heat equation.

For heat flow in two-dimensions the same argument is used but a system of width Δx by Δy in the x and y-directions respectively and a width of W normal to this is used. This system has heat flowing from four directions rather than two as in the one-dimensional case (see Figure 4.2).

If it is assumed that all the heat flow is into the system, this gives an energy balance of

$$E_s = q|_x + q|_{x+\Delta x} + q|_y + q|_{y+\Delta y}$$

where

$$E_s = \rho W\Delta x\Delta yc\frac{\partial T}{\partial t}$$

and

$$q|_x = -\,kW\Delta y\frac{\partial T}{\partial x}\Big|_x$$

$$q|_{x+\Delta x} = kW\Delta y\frac{\partial T}{\partial x}\Big|_{x+\Delta x}$$

$$q|_y = -\,kW\Delta x\frac{\partial T}{\partial y}\Big|_y$$

$$q|_{y+\Delta y} = kW\Delta x\frac{\partial T}{\partial y}\Big|_{y+\Delta y}$$

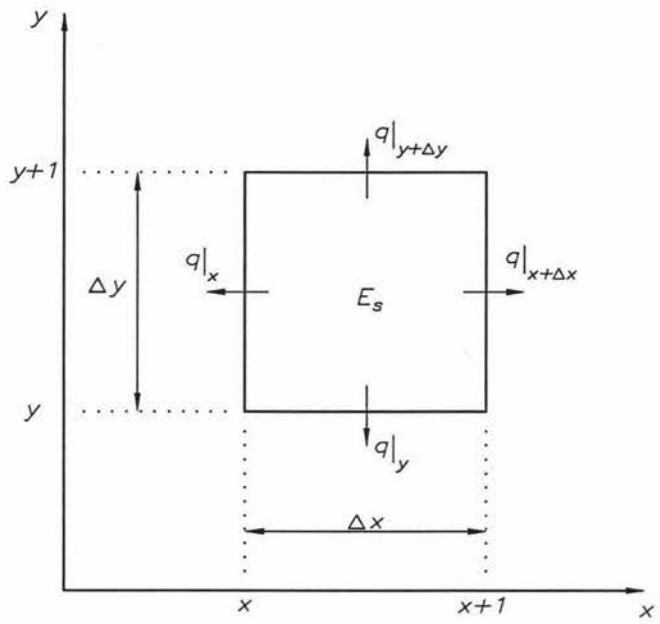

Figure 4.2: Important energy terms for a two-dimensional system

Substitution into the energy balance equation gives

$$\rho W \Delta x \Delta y c \frac{\partial T}{\partial t} = kW\Delta y \left.\frac{\partial T}{\partial x}\right|_{x+\Delta x} - kW\Delta y \left.\frac{\partial T}{\partial x}\right|_{x} + kW\Delta x \left.\frac{\partial T}{\partial y}\right|_{y+\Delta y} - kW\Delta x \left.\frac{\partial T}{\partial y}\right|_{y}$$

which can be rearranged to give

$$\rho W c \frac{\partial T}{\partial t} = \frac{kW \left.\frac{\partial T}{\partial x}\right|_{x+\Delta x} - kW \left.\frac{\partial T}{\partial x}\right|_{x}}{\Delta x} + \frac{kW \left.\frac{\partial T}{\partial y}\right|_{y+\Delta y} - kW \left.\frac{\partial T}{\partial y}\right|_{y}}{\Delta y}$$

As $\Delta x \to 0$ and $\Delta y \to 0$ this becomes

$$\rho W c \frac{\partial T}{\partial t} = \frac{\partial}{\partial x}\left(kW\frac{\partial T}{\partial x}\right) + \frac{\partial}{\partial y}\left(kW\frac{\partial T}{\partial y}\right)$$

Since W is a constant, if k is a constant this can be written as

$$\frac{\partial T}{\partial t} = \alpha\left(\frac{\partial^2 T}{\partial x^2} + \frac{\partial^2 T}{\partial y^2}\right) \tag{4.4}$$

where $\alpha = k/\rho c$. This is the two-dimensional heat equation.

Using a similar argument the three-dimensional heat equation

$$\frac{\partial T}{\partial t} = \alpha\left(\frac{\partial^2 T}{\partial x^2} + \frac{\partial^2 T}{\partial y^2} + \frac{\partial^2 T}{\partial z^2}\right) \tag{4.5}$$

can be found.

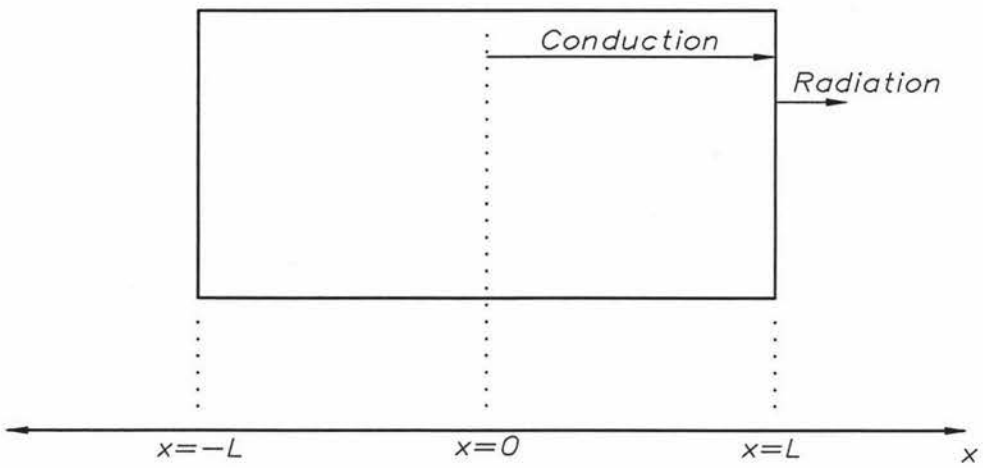

Figure 4.3: Heat flow in a one-dimensional anode

4.2 Boundary and Initial Conditions

Owing to the symmetry of the problem (see Figure 4.3), the solution can be found for just half of the anode. This simplifies the analytical solution and saves a lot of computation time when the solution is found using numerical methods. At $x = 0$ the rate of heat transfer is zero due to symmetry, this gives the following boundary condition at $x = 0$:

$$\left.\frac{\partial T}{\partial x}\right|_{x=0} = 0$$

In Chapter 2 it was shown that at the surface of the anode the energy transfer was due mainly to radiation, the rate of heat transfer being given by

$$q_r = \epsilon\sigma A(T_s^4 - T_\infty^4)$$

Equation (4.1) states that

$$q = -kA\frac{\partial T}{\partial x}$$

therefore the boundary condition at $x = L$ is

$$\left.-kA\frac{\partial T}{\partial x}\right|_{x=L} = \epsilon\sigma A(T(L,t)^4 - T_\infty^4)$$

The initial condition specifies the temperature distribution at $t = 0$. This is a function of position within the anode

$$T(x,0) = f(x)$$

the boundary and initial conditions for the two- and three-dimension problems can be found similarly.

4.3 Summary

One-Dimensional Heat Equation

The one-dimensional heat equation for the problem is

$$\frac{\partial T(x,t)}{\partial t} = \alpha \frac{\partial^2 T(x,t)}{\partial x^2} \tag{4.6}$$

with boundary conditions

$$\left.\frac{\partial T}{\partial x}\right|_{x=0} = 0$$

$$\left.\frac{\partial T}{\partial x}\right|_{x=L_x} = -\frac{\epsilon\sigma}{k}(T(L_x,t)^4 - T_\infty^4)$$

and

$$T(x,0) = f(x)$$

is the initial condition.

Two-Dimensional Heat Equation

The two-dimensional heat equation is

$$\frac{\partial T}{\partial t} = \alpha\left(\frac{\partial^2 T}{\partial x^2} + \frac{\partial^2 T}{\partial y^2}\right) \tag{4.7}$$

with the following boundary conditions

$$\left.\frac{\partial T}{\partial x}\right|_{x=0} = 0$$

$$\left.\frac{\partial T}{\partial y}\right|_{y=0} = 0$$

$$\left.\frac{\partial T}{\partial x}\right|_{x=L_x} = -\frac{\epsilon\sigma}{k}(T(L_x,y,t)^4 - T_\infty^4)$$

$$\left.\frac{\partial T}{\partial y}\right|_{y=L_y} = -\frac{\epsilon\sigma}{k}(T(x,L_y,t)^4 - T_\infty^4)$$

and

$$T(x,y,0) = f(x,y)$$

is the initial condition.

Three-Dimensional Heat Equation

The heat equation in three-dimensions is

$$\frac{\partial T}{\partial t} = \alpha \left(\frac{\partial^2 T}{\partial x^2} + \frac{\partial^2 T}{\partial y^2} + \frac{\partial^2 T}{\partial z^2} \right) \tag{4.8}$$

with the following boundary conditions

$$\left.\frac{\partial T}{\partial x}\right|_{x=0} = 0$$

$$\left.\frac{\partial T}{\partial y}\right|_{y=0} = 0$$

$$\left.\frac{\partial T}{\partial z}\right|_{z=0} = 0$$

$$\left.\frac{\partial T}{\partial x}\right|_{x=L_x} = -\frac{\epsilon\sigma}{k}(T(L_x, y, z, t)^4 - T_\infty^4)$$

$$\left.\frac{\partial T}{\partial y}\right|_{y=L_y} = -\frac{\epsilon\sigma}{k}(T(x, L_y, z, t)^4 - T_\infty^4)$$

$$\left.\frac{\partial T}{\partial z}\right|_{z=L_z} = -\frac{\epsilon\sigma}{k}(T(x, y, L_z, t)^4 - T_\infty^4)$$

and

$$T(x, y, z, 0) = f(x, y, z)$$

is the initial condition.

These equations are solved analytically in Chapter 5. In Chapters 6, 7 and 8 the numerical solution to these equations are found for the one-, two- and three-dimensional models respectively.

Chapter 5

Analytical Solution

The analytic solution can be found if the problem is simplified. While these simplifications make this solution of little practical use, it does give an indication of the expected behavior of the numerical solution.

5.1 One-Dimensional Solution

5.1.1 Linearisation

The one-dimensional heat equation with a radiation boundary condition is nonlinear due to the dependence on the fourth power of the temperature. It is possible to linearise the radiation term, this is done by factoring the fourth power of the temperature as follows

$$\begin{aligned} T_\infty^4 - T_s^4 &= (T_\infty^2 + T_s^2)(T_\infty^2 - T_s^2) \\ &= (T_\infty^2 + T_s^2)(T_\infty + T_s)(T_\infty - T_s) \end{aligned}$$

The radiation boundary condition may now be written

$$\frac{\partial T}{\partial x} = h_r(T_\infty - T_s)$$

where

$$h_r = \epsilon\sigma(T_\infty^2 + T_s^2)(T_\infty + T_s)$$

This gives the boundary equation the same appearance as the convection boundary condition but h_r is really a variable since it depends on the surface temperature

T_s. If the temperature difference between the surface temperature and the ambient temperature is small T_s can be replaced with T_∞. This gives

$$h_r = \epsilon\sigma(T_\infty^2 + T_\infty^2)(T_\infty + T_\infty) = 4\epsilon\sigma T_\infty^3$$

The radiation heat transfer coefficient is now a constant and it is possible to solve the differential equation using analytic methods. It must be noted that this linearisation is only suitable in cases where T_s is close to T_∞.

Restating the differential Equation (4.7) with the linearised boundary condition gives

$$\frac{\partial T}{\partial t} = \alpha \frac{\partial^2 T}{\partial x^2} \tag{5.1}$$

The initial condition at $t = 0$ is

$$T(x, 0) = T_i$$

The boundary condition at $x = 0$ is observed from symmetry to be

$$\frac{\partial T}{\partial x} = 0$$

The linearised radiation boundary condition at $x = L$ is

$$k\frac{\partial T}{\partial x} = h_r \left[T_\infty - T(L, t)\right]$$

5.1.2 Normalisation

These equations can be normalised if the following nondimensional variables are defined

$$\bar{T} = \frac{T - T_\infty}{T_0}$$

$$\bar{x} = \frac{x}{x_0}$$

$$\bar{t} = \frac{t}{t_0}$$

where T_0, x_0 and t_0 are constants to be determined. Substituting these nondimensional variables in to the differential equation gives

$$\frac{T_0}{t_0}\frac{\partial \bar{T}}{\partial \bar{t}} = \alpha \frac{T_0}{x_0^2}\frac{\partial^2 \bar{T}}{\partial \bar{x}^2}$$

This can rearranged to give

$$\frac{\partial \bar{T}}{\partial \bar{t}} = \alpha \frac{t_0}{x_0^2} \frac{\partial^2 \bar{T}}{\partial \bar{x}^2}$$

If t_0 is chosen to be L^2/α and $x_0 = L$ the differential equation reduces to

$$\frac{\partial \bar{T}}{\partial \bar{t}} = \frac{\partial^2 \bar{T}}{\partial \bar{x}^2} \tag{5.2}$$

This is the normalised heat equation. The boundary condition at $x = 0$ that is $\bar{x} = 0$ becomes

$$\frac{\partial \bar{T}}{\partial \bar{x}} = 0 \tag{5.3}$$

the linearised radiation boundary condition at $x = L$ that is $\bar{x} = 1$ is

$$-k \frac{T_0}{x_0} \frac{\partial \bar{T}}{\partial \bar{x}} = h_r T_0 \bar{T}$$

This can be simplified to give

$$-\frac{\partial \bar{T}}{\partial \bar{x}} = \frac{h_r L}{k} \bar{T} = H \bar{T} \tag{5.4}$$

where $H = h_r L/k$ is the normalised heat transfer coefficient. The normalised initial condition is

$$\bar{T} = \frac{T_i - T_\infty}{T_0}$$

If $T_0 = T_i - T_\infty$ then initial condition at $t = 0$ becomes

$$\bar{T} = 1 \tag{5.5}$$

Equation (5.2) to Equation (5.5) are the normalised equations describing the problem.

5.1.3 Separation of Variables

The analytic solution to the normalised[1], linearised problem can be found by the method of separation of variables. If the solution is assumed to be of the form

$$T(x,t) = F(x)G(t) \tag{5.6}$$

then Equation (5.2) can be written as

$$F''(x)G(t) = F(x)G'(t)$$

[1] In this section the normalised variables (*eg* $\bar{x}$) have been written without the bar (eg x).

Separating the variables x and t gives

$$\frac{F''(x)}{F(x)} = \frac{G'(t)}{G(t)} = -\lambda^2 = constant$$

This gives two ordinary differential equations to solve:

$$\frac{F''(x)}{F(x)} = -\lambda^2 \tag{5.7}$$

and

$$\frac{G'(t)}{G(t)} = -\lambda^2 \tag{5.8}$$

Equation (5.7) can be rearranged to give

$$F''(x) + \lambda^2 F(x) = 0$$

which has solutions of the form

$$F(x) = A \sin \lambda x + B \cos \lambda x \tag{5.9}$$

where A and B are constants to be determined.

The boundary condition at $x = 0$ is

$$\frac{\partial T}{\partial x} = 0$$

This can be rewritten using Equation (5.6) as

$$F'(0)G(t) = 0$$

therefore

$$F'(0) = 0$$

Substituting into Equation (5.9) gives

$$A = 0$$

Equation (5.9) can be rewritten as

$$F(x) = B \cos \lambda x$$

The boundary condition at $x = 1$ is

$$\left.\frac{\partial T}{\partial x}\right|_{x=1} = -HT(1,t)$$

This can be rewritten by using Equation (5.6) as

$$F'(1)G(t) = -HF(1)G(t)$$

canceling $G(t)$ gives

$$F'(1) = -HF(1)$$

This gives

$$-B\lambda \sin \lambda = -HB \cos \lambda$$

this can be simplified to give

$$\lambda \tan \lambda = H$$

which is an eigencondition for the solution.

Equation (5.8) is

$$\frac{G'(t)}{G(t)} = -\lambda^2$$

This has a solution of the form

$$G(t) = Ce^{-\lambda^2 t}$$

The partial solution of Equation (5.2) is

$$\begin{aligned} T_n(x,t) &= F_n(x)G_n(t) \\ &= B_n \cos \lambda_n x C_n e^{-\lambda_n^2 t} \\ &= A_n \cos \lambda_n x e^{-\lambda_n^2 t} \end{aligned}$$

where λ_n, the nth eigenvalue, satisfies

$$\lambda_n \tan \lambda_n = H$$

This gives a general solution of the form

$$T(x,t) = \sum_{n=1}^{\infty} A_n e^{-\lambda_n^2 t} \cos \lambda_n x$$

The initial condition $T(x,0) = 1$ gives

$$T(x,0) = 1 = \sum_{n=1}^{\infty} A_n \cos \lambda_n x$$

if both sides are multiplied by $\cos \lambda_m x$ then

$$\cos \lambda_m x = \sum_{n=1}^{\infty} A_n \cos \lambda_n x \cos \lambda_m x$$

Integrating both sides between 0 and 1 gives

$$\int_0^1 \cos \lambda_m x dx = \sum_{n=1}^{\infty} A_n \int_0^1 \cos \lambda_n x \cos \lambda_m x dx$$

It can be shown that $\cos \lambda_m x$ and $\cos \lambda_n x$ are orthogonal[2], that is

$$\int_0^1 \cos \lambda_n x \cos \lambda_m x dx = 0$$

when $m \neq n$. Therefore

$$\int_0^1 \cos \lambda_m x dx = A_m \int_0^1 \cos^2 \lambda_m x dx$$

Rearranging this gives

$$A_m = \frac{\int_0^1 \cos \lambda_m x dx}{\int_0^1 \cos^2 \lambda_m x dx}$$

which can be integrated to give

$$A_m = \frac{1/\lambda_m \sin \lambda_m}{1/4\lambda_m \sin 2\lambda + 1/2}$$

This simplifies to

$$A_m = \frac{4 \sin \lambda_m}{\sin 2\lambda_m + 2\lambda_m}$$

The general solution to the normalised equation can now be written as

$$T(x,t) = \sum_{n=1}^{\infty} \frac{4 \sin \lambda_n}{\sin 2\lambda_n + 2\lambda_n} e^{-\lambda_n^2 t} \cos \lambda_n x \tag{5.10}$$

where λ_n satisfies $\lambda_n \tan \lambda_n = H$. If the original non-normalised variables are used the general solution can be written as

$$T(x,t) = (T_i - T_\infty) \left(\sum_{n=1}^{\infty} \frac{4 \sin \lambda_n}{\sin 2\lambda_n + 2\lambda_n} e^{\frac{-\alpha \lambda_n^2 t}{L^2}} \cos \frac{\lambda_n x}{L} \right) + T_\infty \tag{5.11}$$

[2]See Section 5.1.4

5.1.4 Orthogonality

Function $X_n(x)$ and $X_n(x)$ are said to be orthogonal if

$$\int_0^L X_n(x)X_m(x)dx = 0 \tag{5.12}$$

when $m \neq n$.

Equation (5.7) says that

$$X_n''(x) = -\lambda_n^2 X_n(x)$$

Using this fact, Equation (5.12) can be written as

$$\lambda_n^2 \int_0^L X_n(x)X_m(x)dx = -\int_0^L X_n''(x)X_m(x)dx$$

Using integration by parts the LHS is

$$-\left[X_n'(x)X_m(x)\right]_0^L + \int_0^L X_n'(x)X_m'(x)dx$$

which can be further integrated by parts to give

$$-\left[X_n'(x)X_m(x) - X_n(x)X_m'(x)\right]_0^L - \int_0^L X_n(x)X_m''(x)dx$$

Using Equation (5.7) this can be written as

$$-\left[X_n'(x)X_m(x) - X_n(x)X_m'(x)\right]_0^L + \lambda_m^2 \int_0^L X_n(x)X_m(x)dx$$

Therefore

$$\lambda_n^2 \int_0^L X_n(x)X_m(x)dx = -\left[X_n'(x)X_m(x) - X_n(x)X_m'(x)\right]_0^L + \lambda_m^2 \int_0^L X_n(x)X_m(x)dx$$

rearranging this gives

$$(\lambda_n^2 - \lambda_m^2)\int_0^L X_n(x)X_m(x)dx = -\left[X_n'(x)X_m(x) - X_n(x)X_m'(x)\right]_0^L$$

If the LHS is equal to zero then $X_n(x)$ is orthogonal. Using the boundary conditions the LHS can be written as

$$HX_n(L)X_m(L) - HX_n(L)X_m(L)$$

which is zero.

Therefore

$$(\lambda_n^2 - \lambda_m^2)\int_0^L X_n(x)X_m(x)dx = 0$$

This means that for $m \neq n$

$$\int_0^L X_n(x)X_m(x)dx = 0$$

and the $X_n(x)$ are orthogonal.

5.2 Two-Dimensional Solution

5.2.1 Linearisation

The two-dimensional heat equation can be linearised in the same way as in the one-dimensional case. We have

$$\frac{\partial T}{\partial t} = \alpha \left(\frac{\partial^2 T}{\partial x^2} + \frac{\partial^2 T}{\partial y^2} \right) \tag{5.13}$$

The initial condition at $t = 0$ is

$$T(x, y, 0) = T_i$$

The boundary condition at $x = 0$ is observed from symmetry to be

$$\frac{\partial T}{\partial x} = 0$$

Similarly the boundary condition at $y = 0$ is

$$\frac{\partial T}{\partial y} = 0$$

The linearised radiation boundary condition at $x = L_x$ is

$$k \frac{\partial T}{\partial x} = h_r \left[T_\infty - T(L_x, y, t) \right]$$

and at $y = L_y$

$$k \frac{\partial T}{\partial y} = h_r \left[T_\infty - T(x, L_y, t) \right]$$

5.2.2 Normalisation

These equations can be normalised if the following nondimensional variables are defined

$$\bar{T} = \frac{T - T_\infty}{T_0}$$

$$\bar{x} = \frac{x}{v_0}$$

$$\bar{y} = \frac{y}{v_0}$$

$$\bar{t} = \frac{t}{t_0}$$

where T_0, v_0 and t_0 are constants to be determined. The lengths x and y are divided by the same value v_0 to keep the ratio between the normalised lengths $\bar{x}$ and $\bar{y}$ the

same as the ratio between x and y. Substituting these nondimensional variables into the differential equation gives

$$\frac{T_0}{t_0}\frac{\partial \bar{T}}{\partial \bar{t}} = \alpha\left(\frac{T_0}{v_0^2}\frac{\partial^2 \bar{T}}{\partial \bar{x}^2} + \frac{T_0}{v_0^2}\frac{\partial^2 \bar{T}}{\partial \bar{y}^2}\right)$$

This can rearranged to give

$$\frac{\partial \bar{T}}{\partial \bar{t}} = \alpha\frac{t_0}{v_0^2}\left(\frac{\partial^2 \bar{T}}{\partial \bar{x}^2} + \frac{\partial^2 \bar{T}}{\partial \bar{y}^2}\right)$$

If $v_0 = 1$ and $t_0 = 1/\alpha$ are chosen, this reduces to give

$$\frac{\partial \bar{T}}{\partial \bar{t}} = \frac{\partial^2 \bar{T}}{\partial \bar{x}^2} + \frac{\partial^2 \bar{T}}{\partial \bar{y}^2} \tag{5.14}$$

The boundary condition at $\bar{x} = 0$ becomes

$$\left.\frac{\partial \bar{T}}{\partial \bar{x}}\right|_{\bar{x}=0} = 0 \tag{5.15}$$

At $\bar{y} = 0$ the boundary condition is

$$\left.\frac{\partial \bar{T}}{\partial \bar{y}}\right|_{\bar{y}=0} = 0 \tag{5.16}$$

The linearised radiation boundary condition at $\bar{x} = L_x$ is

$$-k\frac{T_0}{v_0}\left.\frac{\partial \bar{T}}{\partial \bar{x}}\right|_{\bar{x}=L_x} = h_r T_0 \bar{T}$$

which can be simplified to give

$$-\left.\frac{\partial \bar{T}}{\partial \bar{x}}\right|_{\bar{x}=L_x} = \frac{h_r L_x}{k}\bar{T} = H_x \bar{T} \tag{5.17}$$

At $\bar{y} = L_y$ the boundary condition is

$$-\left.\frac{\partial \bar{T}}{\partial \bar{y}}\right|_{\bar{y}=L_y} = \frac{h_r L_y}{k}\bar{T} = H_y \bar{T} \tag{5.18}$$

The initial condition is

$$\bar{T} = \frac{T_i - T_\infty}{T_0}$$

If $T_0 = T_i - T_\infty$. The initial condition at $t = 0$ becomes

$$\bar{T} = 1 \tag{5.19}$$

Equations (5.14) to Equation (5.19) are the normalised equations describing the two-dimensional problem.

5.2.3 Separation of Variables

If the solution to the normalised equation[3] is assumed to be of the form

$$T(x,y,t) = F(x,y)G(t) \tag{5.20}$$

then the differential equation can be written as

$$F(x,y)G(t) = \left[F_{xx}(x,y) + F_{yy}(x,y)\right]G(t)$$

Therefore

$$\frac{F_{xx}(x,y) + F_{yy}(x,y)}{F(x,y)} = \frac{G'(t)}{G(t)} = c_1$$

This gives two equations

$$\frac{F_{xx}(x,y) + F_{yy}(x,y)}{F(x,y)} = c_1$$

and

$$\frac{G'(t)}{G(t)} = c_1$$

The first of these can be rearranged to give

$$F_{xx}(x,y) + F_{yy}(x,y) - c_1 F(x,y) = 0 \tag{5.21}$$

This can also be solved using separation of variables if we assume

$$F(x,y) = X(x)Y(y)$$

Then Equation (5.21) can be written as

$$X''(x)Y(y) + X(x)Y''(y) - c_1 X(x)Y(y) = 0$$

Dividing by $X(x)Y(y)$ gives and rearranging gives

$$\frac{X''(x)}{X(x)} = c_1 - \frac{Y''(y)}{Y(y)} = c_2 \tag{5.22}$$

This gives two equations

$$X''(x) - c_2 X(x) = 0$$

and

$$Y''(y) - (c_1 - c_2)Y(y) = 0$$

[3] In this section the normalised variables (eg $\bar{x}$) have been written without the bar (eg x)

If $c_2 = -\lambda^2$ the first of these equations has solutions of the form

$$X(x) = A \sin \lambda x + B \cos \lambda x$$

where A and B are constants.

From the boundary conditions $A = 0$ and

$$X(x) = B \cos \lambda x$$

where λ satisfies

$$\lambda \tan \lambda L_x = H_x$$

which is an eigencondition.

If $c_1 - c_2 = -\mu^2$ then

$$Y''(y) + \mu^2 Y(y) = 0$$

solving this gives

$$Y(y) = C \sin \mu y + D \cos \mu y$$

The boundary conditions give $C = 0$, so

$$Y(y) = D \cos \mu y$$

and the eigencondition is

$$\mu \tan \mu L_y = H_y$$

The equation

$$\frac{G'(t)}{G(t)} = c_1$$

has a solution of the form

$$G(t) = Ce^{c_1 t}$$

but $c_1 = -(\lambda^2 + \mu^2)$ so this can be written as

$$G(t) = Ce^{-(\lambda^2+\mu^2)t}$$

The particular solution to Equation (5.14) is

$$\begin{aligned} T_{m,n}(x,y,t) &= X_m(x)Y_n(y)G_{m,n}(t) \\ &= B_m \cos \lambda_m x D_n \cos \mu_n y C_{m,n} e^{-(\lambda_m^2+\mu^2)t} \\ &= A_{m,n} \cos \lambda_m x \cos \mu_n y e^{-(\lambda_m^2+\mu_n^2)t} \end{aligned}$$

where λ_m satisfies

$$\lambda_m \tan \lambda_m L_x = H_x$$

and μ_n satisfies

$$\mu_n \tan \mu_n L_y = H_y$$

This gives a general solution of the form

$$T(x,y,t) = \sum_{m=1}^{\infty}\sum_{n=1}^{\infty} A_{m,n} e^{-(\lambda_m^2+\mu_n^2)t} \cos \lambda_m x \cos \mu_n y$$

where $A_{m,n}$ is to be determined. Using the initial condition $T(x,y,0) = 1$ gives

$$T(x,y,0) = 1 = \sum_{m=1}^{\infty}\sum_{n=1}^{\infty} A_{m,n} \cos \lambda_m x \cos \mu_n y$$

If both sides are multiplied by $\cos \lambda_i x$ and $\cos \mu_j y$ then

$$\cos \lambda_i x \cos \mu_j y = \sum_{m=1}^{\infty}\sum_{n=1}^{\infty} A_{m,n} \cos \lambda_i x \cos \lambda_m x \cos \mu_j y \cos \mu_n y$$

Integrating both sides between 0 and 1 gives

$$\int_0^1 \int_0^1 \cos \lambda_i x \cos \mu_j y dx dy =$$
$$\int_0^1 \int_0^1 \sum_{m=1}^{\infty}\sum_{n=1}^{\infty} A_{m,n} \cos \lambda_i x \cos \lambda_m x \cos \mu_j y \cos \mu_n y dx dy$$

It can be shown that $\cos \lambda_i x$ and $\cos \mu_j y$ are orthogonal (see Section 5.1.4) to $\cos \lambda_m x$ and $\cos \mu_n y$ respectively. This gives

$$\int_0^1 \cos \lambda_i x \cos \lambda_m x dx = 0$$

when $m \neq i$, and

$$\int_0^1 \cos \mu_j x \cos \mu_n x dx = 0$$

when $n \neq j$. Therefore

$$\int_0^1 \int_0^1 \cos \lambda_i x \cos \mu_j y dx dy = \int_0^1 \int_0^1 A_{i,j} \cos^2 \lambda_i x \cos^2 \mu_j y dx dy$$

Rearranging for $A_{i,j}$ gives

$$A_{i,j} = \frac{\int_0^1 \int_0^1 \cos \lambda_i x \cos \mu_j y dx dy}{\int_0^1 \int_0^1 \cos^2 \lambda_i x \cos^2 \mu_j y dx dy}$$

Integrating gives

$$A_{i,j} = \frac{4 \sin \lambda_i 4 \sin \mu_j}{(\sin 2\lambda_i + 2\lambda_i)(\sin 2\mu_j + 2\mu_j)}$$

The general solution to the normalised equation can now be written as

$$T(x,y,t) = \sum_{m=1}^{\infty}\sum_{n=1}^{\infty} \frac{16 \sin\lambda_m \sin\mu_n}{(\sin 2\lambda_m + 2\lambda_m)(\sin 2\mu_n + 2\mu_n)} e^{-(\lambda_m^2+\mu_n^2)t} \cos\lambda_m x \cos\mu_n y \tag{5.23}$$

where λ_m satisfies $\lambda_m \tan\lambda_m L_x = H_x$ and μ_n satisfies $\mu_n \tan\mu_n L_y = H_y$. If the original variables are used the general solution can be written as

$$T(x,y,t) = (T_i - T_\infty)\left(\sum_{m=1}^{\infty}\sum_{n=1}^{\infty} A_{m,n} e^{-\alpha(\lambda_m^2+\mu_n^2)t} \cos\lambda_m x \cos\mu_n y\right) + T_\infty \tag{5.24}$$

where

$$A_{m,n} = \frac{16 \sin\lambda_m \sin\mu_n}{(\sin 2\lambda_m + 2\lambda_m)(\sin 2\mu_n + 2\mu_n)}$$

5.3 Three-Dimensional Solution

5.3.1 Linearisation

The three-dimensional problem can be linearised in the same way as in the one-dimensional and two-dimensional cases. The heat equation is

$$\frac{\partial T}{\partial t} = \alpha\left(\frac{\partial^2 T}{\partial x^2} + \frac{\partial^2 T}{\partial y^2} + \frac{\partial^2 T}{\partial z^2}\right) \tag{5.25}$$

The initial condition (at $t = 0$) is

$$T(x,y,z,0) = T_i$$

The boundary condition at $x = 0$ is observed from symmetry to be

$$\frac{\partial T}{\partial x} = 0$$

Similarly the boundary condition at $y = 0$ and $z = 0$ is

$$\frac{\partial T}{\partial y} = 0$$

$$\frac{\partial T}{\partial z} = 0$$

The linearised radiation boundary condition at $x = L_x$ is

$$k\frac{\partial T}{\partial x} = h_r\left[T_\infty - T(L_x,y,z,t)\right]$$

and at $y = L_y$

$$k\frac{\partial T}{\partial y} = h_r\left[T_\infty - T(x,L_y,z,t)\right]$$

and at $z = L_z$

$$k\frac{\partial T}{\partial z} = h_r\left[T_\infty - T(x,y,L_z,t)\right]$$

5.3.2 Normalisation

These equations can be normalised in the same way as the two-dimensional case if the following nondimensional variables are defined

$$\bar{T} = \frac{T - T_\infty}{T_0}$$
$$\bar{x} = \frac{x}{v_0}$$
$$\bar{y} = \frac{y}{v_0}$$
$$\bar{z} = \frac{z}{v_0}$$
$$\bar{t} = \frac{t}{t_0}$$

where T_0, v_0 and t_0 are constants. If $v_0 = 1$ and $t_0 = 1/\alpha$ then Equation (5.25) can be written as

$$\frac{\partial \bar{T}}{\partial \bar{t}} = \frac{\partial^2 \bar{T}}{\partial \bar{x}^2} + \frac{\partial^2 \bar{T}}{\partial \bar{y}^2} + \frac{\partial^2 \bar{T}}{\partial \bar{z}^2} \tag{5.26}$$

The boundary condition at $\bar{x} = 0$ is

$$\frac{\partial \bar{T}}{\partial \bar{x}} = 0 \tag{5.27}$$

at $\bar{y} = 0$ is

$$\frac{\partial \bar{T}}{\partial \bar{y}} = 0 \tag{5.28}$$

at $\bar{z} = 0$ is

$$\frac{\partial \bar{T}}{\partial \bar{z}} = 0 \tag{5.29}$$

The linearised radiation boundary condition at $x = L_x$ is

$$-\frac{\partial \bar{T}}{\partial \bar{x}}\bigg|_{\bar{x}=L_x} = \frac{h_r L_x}{k}\bar{T} = H_x \bar{T} \tag{5.30}$$

at $\bar{y} = L_y$ the boundary condition is

$$-\frac{\partial \bar{T}}{\partial \bar{y}}\bigg|_{\bar{y}=L_y} = \frac{h_r L_y}{k}\bar{T} = H_y \bar{T} \tag{5.31}$$

at $\bar{z} = L_z$ the boundary condition is

$$-\frac{\partial \bar{T}}{\partial \bar{z}}\bigg|_{\bar{z}=L_z} = \frac{h_r L_z}{k}\bar{T} = H_z \bar{T} \tag{5.32}$$

If $T_0 = T_i - T_\infty$ then initial condition at $t = 0$ becomes

$$\bar{T} = 1 \tag{5.33}$$

Equations (5.26) to Equation (5.33) are the normalised equations describing the problem.

5.3.3 Separation of Variables

The solution to the three-dimensional case can be found by extending the two-dimensional case. If the solution to the normalised[4] equation is assumed to be of the form

$$T(x,y,z,t) = X(x)Y(y)Z(z)G(t) \tag{5.34}$$

then four ordinary differential equations can be found using the same method as in the two-dimensional case

$$G'(t) - c_1 G(t) = 0$$

$$X''(x) - c_3 X(x) = 0$$

$$Y''(y) - (c_2 - c_3)Y(y) = 0$$

$$Z''(z) - (c_1 - c_2)Z(z) = 0$$

where $c_3 = -\lambda^2$ and $(c_2 - c_3) = -\mu^2$ and $(c_1 - c_2) = -\nu^2$ so $c_1 = -(\lambda^2 + \mu^2 + \nu^2)$.

Solving these and using the boundary conditions gives

$$X_l(x) = B_x \cos \lambda_l x$$

where λ_l satisfies the eigencondition $\lambda_l \tan \lambda_l L_x = H_x$

$$Y_m(y) = B_y \cos \mu_m y$$

where μ_m satisfies the eigencondition $\mu_m \tan \mu_m L_y = H_y$

$$Z_n(z) = B_z \cos \nu_n z$$

where ν_n satisfies the eigencondition $\nu_n \tan \nu_n L_z = H_z$ and

$$G_{l,m,n}(t) = C e^{-(\lambda_l^2 + \mu_m^2 + \nu_n^2)t}$$

Combining these gives the particular solution

$$T_{l,m,n}(x,y,z,t) = A_{l,m,n} e^{-(\lambda_l^2 + \mu_m^2 + \nu_n^2)t} \cos \lambda_l x \cos \mu_m y \cos \nu_n z$$

this gives the general solution

$$T(x,y,z,t) = \sum_{l=1}^{\infty} \sum_{m=1}^{\infty} \sum_{n=1}^{\infty} A_{l,m,n} e^{-(\lambda_l^2 + \mu_m^2 + \nu_n^2)t} \cos \lambda_l x \cos \mu_m y \cos \nu_n z$$

[4] In this section the normalised variables (*eg* $\bar{x}$) have been written without the bar (eg x).

The constant $A_{l,m,n}$ can be found in the same way as the two dimensional case using the initial condition. The general solution to the normalised equation can now be written as

$$T(x,y,z,t) = \sum_{l=1}^{\infty}\sum_{m=1}^{\infty}\sum_{n=1}^{\infty} \frac{64\sin\lambda_l \sin\mu_m \sin\nu_n}{\sin(2\lambda_l + 2\lambda_l)(2\mu_m + 2\mu_m)(2\nu_n + 2\nu_n)} e^{-(\lambda_l^2+\mu_m^2+\nu_n^2)t}\cos\lambda_l x \cos\mu_m y \cos\nu_n z \tag{5.35}$$

where λ_l satisfies $\lambda_l \tan\lambda_l L_x = H_x$, μ_m satisfies $\mu_m \tan\mu_m L_y = H_y$ and ν_n satisfies $\nu_n \tan\nu_n L_z = H_z$.

If the original variables are used the general solution can be written as

$$T(x,y,z,t) = (T_i - T_\infty)\left(\sum_{l=1}^{\infty}\sum_{m=1}^{\infty}\sum_{n=1}^{\infty} A_{l,m,n} e^{-\alpha(\lambda_l^2+\mu_m^2+\nu_n^2)t}\cos\lambda_l x \cos\mu_m y \cos\nu_n z\right) + T_\infty \tag{5.36}$$

where

$$A_{l,m,n} = \frac{64\sin\lambda_l \sin\mu_m \sin\nu_n}{(\sin 2\lambda_l + 2\lambda_l)(\sin 2\mu_m + 2\mu_m)(\sin 2\nu_n + 2\nu_n)}$$

5.4 Summary

A solution for the linearised problem can be found for each of the cases. Since the solution is given in terms of a series, the temperature at a given point and time is found by calculating the series for a finite number of steps. This is most efficiently done on a computer.

If the following parameters are used for the one-dimensional case:

Length $= L = 0.4\,m$	Thermal Conductivity $= k = 5\,W/mK$
Density $= \rho = 1580\,kg/m^3$	Heat Capacity $= c = 1670\,J/kgK$
Emissivity $= 0.4$	Initial Temperature $= T_i = 1112\,K$
Ambient Temperature $= T_\infty = 293\,K$	

the plot of the analytical solution is shown in Figure 5.1. This gives the expected qualitative results with the surface of the anode cooling more quickly than the centre. As time goes on the entire anode cools down. Since the difference between

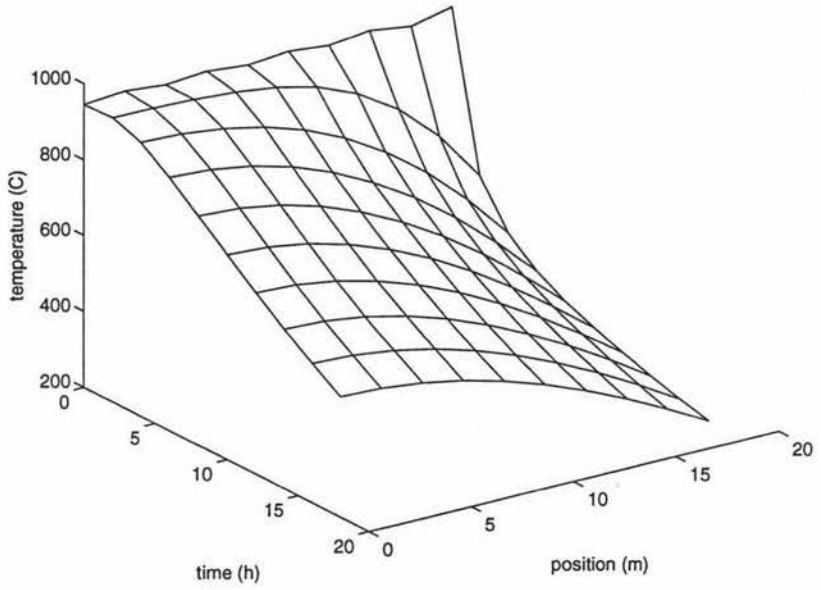

Figure 5.1: Temperature surface for one-dimensional analytic solution

the surface temperature and the ambient temperature is high this does not give a good approximation to the non-linearised problem.

Similar results could be found for the two- and three-dimensional cases also. However since in the physical problem the difference between the temperature at the surface and the ambient temperature is high, numerical methods will be used to solve the non-linearised problem.

Chapter 6

One-Dimensional Numerical Solution

The numerical method used to solve the problem was an explicit finite difference method. The finite difference equations were found initially for constant physical and thermal properties; these were then developed for variable properties. In this chapter solutions are found for one-dimensional problems with one and then two different materials.

All solutions have been computed by code written in FORTRAN running on a DEC AlphaStation 200 4/233. The program writes output to MATLAB-readable files.

6.1 Constant Physical and Thermal Properties

Initially the physical and thermal properties (e.g. thermal conductivity, specific heat capacity and density) will be considered to be constant with both time and position.

6.1.1 Finite Difference Approximations

Finite difference methods involve dividing the region into a finite number of points or nodes. The derivatives in the differential equation are then replaced with an appropriate difference-quotient approximation at each of these points. These can be found by looking at the Taylor series expansion of $T(x,t)$.

Taylor Series Method

Internal Node: Recall the 1-dimensional heat equation is

$$\frac{\partial T}{\partial t} = \alpha \frac{\partial^2 T}{\partial x^2} \tag{6.1}$$

The time derivative in this equation can be found by looking at the Taylor series expansion of $T(x,t)$ about t_m at x_i, t_{m+1} (that is T_i^{m+1})

$$T_i^{m+1} = T_i^m + \left.\frac{\partial T}{\partial t}\right|_i^m \Delta t + O[(\Delta t)^2]$$

This can be solved for for the derivative

$$\left.\frac{\partial T}{\partial t}\right|_i^m = \frac{T_i^{m+1} - T_i^m}{\Delta t} + O[(\Delta t)] \tag{6.2}$$

This is known as the forward difference, alternatively if the Taylor series expansion is found at t_{m-1} the backwards difference can be found

$$\left.\frac{\partial T}{\partial t}\right|_i^m = \frac{T_i^m - T_i^{m-1}}{\Delta t} + O[(\Delta t)] \tag{6.3}$$

The second derivative with respect to x of $T(x,t)$ in Equation (6.1) can be found by looking at the Taylor series expansion about x_i at x_{i+1} and x_{i-1}

$$T_{i+1}^m = T_i^m + \left.\frac{\partial T}{\partial x}\right|_i^m \Delta x + \frac{1}{2}\left.\frac{\partial^2 T}{\partial x^2}\right|_i^m (\frac{\Delta x}{2})^2 + \frac{1}{6}\left.\frac{\partial^3 T}{\partial x^3}\right|_i^m (\frac{\Delta x}{2})^3 + O[(\Delta x)^4]$$

$$T_{i-1}^m = T_i^m - \left.\frac{\partial T}{\partial x}\right|_i^m \Delta x + \frac{1}{2}\left.\frac{\partial^2 T}{\partial x^2}\right|_i^m (\frac{\Delta x}{2})^2 - \frac{1}{6}\left.\frac{\partial^3 T}{\partial x^3}\right|_i^m (\frac{\Delta x}{2})^3 + O[(\Delta x)^4]$$

adding these two equations gives

$$T_{i+1}^m + T_{i-1}^m = 2T_i^m + \left.\frac{\partial^2 T}{\partial x^2}\right|_i^m (\frac{\Delta x}{2})^2 + O[(\Delta x)^4]$$

This may now be solved to give the second derivative

$$\left.\frac{\partial^2 T}{\partial x^2}\right|_i^m = \frac{T_{i+1}^m + 2T_i^m + T_{i-1}^m}{(\Delta x)^2} + O[(\Delta x)^2] \tag{6.4}$$

The explicit finite difference approximation to Equation (6.1) can be found by substituting Equations (6.3) and (6.4) into Equation (6.1) which gives

$$\frac{T_i^{m+1} - T_i^m}{\Delta t} = \frac{T_{i+1}^m - 2T_i^m + T_{i-1}^m}{(\Delta x)^2}$$

where terms of $O[(\Delta x)^2, \Delta t]$ have been disregarded.This equation can be rearranged to give an explicit finite difference formula for an internal node

$$T_i^{m+1} = \frac{\alpha \Delta t}{(\Delta x)^2}(T_{i+1}^m - 2T_i^m + T_{i-1}^m) + T_i^m \tag{6.5}$$

The implicit finite difference formula can be found by using the backward difference approximation for the time derivative. Using the Fourier number $Fo = \alpha \Delta t/(\Delta x)^2$, Equation (??) becomes

$$T_i^{m+1} = Fo\left(T_{i+1}^m - 2T_i^m + T_{i-1}^m\right) + T_i^m \tag{6.6}$$

Surface Node: If the boundary condition is of the form

$$k\frac{\partial T}{\partial x} = q'' \tag{6.7}$$

it represents a surface with heat flux. This partial derivative can be approximated by finding the Taylor series expansion of $T(x,t)$ about x_m.

$$T_{i+1}^m = T_i^m + \left.\frac{\partial T}{\partial x}\right|_i^m \Delta x + \left.\frac{\partial^2 T}{\partial x^2}\right|_i^m (\Delta x)^2 + O[(\Delta x)^3]$$

$$T_{i-1}^m = T_i^m - \left.\frac{\partial T}{\partial x}\right|_i^m \Delta x + \left.\frac{\partial^2 T}{\partial x^2}\right|_i^m (\Delta x)^2 + O[(\Delta x)^3]$$

Subtracting these gives

$$T_{i+1}^m - T_{i-1}^m = 2\left.\frac{\partial T}{\partial x}\right|_i^m \Delta x + O[(\Delta x)^3]$$

solving for the derivative gives

$$\left.\frac{\partial T}{\partial x}\right|_i^m = \frac{T_{i+1}^m - T_{i-1}^m}{2\Delta x} + O[(\Delta x)^2]$$

Substituting this into Equation (6.7) and neglecting $0[(\Delta x)^2]$ gives

$$k\frac{T_{i+1}^m - T_{i-1}^m}{2\Delta x} = q''$$

Solving for T_{i+1}^m gives

$$T_{i+1}^m = 2\frac{\Delta x q''}{k} + T_{i-1}^m \tag{6.8}$$

At the boundary x_i is the final node and there is no node i+1 this means Equation (6.8) must be substituted into Equation (6.5) giving

$$T_i^{m+1} = \frac{\alpha \Delta t}{(\Delta x)^2}(2\frac{\Delta x q''}{k} - 2T_i^m + 2T_{i-1}^m) + T_i^m \tag{6.9}$$

A similar argument can be used at the other boundary. In the model developed the boundary condition at $x = x_1 = 0$ is

$$k\frac{\partial T}{\partial x} = q'' = 0$$

Therefore Equation (6.9) becomes

$$T_1^{m+1} = \frac{\alpha \Delta t}{(\Delta x)^2}(2T_2^m - 2T_1^m) + T_1^m$$

and the boundary condition at $x = x_N = L$ is

$$k\frac{\partial T}{\partial x} = q'' = \epsilon\sigma(T_\infty^4 - (T_N^m)^4)$$

Therefore Equation (6.9) becomes

$$T_N^{m+1} = Fo\left\{2T_{N-1}^m - 2T_N^m + 2\frac{\epsilon\sigma}{k}\left[T_\infty^4 - (T_N^m)^4\right]\Delta x\right\} + T_N^m$$

Heat Flow Method

Internal Node: Alternatively the finite difference equations can be found by looking at the heat flow into and out of the strip surrounding a node as in Figure 6.1. Using the first law of thermodynamics

$$\rho \Delta x W c \left.\frac{\partial T}{\partial t}\right|_i^m = q_l + q_r \tag{6.10}$$

where q_1 and q_2 are the heat flux from the left and right nodes respectively. The heat flux is proportional to the temperature gradient, which can be approximated by the difference in temperatures between adjacent nodes, divided by the distance between these nodes Δx. The heat fluxes q_1 and q_2 can be written as

$$q_1 = kW(\frac{T_{i-1}^m - T_i^m}{\Delta x})$$

$$q_2 = kW(\frac{T_{i+1}^m - T_i^m}{\Delta x})$$

Taking the forward difference for the time derivative

$$\left.\frac{\partial T}{\partial t}\right|_i^m = \frac{T_i^{m+1} - T_i^m}{\Delta t}$$

and substitution into Equation (6.10) gives

$$\rho \Delta x W c \frac{T_i^{m+1} - T_i^m}{\Delta t} = kW(\frac{T_{i-1}^m - T_i^m}{\Delta x}) + kW(\frac{T_{i+1}^m - T_i^m}{\Delta x})$$

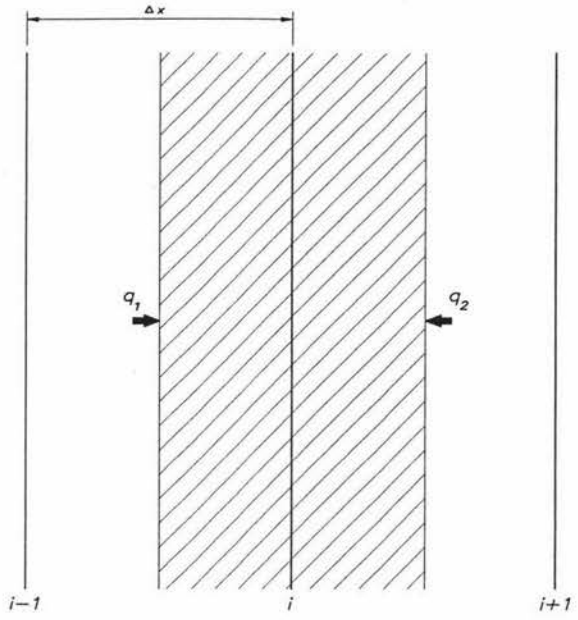

Figure 6.1: One-dimensional internal node

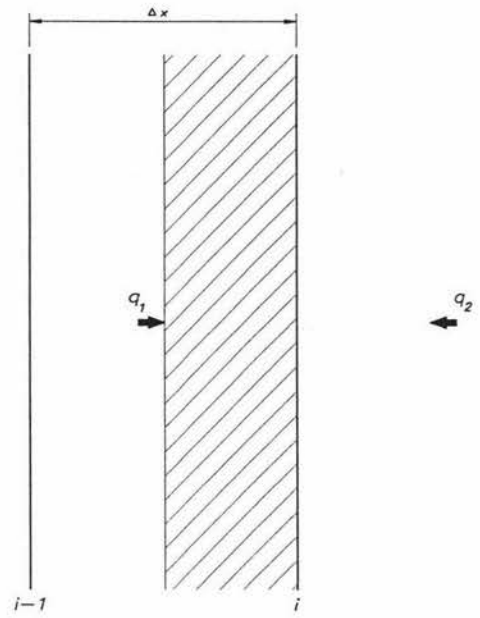

Figure 6.2: One-dimensional surface node

This can be rearranged to give the finite difference equation

$$T_i^{m+1} = Fo(T_{i-1}^m - 2T_i^m + T_{i+1}^m) + T_i^m \tag{6.11}$$

for an internal node.

Surface Node: The same method can also be used for a surface node where the heat flux from the surface is given by q''. The volume which the node represents is $1/2\Delta xW$ so

$$\frac{1}{2}\rho\Delta xWc\frac{T_i^{m+1} - T_i^m}{\Delta t} = kW(\frac{T_{i-1}^m - T_i^m}{\Delta x}) + q''$$

therefore

$$T_i^{m+1} = Fo(2T_{i-1}^m - 2T_i^m + \frac{2\Delta x q''}{k}) + T_i^m \tag{6.12}$$

6.1.2 Numerical Results

The one dimensional equation was solved with the following values

Thickness $= L = 0.4\,m$	Thermal Conductivity $= k = 5\,W/mK$
Density $= \rho = 1580\,kg/m^3$	Heat Capacity $= c = 1670\,J/kgK$
Emissivity $= 0.4$	Initial Temperature $= T_i = 1112\,K$
Ambient Temperature $= T_\infty = 293\,K$	

This means the thermal diffusivity $\alpha = k/\rho C_p = 1.89 \times 10^{-6}\,m^2/s$. The length L was divided into 20 nodes so $\Delta x = 0.02m$, the solution was found for $t = 20hr$ using a time step $\Delta t = 4\,s$. Plotting temperature against time and position x (Figure 6.3) shows how the anode initially cools at the surface and how as time goes on the temperature within the anode decreases. It can be seen that this solution is similar to the analytic solution found earlier.

The one-dimensional equation was solved for various thermal properties and anodes of different lengths. Results are shown in Table 6.1. It can be seen that the length of the anode has a large effect on the temperature both at the surface and the centre of the anode. The properties of the material mainly affect the temperature within the anode but also affect the surface temperature. The emissivity does not have as large an effect on the temperatures as some of the other parameters; it mainly affects the surface temperature. A high initial temperature cools down very quickly and the low initial temperature cools down quite slowly. The ambient temperature has little affect when it is varied from $0\,^\circ C$ to $40\,^\circ C$.

Table 6.1: Temperature at surface and centre for various physical and thermal properties

L (m)	k (W/mK)	ρ (kg/m^3)	C_p (kJ/kgK)	ϵ	T_i (K)	T_∞ (K)	T_s (1 hr) (K)	T_c (1 hr) (K)	T_s (10 hr) (K)	T_c (10 hr) (K)	T_s (20 hr) (K)	T_c (20 hr) (K)
0.4	5.0	1580	1670	0.4	1112	293	854	1112	698	931	622	765
0.6	5.0	1580	1670	0.4	1112	293	853	1112	705	1052	656	930
0.2	5.0	1580	1670	0.4	1112	293	854	1084	617	683	509	537
0.1	5.0	1580	1670	0.4	1112	293	835	952	496	509	406	411
0.4	1.0	1580	1670	0.4	1112	293	749	1112	607	1101	567	1039
0.4	10.0	1580	1670	0.4	1112	293	896	1109	716	841	617	682
0.4	5.0	2500	1670	0.4	1112	293	882	1112	734	1016	675	879
0.4	5.0	500	1670	0.4	1112	293	780	1089	560	649	460	496
0.4	5.0	1580	1670	1.0	1112	293	736	1112	584	869	513	672
0.4	5.0	1580	1670	0.8	1112	293	764	1112	611	884	538	694
0.4	5.0	1580	1670	0.6	1112	293	802	1112	646	903	572	723
0.4	5.0	1580	1670	0.2	1112	293	935	1112	789	977	716	841
0.4	5.0	1580	1670	0.4	1500	293	993	1500	785	1172	686	904
0.4	5.0	1580	1670	0.4	500	293	480	500	450	482	432	457
0.4	5.0	1580	1670	0.4	1112	303	854	1112	698	931	623	766
0.4	5.0	1580	1670	0.4	1112	273	853	1112	696	930	621	764

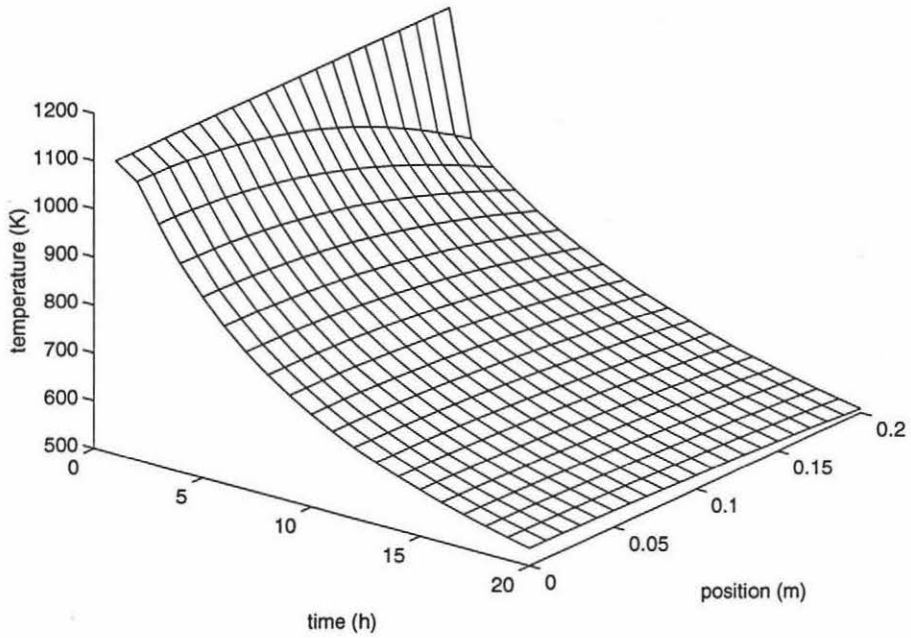

Figure 6.3: Temperature surface for one-dimensional numerical solution

6.2 Variable Physical and Thermal Properties

In this section we include in the model the possibility of the thermal and physical properties changing with position within the anode. This means that more than one material (eg carbon and bath) can be included in the model. It is also possible to extend this to include the thermal properties varying with temperature.

6.2.1 Finite Difference approximations

The heat flux between adjacent nodes can be calculated by taking the average of the thermal conductivity of the two nodes

$$q_1 = \frac{k_{i-1} + k_i}{2} W \left(\frac{T_{i-1}^m - T_i^m}{\Delta x}\right)$$

$$q_2 = \frac{k_i + k_{i+1}}{2} W \left(\frac{T_{i+1}^m - T_i^m}{\Delta x}\right)$$

The first law of thermodynamics can be written as

$$(\rho c)_i \Delta x W \left.\frac{\partial T}{\partial t}\right|_i^m = q_1 + q_2$$

substituting in q_1 and q_2 gives

$$(\rho c)_i \Delta x W \left.\frac{\partial T}{\partial t}\right|_i^m = \frac{W}{\Delta x}\left(\frac{k_{i-1}+k_i}{2}T_{i-1} - \frac{k_{i-1}+2k_i+k_{i+1}}{2}T_i + \frac{k_i+k_{i+1}}{2}T_{m+1}\right)$$

The finite difference equation may now be rewritten as

$$T_i^{m+1} = Fo(a_i T_{i-1}^m - 2b_i T_i^m + c_i T_{i+1}^m) + T_i^m$$

where

$$a_i = \frac{k_{i-1}+k_i}{2(\rho c)_i}$$

$$2b_i = \frac{k_{i-1}+2k_i+k_{i+1}}{2(\rho c)_i}$$

$$c_i = \frac{k_i+k_{i+1}}{2(\rho c)_i}$$

If the thermal properties also varied with temperature (i.e. $k = k(x,T)$) then at each time step m, T_i^m could be used to find k_i^m.

6.2.2 Numerical Simulation

The one-dimensional model was solved for a butt of total thickness of $0.4\,m$, while the bath thickness was varied from being $0.0\,m$ to be $0.4\,m$. The carbon had the following thermal properties:

Emissivity = 0.4	Thermal Conductivity = $k_c = 5\,W/mK$
Density = $\rho_c = 1580\,kg/m^3$	Heat Capacity = $c_c = 1670\,J/kgK$

and the bath had:

Emissivity = 0.4	Thermal Conductivity = $k_b = 0.4\,W/mK$
Density = $\rho_b = 2050\,kg/m^3$	Heat Capacity = $c_b = 2287\,J/kgK$

Figure 6.4 shows the temperature profile every two hours for up to twenty hours. It can be seen that the surface of the bath cools down more quickly than the carbon surface, however the interior of the bath stays hotter for longer. This suggests that removing the bath from a hot anode would help speed up the cooling process.

The calculated temperature with time of a point of depth $0.05\,m$ into the surface of the carbon for a butt of thickness $0.4\,m$ with a bath cover of thickness $0.2\,m$

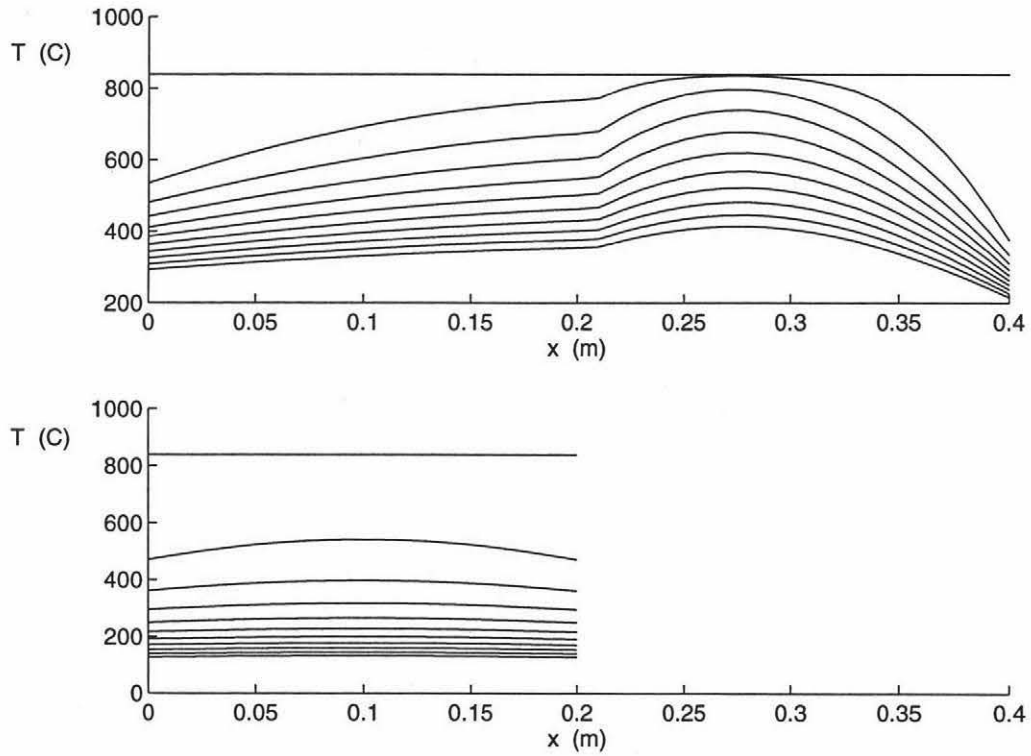

Figure 6.4: Temperature profiles for butts with various bath thicknesses

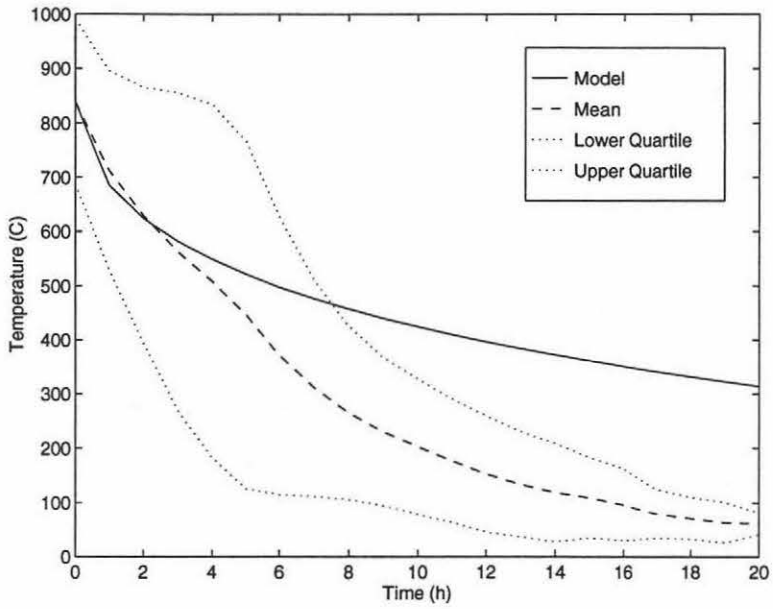

Figure 6.5: Cooling curve of a point in carbon compared to experimental data

is shown Figure 6.5 where this is compared with the data given in [9]. Figure 6.6 shows the temperature change with time for a point of depth $0.05\,m$ into the bath. As can be seen this model starts of reasonably well but as time goes on it starts to give a higher temperature for both the carbon and the bath compared with experimental data.

The temperature change with time for a point of depth $0.05\,m$ in an anode with the bath removed before any cooling has taken place is shown in Figure 6.7. The temperature profiles within both the clean and dirty anodes are shown in Figure 6.8 which shows that, the clean anode cools at a much faster rate.

6.3 Accuracy and Stability of Numerical Method

The accuracy of the solution depends on the size of the grid Δx and on the size of the time step Δt. The sizes of Δx and Δt also affect the computation time. For the one dimensional problem this is time is insignificant (less than $5\,s$); however this is more important in the higher dimensional cases as the number of nodes increases significantly. The stability of the numerical method used depends on the coefficient of T_n^m in Equation (6.11). If this value is negative the numerical solution becomes

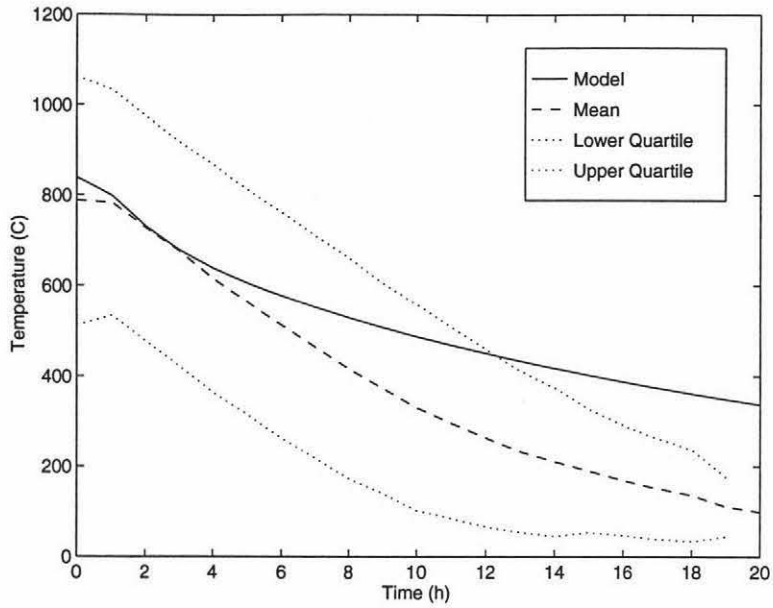

Figure 6.6: Cooling curve of a point in bath compared to experimental data

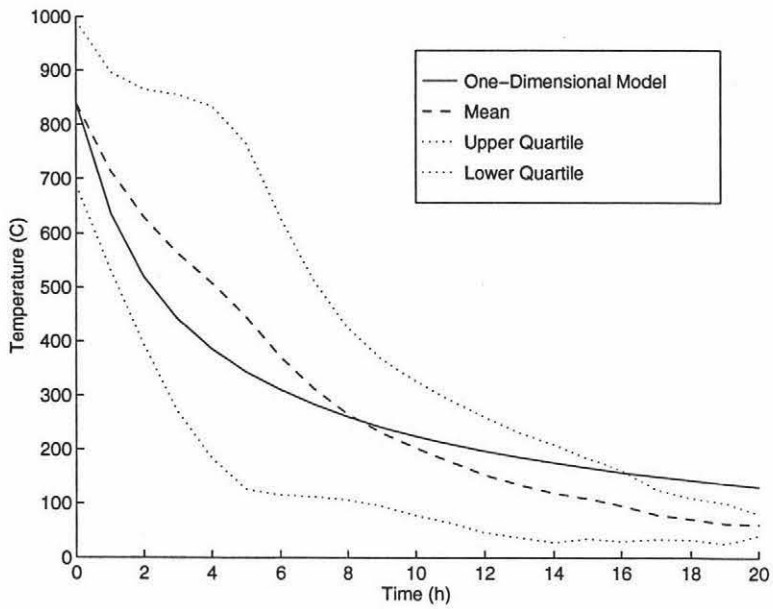

Figure 6.7: Temperature of clean node

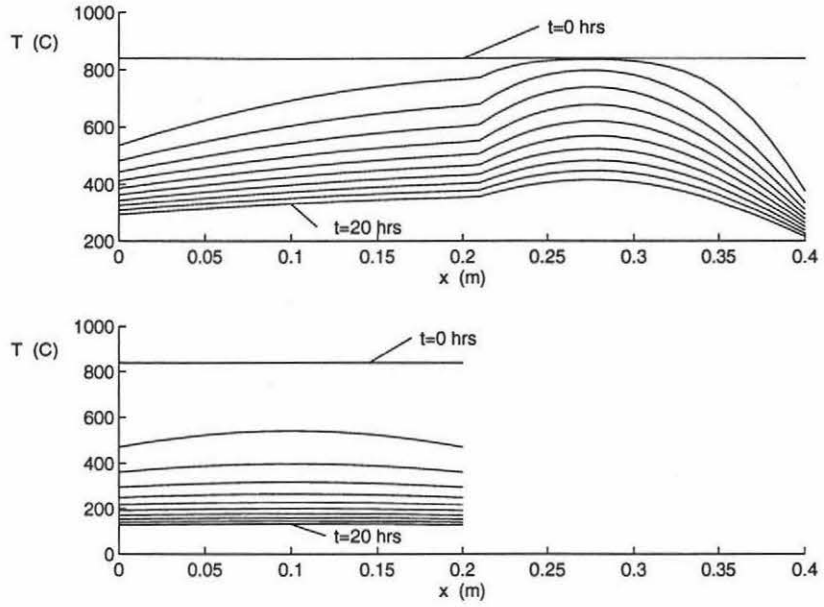

Figure 6.8: Temperature profiles of dirty anode (top) and clean anode (bottom)

unstable (see [1]). For a given mesh size Δx a maximum time step Δt can be found which gives a stable solution. For an internal node the coefficient of T_n^m is

$$1 - 2Fo \geq 0$$

Since $Fo = \alpha \Delta t/(\Delta x)^2$ this can be written as

$$\Delta t \leq \frac{(\Delta x)^2}{2\alpha}$$

For the problem solved in Section 6.1.2, $\Delta x = 0.01\,m$ so for an internal node the maximum Δt is $26.386\,s$. This can be seen in Table 6.2 in the first section where $\Delta t = 26\,s$ gives good results, but if this is increased to $\Delta t = 27\,s$ the method is unstable.

The results for a number of simulations using the same data as in Section 6.1.2 were done with various mesh sizes and different sized time steps. These are shown in Table 6.2. It can be seen that for all grid sizes up to $\Delta x = 0.04\,m$ the method gives similar results. When $\Delta x = 0.08\,m$ the method starts to lose some accuracy, the temperatures varying by up to $10K$ from the smaller grid sizes. Changing the size of the time steps does make some difference but this is fairly small if the time step is less than the critical value for stability.

Table 6.2: Temperature at surface and centre for various grid and timestep sizes

Δx (m)	Δt (s)	T_c (1 hr) (K)	T_s (1 hr) (K)	T_c (5 hr) (K)	T_s (5 hr) (K)	T_c (10 hr) (K)	T_s (10 hr) (K)	T_c (20 hr) (K)	T_s (20 hr) (K)
0.01	4	851	1081	709	830	609	672	501	528
0.01	8	851	1081	709	830	609	672	501	528
0.01	16	851	1081	709	830	609	672	501	528
0.01	26	851	1082	709	830	609	672	501	528
0.01	27	unstable							
0.02	4	851	1081	709	830	609	672	501	528
0.02	8	851	1081	709	830	609	672	501	528
0.02	16	851	1081	709	830	609	672	501	528
0.04	4	850	1081	709	830	609	671	501	528
0.04	8	850	1081	709	830	609	671	501	528
0.04	16	850	1081	709	830	609	671	501	528
0.08	4	849	1071	707	824	608	668	501	526
0.08	80	849	1071	707	824	608	668	501	526
0.08	16	849	1071	707	824	608	668	501	526

6.4 Summary

The one-dimensional model of the problem allows for a much greater range of features to be incorporated into the model than the lumped system model, including different types of materials. The major problem with this model is the fact that the geometric shape of the anodes cannot be incorporated into the model; this will be done in Chapters 7 and 8. The results above show that although the model has the correct qualitative properties it does not follow the cooling data from the experiments.

The model shows that the removal of bath from the butt has a large effect on the temperature within the butt as expected. It can also be seen that for a position near the surface of the carbon such as that measured in the experiment in [9], there is little difference in temperature between clean and dirty anodes.

Chapter 7

Two-Dimensional Numerical Solution

The finite difference equations can be found for both the constant and variable physical and thermal property cases. Various cases will be modelled including the same case as the analytical solution. By changing the thermal properties with position an anode covered in bath will be modelled. A more complicated shape which includes the assembly yoke (see Figure 1.3) from which the anode hangs is also modelled.

7.1 Constant Physical and Thermal Properties

7.1.1 Finite Difference Approximation

The formulation of the finite difference equations in the two-dimensional case is similar to the one-dimensional case. The main difference is that there are four types of nodes: internal, surface, external corner and internal corner nodes. Different finite difference equations must be found for each type.

Internal Node

An internal node is surrounded by four other nodes as shown in Figure 7.1. The two-dimensional heat equation is

$$\frac{\partial T}{\partial t} = \alpha\left(\frac{\partial^2 T}{\partial x^2} + \frac{\partial^2 T}{\partial y^2}\right) \tag{7.1}$$

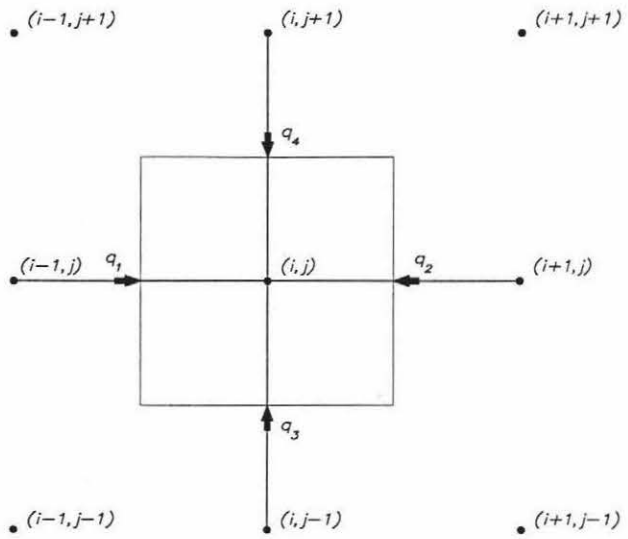

Figure 7.1: Two-dimensional internal node

The finite difference equations can be found by two different methods. The first uses Taylor series expansions while the other uses the energy balance equation.

Taylor Series Method: The Taylor series expansion of $T(x,y,t)$ about t_m at (x_i, y_j, t_{m+1}), that is $T_{i,j}^{m+1}$, is given by

$$T_{i,j}^{m+1} = T_{i,j}^{m} + \left.\frac{\partial T}{\partial t}\right|_{i,j}^{m} \Delta x + O[(\Delta x)^2]$$

This can be solved for for the derivative

$$\left.\frac{\partial T}{\partial t}\right|_{i,j}^{m} = \frac{T_{i,j}^{m+1} - T_{i,j}^{m}}{\Delta x} + O[(\Delta x)] \tag{7.2}$$

The second derivative with respect to x of $T(x,y,t)$ in Equation (7.1) can be found by looking at the Taylor series expansion about x_i at x_{i+1} and x_{i-1}:

$$T_{i+1,j}^{m} = T_{i,j}^{m} + \left.\frac{\partial T}{\partial x}\right|_{i,j}^{m} \Delta x + \frac{1}{2}\left.\frac{\partial^2 T}{\partial x^2}\right|_{i,j}^{m} (\frac{\Delta x}{2})^2 + \frac{1}{6}\left.\frac{\partial^3 T}{\partial x^3}\right|_{i,j}^{m} (\frac{\Delta x}{2})^3 + O[(\Delta x)^4]$$

$$T_{i-1,j}^{m} = T_{i,j}^{m} - \left.\frac{\partial T}{\partial x}\right|_{i,j}^{m} \Delta x + \frac{1}{2}\left.\frac{\partial^2 T}{\partial x^2}\right|_{i,j}^{m} (\frac{\Delta x}{2})^2 - \frac{1}{6}\left.\frac{\partial^3 T}{\partial x^3}\right|_{i,j}^{m} (\frac{\Delta x}{2})^3 + O[(\Delta x)^4]$$

adding these two equations gives

$$T_{i+1,j}^{m} + T_{i-1,j}^{m} = 2T_{i,j}^{m} + \left.\frac{\partial^2 T}{\partial x^2}\right|_{i,j}^{m} (\frac{\Delta x}{2})^2 + O[(\Delta x)^4]$$

This may now be solved to give the second derivative

$$\left.\frac{\partial^2 T}{\partial x^2}\right|_{i,j}^{m} = \frac{T_{i+1,j}^{m} + 2T_{i,j}^{m} + T_{i-1,j}^{m}}{(\Delta x)^2} + O[(\Delta x)^2] \tag{7.3}$$

Similarly the second derivative with respect to y of $T(x, y, t)$ in Equation (7.1) can be found by looking at the Taylor series expansion about y_j at y_{j+1} and y_{j-1}

$$T_{i,j+1}^{m} = T_{i,j}^{m} + \left.\frac{\partial T}{\partial y}\right|_{i,j}^{m} \Delta y + \frac{1}{2}\left.\frac{\partial^2 T}{\partial y^2}\right|_{i,j}^{m} (\frac{\Delta y}{2})^2 + \frac{1}{6}\left.\frac{\partial^3 T}{\partial y^3}\right|_{i,j}^{m} (\frac{\Delta y}{2})^3 + O[(\Delta y)^4]$$

$$T_{i,j-1}^{m} = T_{i,j}^{m} - \left.\frac{\partial T}{\partial y}\right|_{i,j}^{m} \Delta y + \frac{1}{2}\left.\frac{\partial^2 T}{\partial y^2}\right|_{i,j}^{m} (\frac{\Delta y}{2})^2 - \frac{1}{6}\left.\frac{\partial^3 T}{\partial y^3}\right|_{i,j}^{m} (\frac{\Delta y}{2})^3 + O[(\Delta y)^4]$$

adding these two equations gives

$$T_{i,j+1}^{m} + T_{i,j-1}^{m} = 2T_{i,j}^{m} + \left.\frac{\partial^2 T}{\partial y^2}\right|_{i,j}^{m} (\frac{\Delta y}{2})^2 + O[(\Delta y)^4]$$

This may now be solved to give the second derivative with respect to y

$$\left.\frac{\partial^2 T}{\partial y^2}\right|_{i,j}^{m} = \frac{T_{i,j+1}^{m} + 2T_{i,j}^{m} + T_{i,j-1}^{m}}{(\Delta y)^2} + O[(\Delta y)^2] \tag{7.4}$$

The explicit finite difference approximation to Equation (7.1) can be found by substituting Equations (7.2), (7.3) and (7.4) into Equation (7.1) which gives

$$\frac{T_{i,j}^{m+1} - T_{i,j}^{m}}{\Delta t} = \alpha\left(\frac{T_{i+1,j}^{m} - 2T_{i,j}^{m} + T_{i-1,j}^{m}}{(\Delta x)^2} + \frac{T_{i,j+1}^{m} - 2T_{i,j}^{m} + T_{i,j-1}^{m}}{(\Delta y)^2}\right)$$

If a square grid is used, that is $\Delta x = \Delta y$ this equation can be simplified to give

$$\frac{T_{i,j}^{m+1} - T_{i,j}^{m}}{\Delta t} = \alpha\left(\frac{T_{i+1,j}^{m} + T_{i,j+1}^{m} - 4T_{i,j}^{m} + T_{i-1,j}^{m} + T_{i,j-1}^{m}}{(\Delta x)^2}\right)$$

This can be rearranged to give

$$T_{i,j}^{m+1} = \alpha\Delta t\left(\frac{T_{i+1,j}^{m} + T_{i,j+1}^{m} - 4T_{i,j}^{m} + T_{i-1,j}^{m} + T_{i,j-1}^{m}}{(\Delta x)^2}\right) + T_{i,j}^{m}$$

If $Fo = \alpha\Delta t/(\Delta x)^2$ then

$$T_{i,j}^{m+1} = Fo\left(T_{i+1,j}^{m} + T_{i,j+1}^{m} - 4T_{i,j}^{m} + T_{i-1,j}^{m} + T_{i,j-1}^{m}\right) + T_{i,j}^{m} \tag{7.5}$$

where Fo is called the Fourier number.

Energy Balance Method: The equation can alternatively be found by looking at the energy balance equation for the volume around each node. For the internal node (see Figure 7.1) the heat flow from $(i-1,j,k)$ is

$$q_1 = k_x \frac{T_{i-1,j} - T_{i,j}}{\Delta x} \Delta y$$

similar expressions can be found for the three other surrounding nodes.

The energy balance

$$E_s = q_1 + q_2 + q_3 + q_4$$

can be written as

$$\begin{aligned} \rho C \Delta x \Delta y \frac{\partial T_{i,j}}{\partial t} &= k_x \frac{T_{i-1,j} - T_{i,j}}{\Delta x} \Delta y + k_x \frac{T_{i+1,j} - T_{i,j}}{\Delta x} \Delta y + k_y \frac{T_{i,j-1} - T_{i,j}}{\Delta y} \Delta x \\ &\quad + k_y \frac{T_{i,j+1} - T_{i,j}}{\Delta y} \Delta x \end{aligned}$$

If $k_x = k_y = k$ and $\Delta x = \Delta y$ this can be written as

$$\rho C \frac{\partial T_{i,j}}{\partial t} = k \left(\frac{T_{i-1,j} - T_{i,j}}{(\Delta x)^2} + \frac{T_{i+1,j} - T_{i,j}}{(\Delta x)^2} + \frac{T_{i,j-1} - T_{i,j}}{(\Delta x)^2} + \frac{T_{i,j+1} - T_{i,j}}{(\Delta x)^2} \right)$$

If $\alpha = k/\rho C$ this becomes

$$\frac{\partial T_{i,j}}{\partial t} = \frac{\alpha}{(\Delta x)^2} \left(T_{i-1,j} + T_{i,j-1} - 4T_{i,j} + T_{i+1,j} + T_{i,j+1} \right)$$

If the finite difference approximation for the derivative with respect to time is used this becomes Equation (7.5)

$$T_{i,j}^{m+1} = Fo \left(T_{i+1,j}^m + T_{i,j+1}^m - 4T_{i,j}^m + T_{i-1,j}^m + T_{i,j-1}^m \right) + T_{i,j}^m$$

where $Fo = \alpha \Delta t / (\Delta x)^2$ is the Fourier Number.

Surface Node

If the node is on the surface of the anode (see Figure 7.2) there is no node $(i+1,j)$ but heat is transferred across the surface by radiation. The energy balance method will be used to find the finite difference equations.

The heat transfer from the internal node $(i-1,j)$ is given by

$$q_1 = k_x \frac{T_{i-1,j} - T_{i,j}}{\Delta x} \Delta y$$

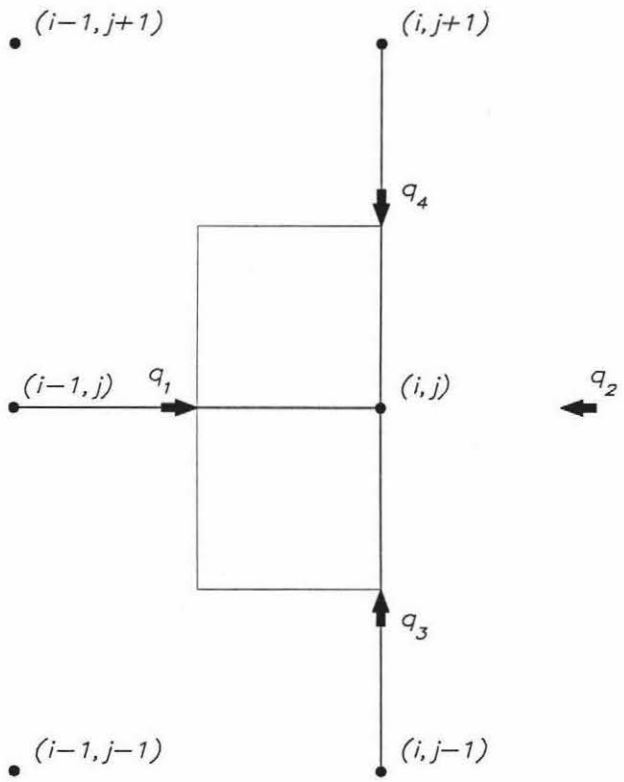

Figure 7.2: Two-dimensional surface node

the heat transfer from the adjacent surface node $(i, j-1)$ is

$$q_3 = \frac{1}{2}k_y \frac{T_{i,j-1} - T_{i,j}}{\Delta y}\Delta x$$

since the area for conduction is half that of the internal node. A similar expression can be found for q_4. The heat transfer across the surface is

$$q_2 = q''\Delta y$$

The volume which the node represents is $\Delta x \Delta y/2$, which means the energy balance is

$$\frac{1}{2}\rho C \Delta x \Delta y \frac{\partial T_{i,j}}{\partial t} = k_x \frac{T_{i-1,j} - T_{i,j}}{\Delta x}\Delta y + q''\Delta y + k_y \frac{T_{i,j-1} - T_{i,j}}{2\Delta y}\Delta x + k_y \frac{T_{i,j+1} - T_{i,j}}{2\Delta y}\Delta x$$

If $k_x = k_y = k$ and $\Delta x = \Delta y$ this can be written as

$$\frac{1}{2}\rho C \frac{\partial T_{i,j}}{\partial t} = k\left(\frac{T_{i-1,j} - T_{i,j}}{(\Delta x)^2} + \frac{T_{i,j-1} - T_{i,j}}{2(\Delta x)^2} + \frac{T_{i,j+1} - T_{i,j}}{2(\Delta x)^2}\right) + \frac{q''}{\Delta x}$$

If $\alpha = k/\rho C$ this becomes

$$\frac{\partial T_{i,j}}{\partial t} = \frac{\alpha}{(\Delta x)^2}\left(2T_{i-1,j} + T_{i,j-1} - 4T_{i,j} + T_{i,j+1} + 2\frac{q''\Delta x}{k}\right)$$

If the finite difference approximation for the derivative with respect to time is used this gives the finite difference equation for the surface node

$$T_{i,j}^{m+1} = Fo\left(2T_{i-1,j}^{m} + T_{i,j-1}^{m} - 4T_{i,j}^{m} + T_{i,j+1}^{m} + 2\frac{q''\Delta x}{k}\right) + T_{i,j}^{m} \qquad (7.6)$$

where $Fo = \alpha\Delta t/(\Delta x)^2$ is the Fourier Number.

External Corner Node

If the node is on an external corner of the anode (see Figure 7.3) there is no node $(i+1, j)$ or $(i, j+1)$ but heat is transferred across the surfaces by radiation. The energy balance method will be used to find the finite difference equations.

The heat transfer from the surface node $(i-1, j)$ is given by

$$q_1 = \frac{1}{2}k_x \frac{T_{i-1,j} - T_{i,j}}{\Delta x}\Delta y$$

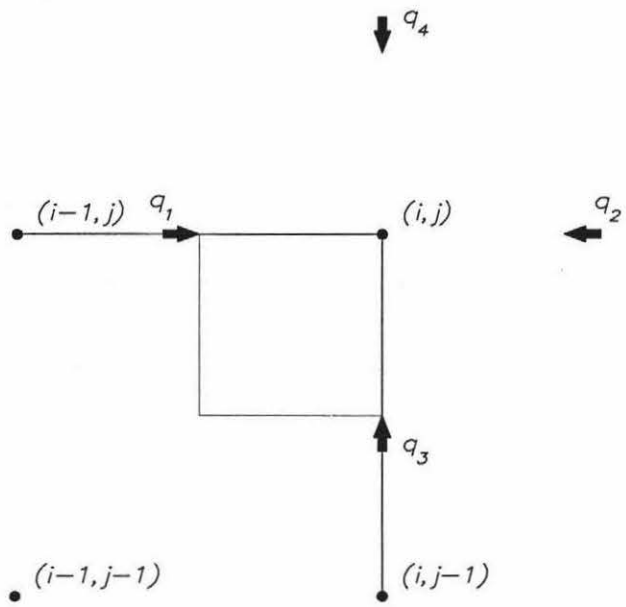

Figure 7.3: Two-dimensional external corner node

since the area for conduction is half that of the internal node. A similar expression can be found for q_3. The heat transfer across the surface in the x-direction is

$$q_2 = \frac{q''_x \Delta y}{2}$$

since there is only $\Delta y/2$ surface area for heat to be transferred across. A similar expression can be found for q_4. The volume which the node represents is $\Delta x \Delta y/4$, which means the energy balance is

$$\frac{1}{4}\rho C \Delta x \Delta y \frac{\partial T_{i,j}}{\partial t} = k_x \frac{T_{i-1,j} - T_{i,j}}{2\Delta x}\Delta y + \frac{q''_x \Delta y}{2} + k_y \frac{T_{i,j-1} - T_{i,j}}{2\Delta y}\Delta x + \frac{q''_y \Delta x}{2}$$

If $k_x = k_y = k$,$\Delta x = \Delta y$ and $q''_x = q''_y$ this can be written as

$$\frac{1}{4}\rho C \frac{\partial T_{i,j}}{\partial t} = k\left(\frac{T_{i-1,j} - T_{i,j}}{2(\Delta x)^2} + \frac{T_{i,j-1} - T_{i,j}}{2(\Delta x)^2} + \right) + \frac{q''}{\Delta x}$$

If $\alpha = k/\rho C$ this becomes

$$\frac{\partial T_{i,j}}{\partial t} = \frac{\alpha}{(\Delta x)^2}\left(2T_{i-1,j} + 2T_{i,j-1} - 4T_{i,j} + 4\frac{q''\Delta x}{k}\right)$$

If the finite difference approximation for the derivative with respect to time is used the finite difference equation for the external corner node is

$$T^{m+1}_{i,j} = Fo\left(2T^m_{i-1,j} + 2T^m_{i,j-1} - 4T^m_{i,j} + 4\frac{q''\Delta x}{k}\right) + T^m_{i,j} \tag{7.7}$$

where $Fo = \alpha \Delta t/(\Delta x)^2$ is the Fourier Number.

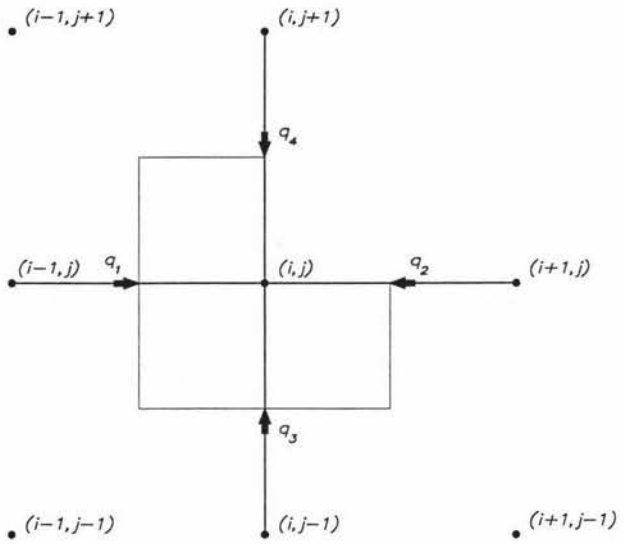

Figure 7.4: Two-dimensional internal corner node

Internal Corner Node

If the node is on an internal corner (see Figure 7.4) there is combined radiation and conduction from the two adjacent surface nodes and conduction from the two adjacent internal nodes. The energy balance method will be used to find the finite difference equations. The heat transfer from the internal node $(i-1,j)$ is given by

$$q_1 = k_x \frac{T_{i-1,j} - T_{i,j}}{\Delta x} \Delta y$$

A similar expression can be found for q_3. The heat transfer from the surface node $(i+1,j)$ in the x direction is

$$q_2 = k_x \frac{T_{i-1,j} - T_{i,j}}{2\Delta x} \Delta y + \frac{q''_x \Delta y}{2}$$

since half of the area for heat to be transferred across is by radiation and half by conduction, a similar expression can be found for q_4.

The volume which the node represents is $3\Delta x \Delta y/4$, which means the energy balance is

$$\begin{aligned} \frac{3}{4}\rho C \Delta x \Delta y \frac{\partial T_{i,j}}{\partial t} = {} & k_x \frac{T_{i-1,j} - T_{i,j}}{\Delta x} \Delta y + k_x \frac{T_{i+1,j} - T_{i,j}}{2\Delta x} \Delta y + \frac{q''_x \Delta y}{2} \\ & + k_y \frac{T_{i,j-1} - T_{i,j}}{\Delta y} \Delta x + k_y \frac{T_{i-1,j} - T_{i,j}}{2\Delta y} \Delta x + \frac{q''_y \Delta x}{2} \end{aligned}$$

If $k_x = k_y = k$,$\Delta x = \Delta y$ and $q''_x = q''_y$ this can be written as

$$\frac{3}{4}\rho C\frac{\partial T_{i,j}}{\partial t} = k\left(\frac{T_{i-1,j}-T_{i,j}}{(\Delta x)^2}+\frac{T_{i,j-1}-T_{i,j}}{(\Delta x)^2}+\frac{T_{i+1,j}-T_{i,j}}{(2\Delta x)^2}+\frac{T_{i,j+1}-T_{i,j}}{2(\Delta x)^2}+\right)+\frac{q''}{\Delta x}$$

If $\alpha = k/\rho C$ this becomes

$$\frac{\partial T_{i,j}}{\partial t} = \frac{2\alpha}{3(\Delta x)^2}\left(2T_{i-1,j}+2T_{i,j-1}-6T_{i,j}+T_{i+1,j}+T_{i,j+1}+2\frac{q''\Delta x}{k}\right)$$

If the finite difference approximation for the derivative with respect to time is used then the finite difference equation for the internal corner node is

$$T^{m+1}_{i,j} = \frac{2}{3}Fo\left(2T^m_{i-1,j}+2T^m_{i,j-1}-4T^m_{i,j}+T_{i+1,j}+T^m_{i,j+1}+2\frac{q''\Delta x}{k}\right)+T^m_{i,j} \quad (7.8)$$

where $Fo = \alpha\Delta t/(\Delta x)^2$ is the Fourier Number.

7.1.2 Anode with no bath or yoke

The solution was found for a butt with constant physical and thermal properties throughout. This represents a butt which consists of just carbon without any bath.

Length $= L = 0.8m$	Thermal Conductivity $= k = 5.5W/mK$
Height $= 0.2m$	Heat Capacity $= c = 980kJ/kgK$
Density $= \rho = 1550kg/m^3$	Ambient Temperature $= T_\infty = 293K$
Emissivity $= 0.4$	Initial Temperature $= T_i = 1112K$

A square mesh with $\Delta x = 0.02\,m$ was used, this means 10 nodes were used in the vertical direction and 40 horizontally. The solution was found out to a time of twenty hours.

The temperature profile at four different times is shown in Figure 7.5. It can be seen that the surface of the anode cools more quickly as would be expected. After about ten hours it can be seen that the temperature is fairly uniform throughout the anode. The temperature of a point $0.05\,m$ in from the edge and $0.05\,m$ from the bottom of the anode (Point A in Figure 7.7) is shown in Figure 7.6. It can be seen that initially the temperature drops very quickly but the rate of cooling slows as time increases.

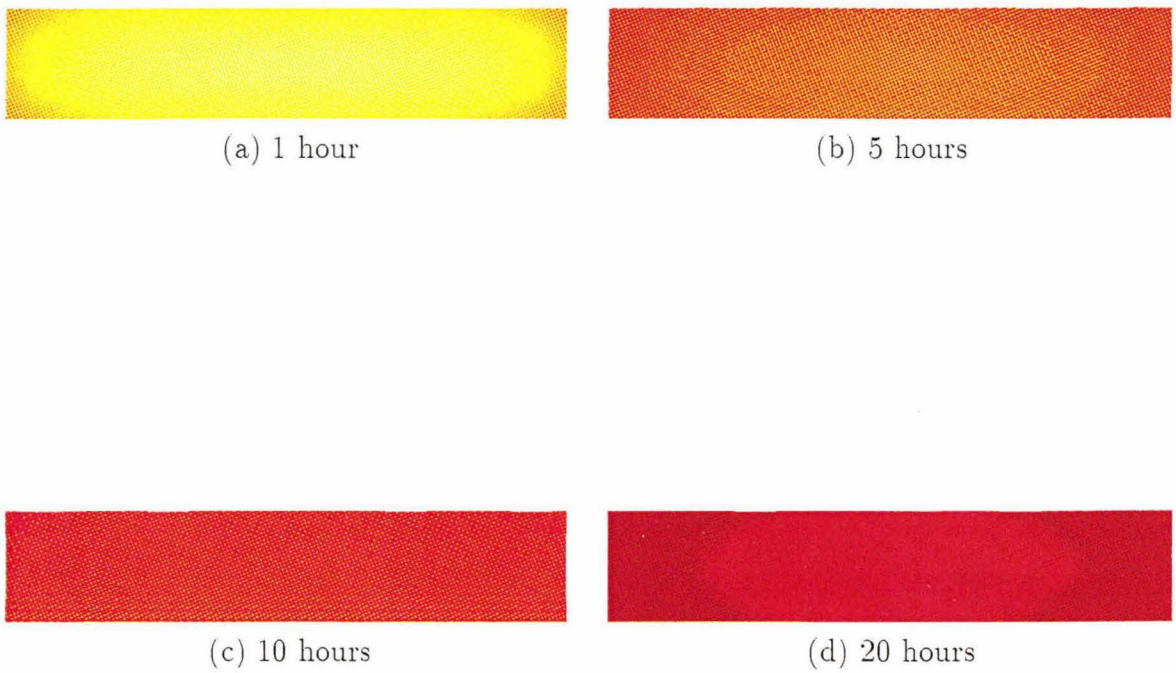

(a) 1 hour

(b) 5 hours

(c) 10 hours

(d) 20 hours

Figure 7.5: Temperature profile for clean anode without steel yoke

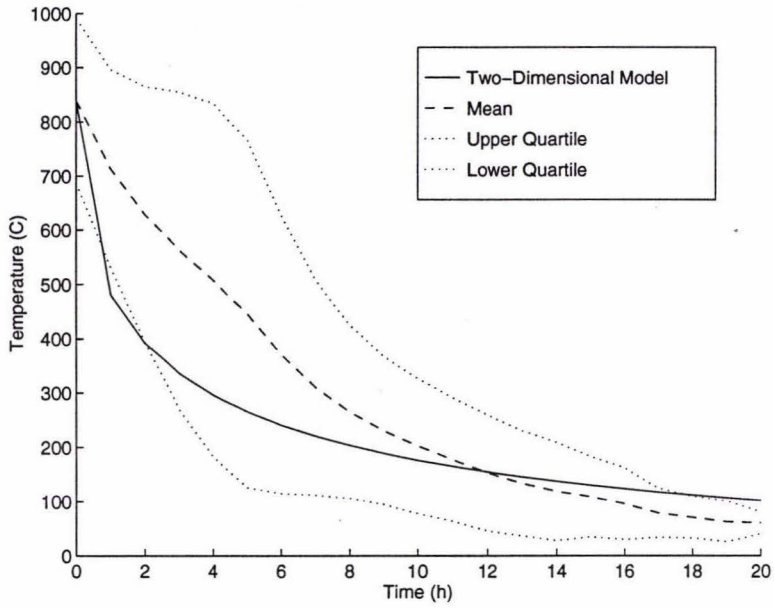

Figure 7.6: Temperature of point in carbon for clean anode without steel yoke

7.2 Variable Physical and Thermal Properties

As in the one-dimensional case, the thermal and physical properties may vary with position in the anode. In the one-dimensional case this meant a layer of bath could be included in the model and in the two-dimensional case this can also be done.

The anode assembly (shown in Figure 1.3) from which the anode hangs has been approximated in two dimensions by the shape in Figure 7.7. The steel yoke consists of four stubs which have a depth of $100mm$ into the carbon. Since steel has a high thermal conductivity compared to carbon (see values on Page 65) it would be expected that these stubs would help cool the centre of the butt more quickly. These stubs and the entire assembly can be included in the two-dimensional model. In the model the geometry of the assembly has been simplified to be as shown in Figure 7.7, although it would be possible to have a more detailed geometry.

The shape of the carbon shown in Figure 1.2 is not square as in Figure 7.7, but has rounded ends. Similarly the shape of the bath is highly irregular. They have been approximated by rectangular-shaped areas for simplicity.

Modelling of the boundaries between materials is an important consideration as the nodes are located along the boundaries of the materials. If the method of averaging

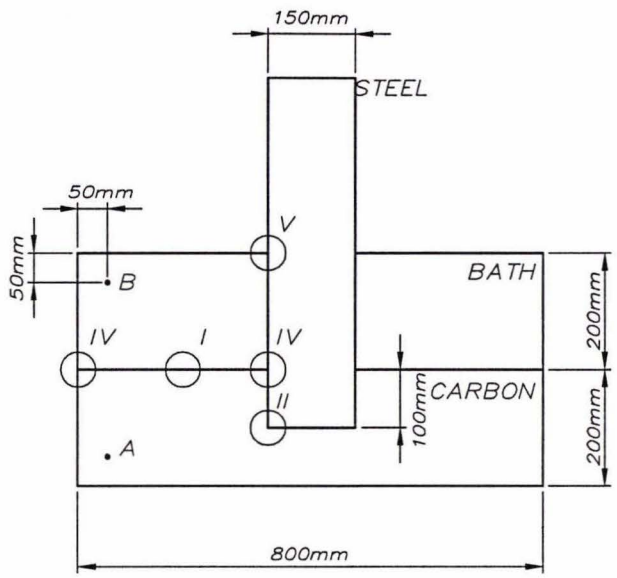

Figure 7.7: Two-Dimensional approximation of butt

the thermal properties between two nodes as in the one-dimensional case is used, the boundary is shifted to half way between the where the boundary actually is and the adjacent node. An alternative method is to set up the equations at each node so that the correct thermal properties from each direction are used.

7.2.1 Finite Difference Approximation

There are five types of interfaces between materials in the anode. These are shown in Figure 7.7. Three of these are internal nodes, one is a surface node and one is an internal corner node.

Internal Node

The finite difference equation for the internal nodes can be written as

$$T_{i,j}^{m+1} = \delta(a_{i,j}T_{i-1,j}^{m} + b_{i,j}T_{i,j-1}^{m} + c_{i,j}T_{i,j}^{m} + d_{i,j}T_{i+1,j}^{m} + e_{i,j}T_{i,j+1}^{m}) + T_{i,j}^{m}$$

where $\delta = \Delta t/(\Delta x)^2$. The coefficients $a_{i,j}$, $b_{i,j}$, $d_{i,j}$ and $e_{i,j}$ are found by taking the average of the diffusivities between each node and the node $T_{i,j}$. The coefficient $c_{i,j}$ is the sum of the other four coefficients.

For the three internal nodes on material interfaces shown in Figure 1.3 the coefficients are: **Interface Type I**: The coefficients are

$$a_{i,j} = \frac{\alpha_c + \alpha_b}{2}$$

$$b_{i,j} = \alpha_c$$

$$c_{i,j} = 2\alpha_b + 2\alpha_c$$

$$d_{i,j} = \frac{\alpha_c + \alpha_b}{2}$$

$$e_{i,j} = \alpha_b$$

Interface Type II: The coefficients are

$$a_{i,j} = \alpha_c$$

$$b_{i,j} = \alpha_c$$

$$c_{i,j} = \alpha_s + 3\alpha_c$$

$$d_{i,j} = \frac{\alpha_c + \alpha_s}{2}$$

$$e_{i,j} = \frac{\alpha_c + \alpha_s}{2}$$

Interface Type III: The coefficients are

$$a_{i,j} = \frac{\alpha_c + \alpha_b}{2}$$

$$b_{i,j} = \frac{\alpha_c + \alpha_s}{2}$$

$$c_{i,j} = \alpha_b + \alpha_c + 2\alpha_s$$

$$d_{i,j} = \alpha_s$$

$$e_{i,j} = \frac{\alpha_b + \alpha_s}{2}$$

Surface Node

For the surface material interface the finite difference equation is

$$T_{i,j}^{m+1} = \delta \left(b_{i,j} T_{i,j-1}^{m} - c_{i,j} T_{i,j}^{m} + 2 d_{i,j} T_{i+1,j} + e_{i,j} T_{i,j+1}^{m} + 2 \frac{q'' \Delta x}{k} \right) + T_{i,j}^{m} \qquad (7.9)$$

Interface Type IV: The coefficients are

$$b_{i,j} = \frac{\alpha_c}{2}$$

$$c_{i,j} = \alpha_c + \alpha_b$$

$$d_{i,j} = \frac{\alpha_c + \alpha_b}{2}$$

$$e_{i,j} = \frac{\alpha_b}{2}$$

Internal Corner Node

For the internal corner node

$$T_{i,j}^{m+1} = \frac{2}{3} \delta \left(2 a_{i,j} T_{i-1,j}^{m} + 2 b_{i,j} T_{i,j-1}^{m} - 4 c_{i,j} T_{i,j}^{m} + d_{i,j} T_{i+1,j} + e_{i,j} T_{i,j+1}^{m} + 2 \frac{q'' \Delta x}{k} \right) + T_{i,j}^{m} \qquad (7.10)$$

Interface Type V: The coefficients are

$$a_{i,j} = \frac{\alpha_b}{2}$$

$$b_{i,j} = \frac{\alpha_b + \alpha_s}{2}$$

$$c_{i,j} = \alpha_b + 2\alpha_s$$

$$d_{i,j} = \frac{\alpha_s}{2}$$

$$e_{i,j} = \alpha_s$$

If these equations are used, a large range of geometric layouts can be modelled. For example the yoke assembly can be included or removed from the model. Some of these different setups are shown in the next section.

7.2.2 Two-dimensional Simulations

The solution will be found for three different cases in addition to the previous configuration. They are: an anode consisting of carbon without a bath cover but steel rods from the yoke enter the top of the anode, an anode with a bath cover without the steel rods, and an anode with a bath cover and the steel rods. The same thermal properties as in the one-dimensional case were used. Each of the materials had the following properties: Carbon:

Emissivity = 0.4	Thermal Conductivity = $k_c = 5\,W/mK$
Density = $\rho_c = 1580\,kg/m^3$	Heat Capacity = $c_c = 1670\,J/kgK$

Bath:

Emissivity = 0.4	Thermal Conductivity = $k_b = 0.4\,W/mK$
Density = $\rho_b = 2050\,kg/m^3$	Heat Capacity = $c_b = 2287\,J/kgK$

Steel:

Emissivity = 0.4	Thermal Conductivity = $k_s = 36\,W/mK$
Density = $\rho_s = 7753\,kg/m^3$	Heat Capacity = $c_s = 486\,J/kgK$

The thermal properties for carbon and bath are from [5]. The thermal properties for steel were given in [1].

Clean Anode with Yoke

An anode with a length of $0.8\,m$ and a thickness of $0.2\,m$ with a steel rod $0.15\,m$ wide and $0.4\,m$ long inserted into the top of the anode, as shown in Figure 7.7, was modelled. The steel rod represented the assembly yoke from which the anode hangs.

The temperature profiles within the anode can be seen for four different times in Figure 7.8. It can be seen that the rod cools down quickly compared to the rest of the anode. The rod causes the centre of the anode to cool more quickly. Comparison of Figure 7.9 and Figure 7.6 shows that the yoke has little effect on the temperature at a point near the surface.

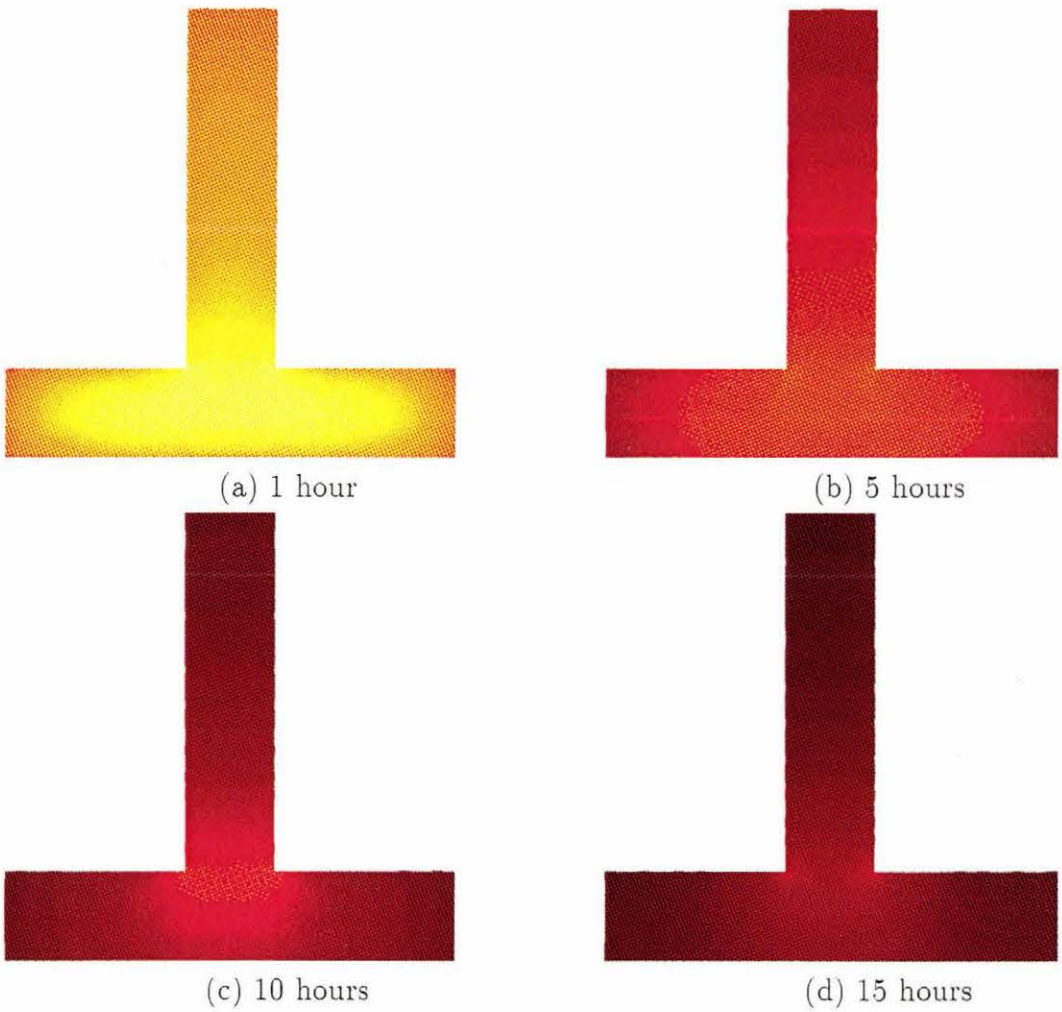

(a) 1 hour (b) 5 hours

(c) 10 hours (d) 15 hours

Figure 7.8: Temperature profile for a clean anode with steel yoke

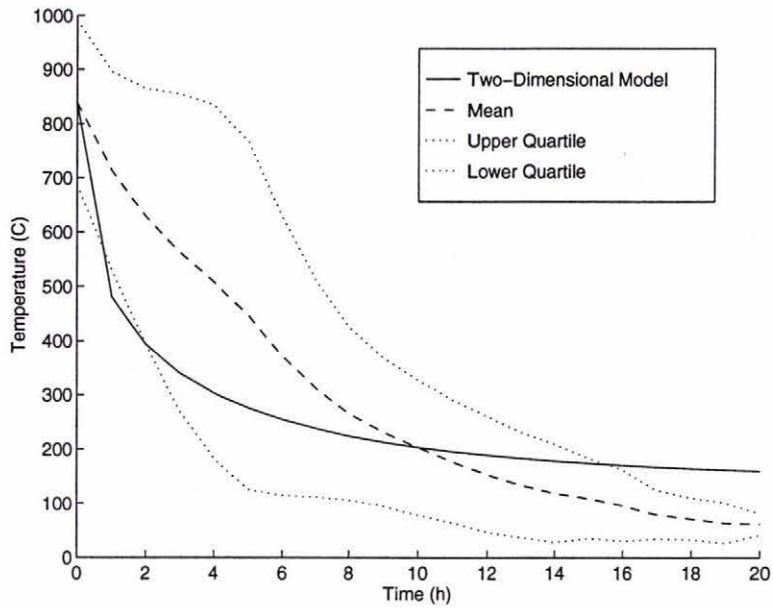

Figure 7.9: Temperature of point in carbon for a clean anode with a steel yoke

Dirty Anode without Yoke

The carbon was taken to be $0.2\,m$ thick with a layer of bath on top $0.2\,m$ thick, the anode was $0.8\,m$ wide. The temperature profile at four different times are shown in Figure 7.10. It can be seen that the bath stays a lot hotter than the carbon. It also has the effect of slowing the cooling of the carbon.

Figure 7.11 shows that the temperature the model predicts initially drops below the temperature in the experimental data. As the temperature decreases the model starts to get higher values for the temperature than the data. The lower initial temperatures could be due to the fact that this model assumes the anodes are in isolation whereas in reality they are affected by surrounding anodes. It would be expected that they would keep each other hotter. As the temperature drops heat loss due to convection could also be important; this could explain the higher temperatures from the model for later times.

The temperature change with time of a point in the bath is shown in Figure 7.12, it can be seen that the bath does not cool as quickly as the carbon.

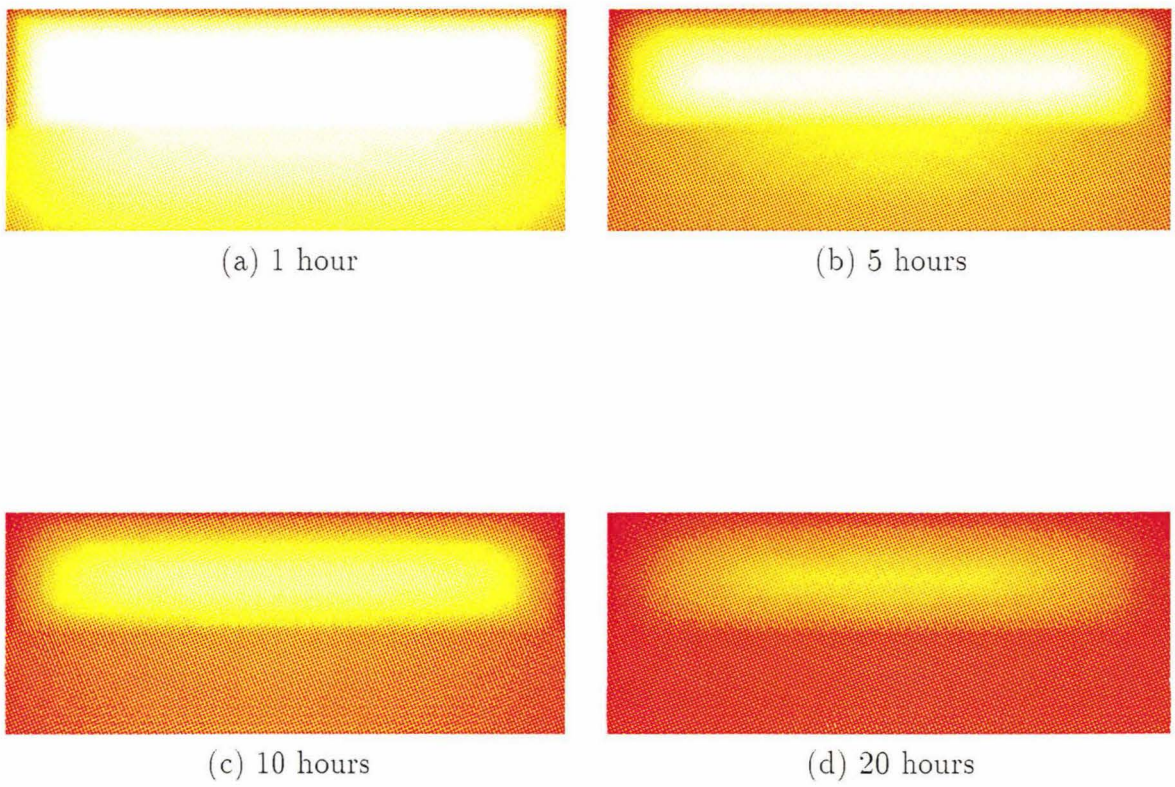

(a) 1 hour

(b) 5 hours

(c) 10 hours

(d) 20 hours

Figure 7.10: Temperature profile in carbon for a dirty anode without steel yoke

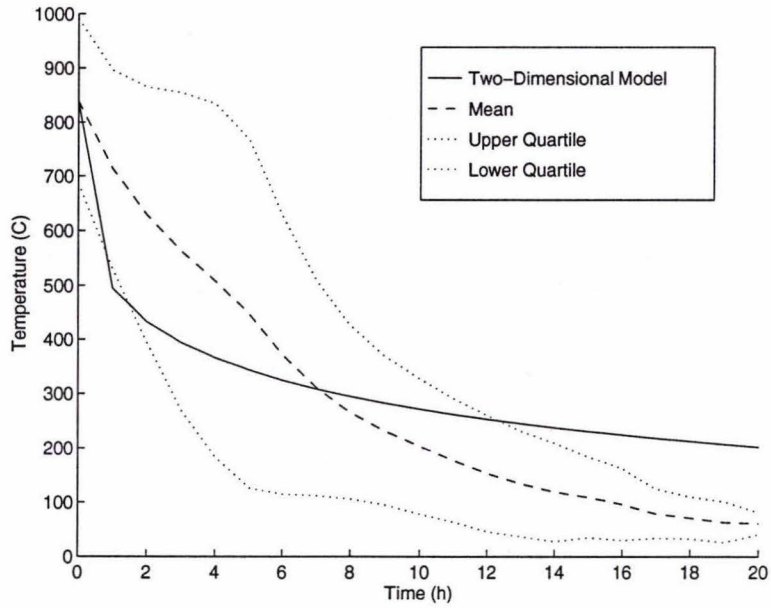

Figure 7.11: Temperature of point in carbon for a dirty anode without steel yoke

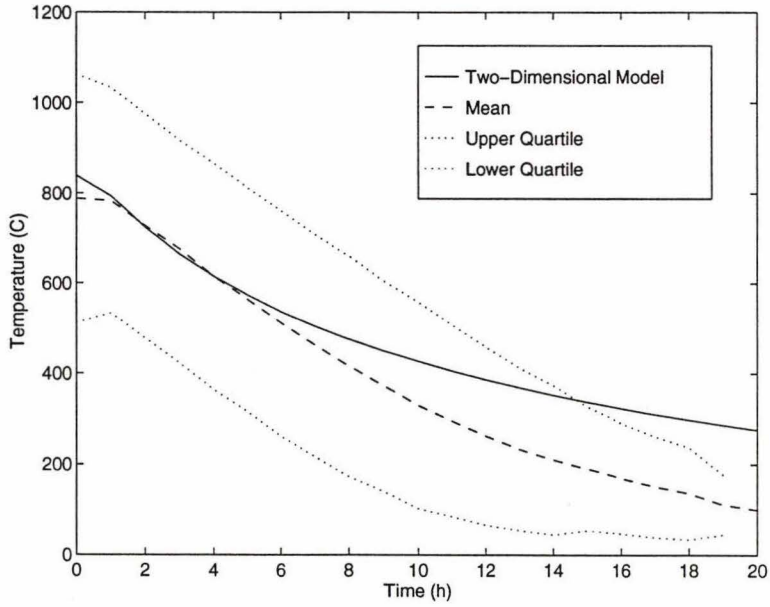

Figure 7.12: Temperature of point in bath for a dirty anode without steel yoke

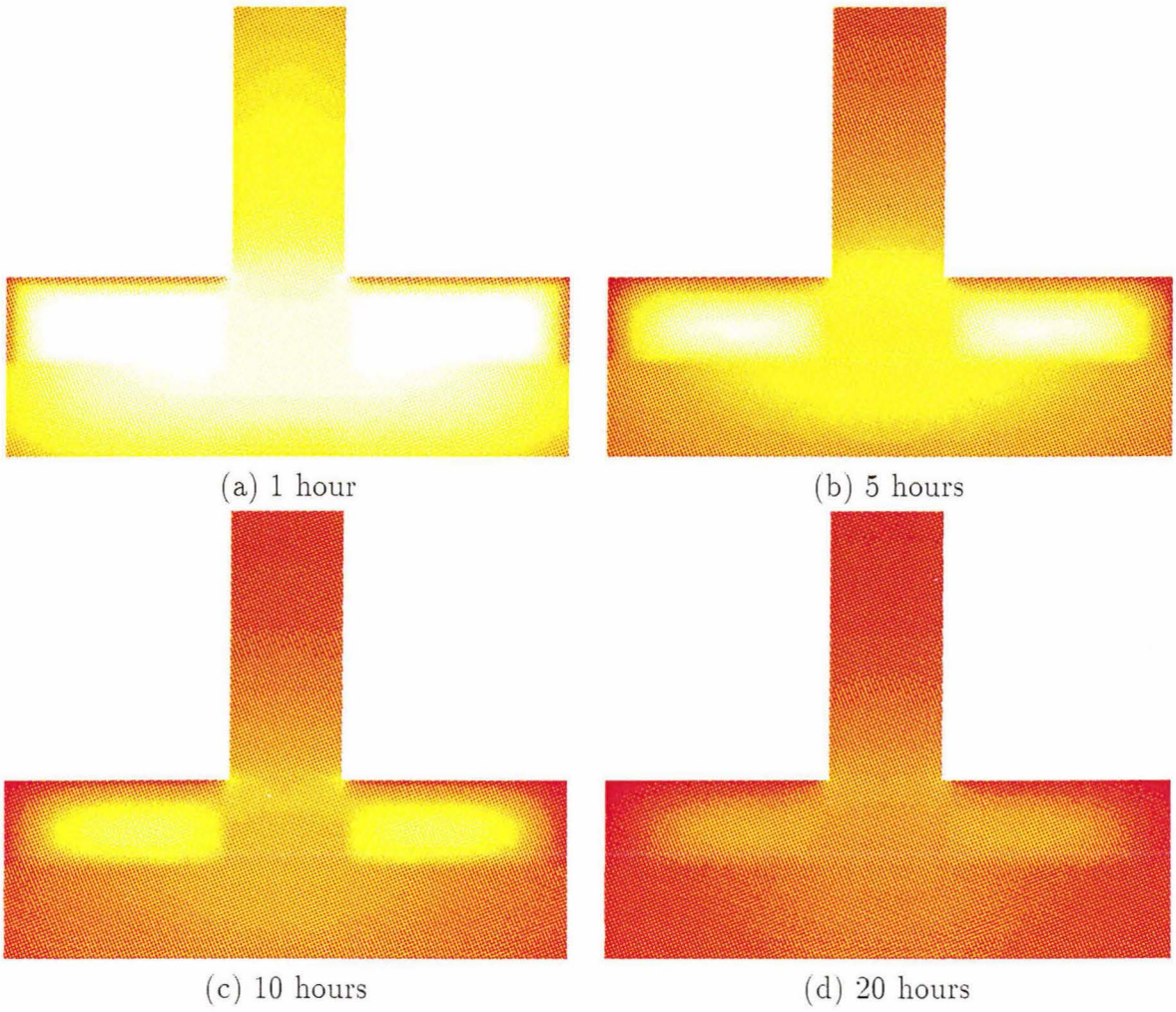

(a) 1 hour (b) 5 hours

(c) 10 hours (d) 20 hours

Figure 7.13: Temperature profile for a dirty anode with steel yoke

Dirty Anode with Yoke

The solution was found for an anode with a bath cover of $0.2\,m$ and a yoke with rods entering the carbon from above to a depth of $0.05\,m$ as shown in Figure 7.7. The temperature profile for four different times is shown in Figure 7.13.

The temperature of a point a depth of $0.05\,m$ into the top of the bath and $0.05\,m$ in from the edge of the anode is shown in Figure 7.15. It can be seen from the temperature profiles shown in Figure 7.13 show that the carbon cools down more quickly than the bath. The effect of the steel rods can also be seen; the centre of the anode cools down more quickly as heat is conducted up the rod.

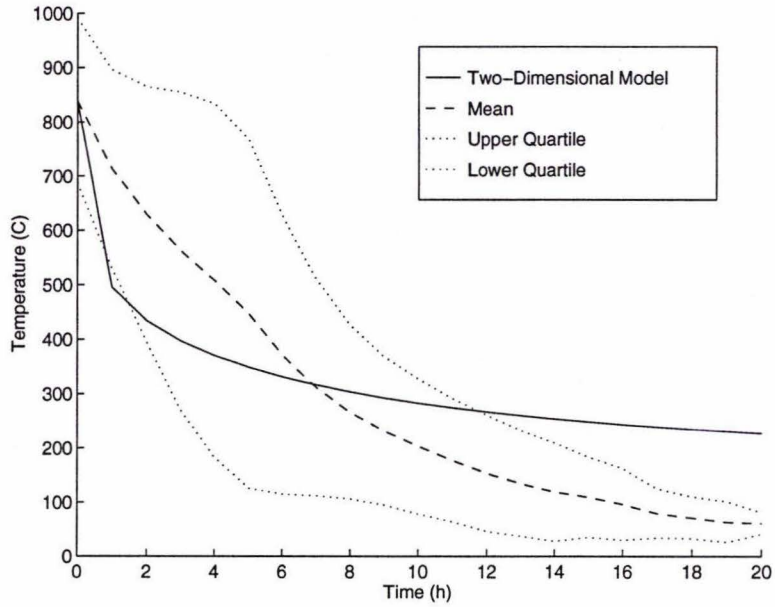

Figure 7.14: Temperature of point in carbon for a dirty anode with steel yoke

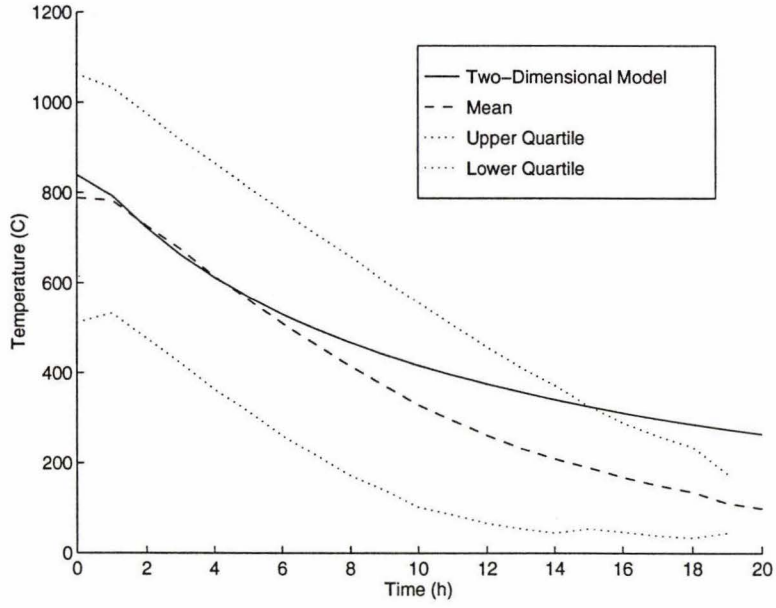

Figure 7.15: Temperature of point in bath for a dirty anode with steel yoke

7.3 Summary

The two-dimensional model meant that it was possible to include more geometry into the problem than the one-dimensional case. A bath cover can be included into the model as can the steel rods which go through the bath and into the carbon.

It was shown that the bath cover held its heat and the temperature of the carbon was hotter as a result. The steel rods had little effect on the point near the surface of the anode. However it can be seen that the internal temperatures around the rod were cooler due to heat being conducted up the rods.

The difference in the experimental data and the model is thought to be due to the effect of surrounding anodes. As the temperature drops the heat loss due to convection may be significant.

In the next chapter the three-dimensional finite difference equations will be found for a clean and a dirty anode.

Chapter 8

Three-Dimensional Numerical Solution

The finite difference equations for heat flows in three dimensions are found similarly to the one- and two-dimensional cases. In three dimensions there are eight different cases to be considered; these are developed in Section 8.1. The three-dimensional solution is initially found for a clean butt and this is then compared to that for a dirty butt.

8.1 Finite Difference Equations

There are eight different finite difference equations. These are not as obvious as in the one- and two-dimensional cases.

Internal Node

For each internal node (see Figure 8.1) the heat transfer from each of the surrounding nodes is proportional to the respective temperature gradients. If the distance between each node is small enough the heat transfer from the node $(i-1, j, k)$ to (i, j, k) can be approximated by

$$q_1 = k_x \frac{T_{i-1,j,k} - T_{i,j,k}}{\Delta x} \Delta y \Delta z$$

The heat transfer from the other surrounding node can be found similarly.

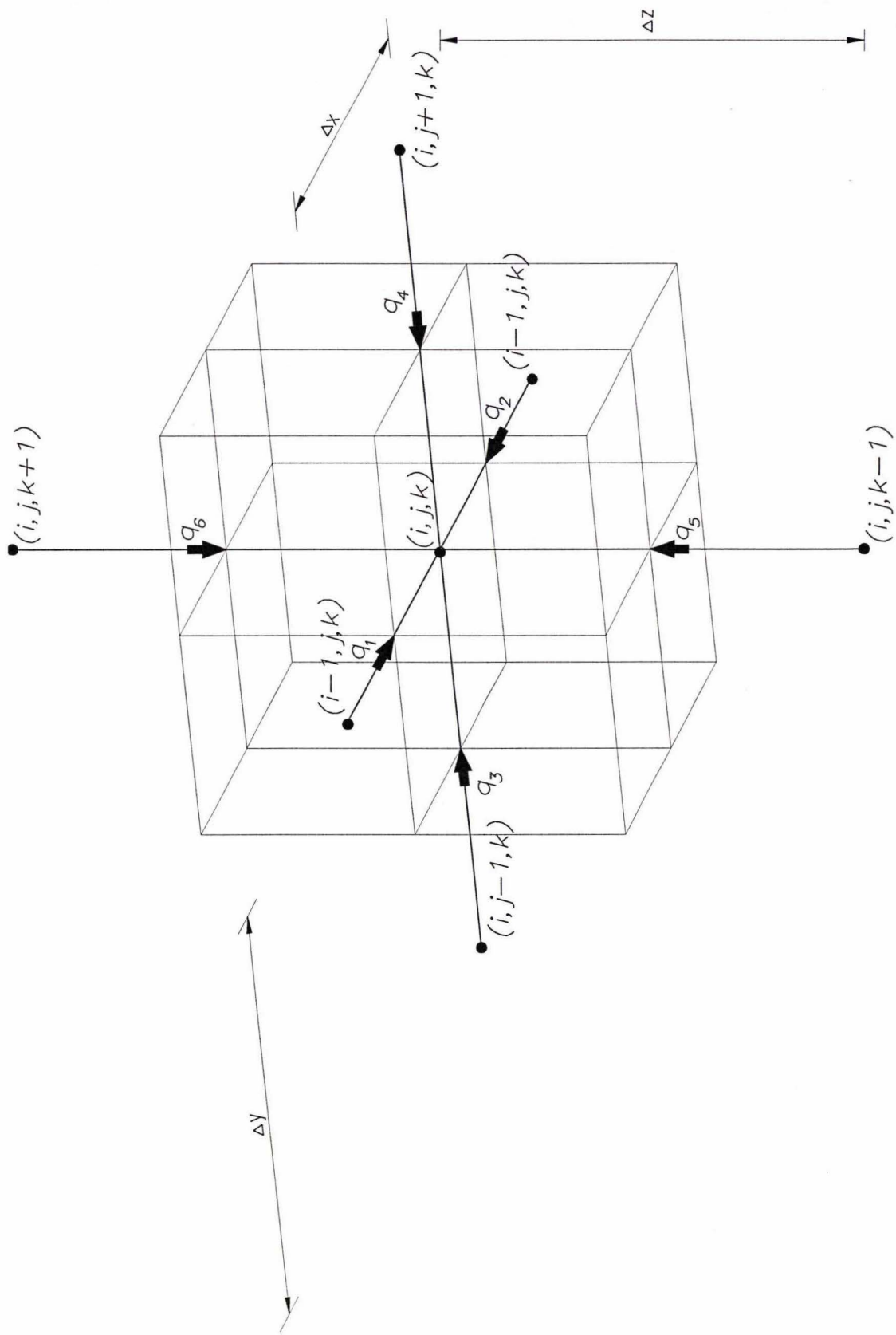

Figure 8.1: Three-dimensional internal node

This means the heat balance equation can be written as

$$\rho C \Delta x \Delta y \Delta z \frac{\partial T_{i,j,k}}{\partial t} =$$
$$k_x \frac{T_{i-1,j,k} - T_{i,j,k}}{\Delta x} \Delta y \Delta z + k_x \frac{T_{i+1,j,k} - T_{i,j,k}}{\Delta x} \Delta y \Delta z + k_y \frac{T_{i,j-1,k} - T_{i,j,k}}{\Delta y} \Delta x \Delta z$$
$$+ k_y \frac{T_{i,j+1,k} - T_{i,j,k}}{\Delta y} \Delta x \Delta z + k_z \frac{T_{i,j,k-1} - T_{i,j,k}}{\Delta z} \Delta x \Delta y + k_z \frac{T_{i,j,k+1} - T_{i,j,k}}{\Delta z} \Delta x \Delta y$$

If $k_x = k_y = k_z$ and $\Delta x = \Delta y = \Delta z$ this can be written as

$$\rho C \frac{\partial T_{i,j,k}}{\partial t} = k_x \left(\frac{T_{i-1,j,k} - T_{i,j,k}}{(\Delta x)^2} + \frac{T_{i+1,j,k} - T_{i,j,k}}{(\Delta x)^2} + \frac{T_{i,j-1,k} - T_{i,j,k}}{(\Delta x)^2} + \right.$$
$$\left. \frac{T_{i,j+1,k} - T_{i,j,k}}{(\Delta x)^2} + \frac{T_{i,j,k-1} - T_{i,j,k}}{(\Delta x)^2} + \frac{T_{i,j,k+1} - T_{i,j,k}}{(\Delta x)^2} \right)$$

If $\alpha = k_x / \rho C$ this becomes

$$\frac{\partial T_{i,j,k}}{\partial t} = \frac{\alpha}{(\Delta x)^2} \left(T_{i-1,j,k} + T_{i,j-1,k} + T_{i,j,k-1} - 6T_{i,j,k} + T_{i+1,j,k} + T_{i,j+1,k} + T_{i,j,k+1} \right)$$

If the derivative with respect to time is written as a forward finite difference approximation this becomes

$$T^{m+1}_{i,j,k} = Fo \left(T^m_{i-1,j,k} + T^m_{i,j-1,k} + T^m_{i,j,k-1} - 6T^m_{i,j,k} + T^m_{i+1,j,k} + T^m_{i,j+1,k} + T^m_{i,j,k+1} \right) + T^m_{i,j,k} \tag{8.1}$$

where $Fo = \alpha \Delta t / (\Delta x)^2$ is the Fourier number.

Internal Corner Node

An internal corner node is shown in Figure 8.2. The volume is $7/8 \Delta x \Delta y \Delta z$. The heat transfer from the surrounding internal nodes is the same as for the internal node:

$$q_1 = k_x \frac{T_{i-1,j,k} - T_{i,j,k}}{\Delta x} \Delta y \Delta z$$

but the heat transfer from the surface nodes is

$$q_2 = \frac{3}{4} k_x \frac{T_{i+1,j,k} - T_{i,j,k}}{\Delta x} \Delta y \Delta z + \frac{1}{4} q''_x \Delta y \Delta z$$

In this case there are three adjacent nodes which are internal and three which are on the surface. This gives the following equation:

$$\frac{7}{8} \rho C \Delta x \Delta y \Delta z \frac{\partial T_{i,j,k}}{\partial t} =$$

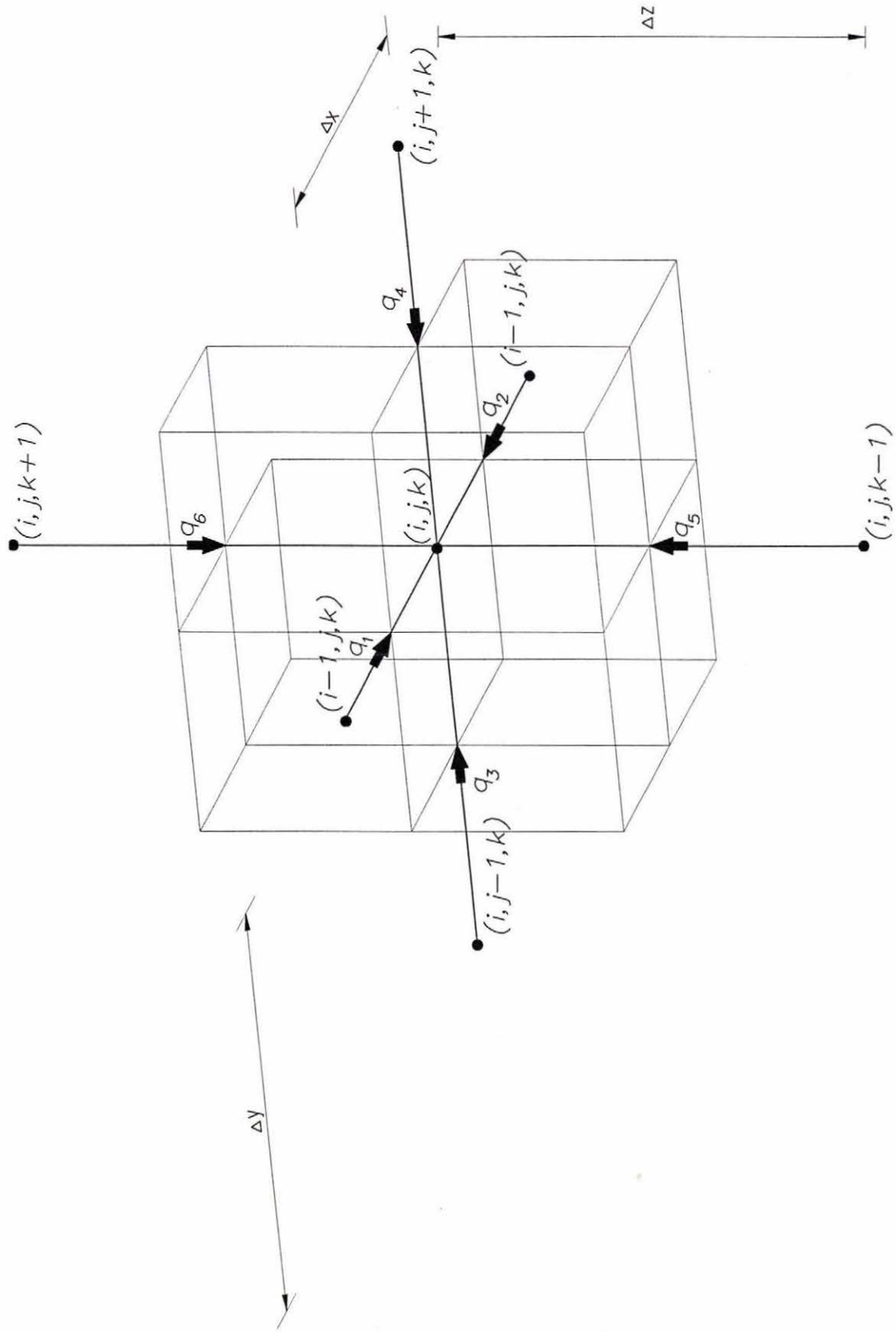

Figure 8.2: Three-dimensional internal corner node

$$k_x \frac{T_{i-1,j,k} - T_{i,j,k}}{\Delta x} \Delta y \Delta z + \frac{3}{4} k_x \frac{T_{i+1,j,k} - T_{i,j,k}}{\Delta x} \Delta y \Delta z + \frac{1}{4} q''_x \Delta y \Delta z$$
$$+ k_y \frac{T_{i,j-1,k} - T_{i,j,k}}{\Delta y} \Delta x \Delta z + \frac{3}{4} k_y \frac{T_{i,j+1,k} - T_{i,j,k}}{\Delta y} \Delta x \Delta z + \frac{1}{4} q''_y \Delta x \Delta z$$
$$+ k_z \frac{T_{i,j,k-1} - T_{i,j,k}}{\Delta z} \Delta x \Delta y + \frac{3}{4} k_z \frac{T_{i,j,k+1} - T_{i,j,k}}{\Delta z} \Delta x \Delta y + \frac{1}{4} q''_z \Delta x \Delta y$$

If $k_x = k_y = k_z$ and $\Delta x = \Delta y = \Delta z$ this can be written as

$$\frac{7}{8} \rho C \frac{\partial T_{i,j,k}}{\partial t} = k_x \left(\frac{T_{i-1,j,k} - T_{i,j,k}}{(\Delta x)^2} + \frac{3(T_{i+1,j,k} - T_{i,j,k})}{4(\Delta x)^2} + \frac{T_{i,j-1,k} - T_{i,j,k}}{(\Delta x)^2} + \right.$$
$$\left. \frac{3(T_{i,j+1,k} - T_{i,j,k})}{4(\Delta x)^2} + \frac{T_{i,j,k-1} - T_{i,j,k}}{(\Delta x)^2} + \frac{3(T_{i,j,k+1} - T_{i,j,k})}{4(\Delta x)^2} \right) + \frac{3q''}{4\Delta x}$$

If $\alpha = k_x / \rho C$ this becomes

$$\frac{\partial T_{i,j,k}}{\partial t} = \frac{2\alpha}{7(\Delta x)^2} (4T_{i-1,j,k} + 4T_{i,j-1,k} + 4T_{i,j,k-1} - 21T_{i,j,k} + 3T_{i+1,j,k} + 3T_{i,j+1,k} +$$
$$3T_{i,j,k+1} + 3\frac{q''\Delta x}{k_x} \Big)$$

If the derivative with respect to time is written as a forward finite difference approximation this becomes

$$T^{m+1}_{i,j,k} = \frac{2}{7} Fo \left(4T^m_{i-1,j,k} + 4T^m_{i,j-1,k} + 4T^m_{i,j,k-1} - 21T^m_{i,j,k} + 3T^m_{i+1,j,k} + 3T^m_{i,j+1,k} \right.$$
$$\left. + 3T^m_{i,j,k+1} + 3\frac{q''\Delta x}{k_x} \right) + T^m_{i,j,k} \quad (8.2)$$

where the Fourier number is $Fo = \alpha \Delta t / (\Delta x)^2$.

Internal Edge Node

An internal edge node is shown in Figure 8.3. The volume is $3/4 \Delta x \Delta y \Delta z$. The heat transfer to the two adjacent internal nodes is the same as for the internal node

$$q_1 = k_x \frac{T_{i-1,j,k} - T_{i,j,k}}{\Delta x} \Delta y \Delta z$$

but the heat transfer to the two adjacent surface nodes is

$$q_2 = \frac{1}{2} k_x \frac{T_{i+1,j,k} - T_{i,j,k}}{\Delta x} \Delta y \Delta z + \frac{1}{2} q''_x \Delta y \Delta z$$

and the heat transfer to the two adjacent edge nodes is

$$q_3 = \frac{3}{4} k_y \frac{T_{i,j-1,k} - T_{i,j,k}}{\Delta y} \Delta x \Delta z$$

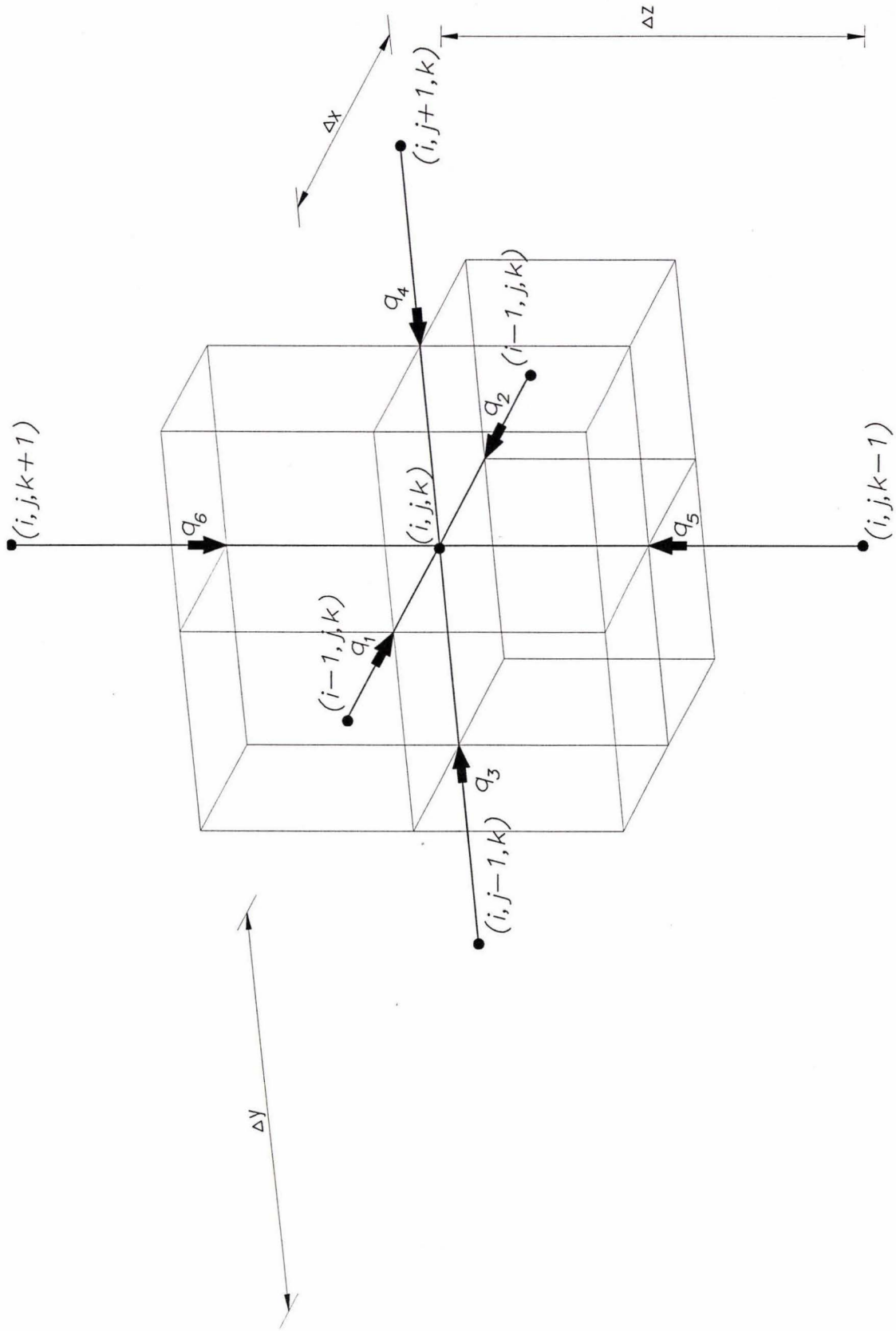

Figure 8.3: Three-dimensional internal edge node

In this case there are two adjacent nodes which are internal and two which are on the surface and two on edges. This gives the following equation

$$\frac{3}{4}\rho C\Delta x\Delta y\Delta z\frac{\partial T_{i,j,k}}{\partial t} =$$
$$k_x\frac{T_{i-1,j,k}-T_{i,j,k}}{\Delta x}\Delta y\Delta z+\frac{1}{2}k_x\frac{T_{i+1,j,k}-T_{i,j,k}}{\Delta x}\Delta y\Delta z+\frac{1}{2}q''_x\Delta y\Delta z$$
$$+\frac{3}{4}k_y\frac{T_{i,j-1,k}-T_{i,j,k}}{\Delta y}\Delta x\Delta z+\frac{3}{4}k_y\frac{T_{i,j+1,k}-T_{i,j,k}}{\Delta y}\Delta x\Delta z$$
$$+k_z\frac{T_{i,j,k-1}-T_{i,j,k}}{\Delta z}\Delta x\Delta y+\frac{1}{2}k_z\frac{T_{i,j,k+1}-T_{i,j,k}}{\Delta z}\Delta x\Delta y+\frac{1}{2}q''_z\Delta x\Delta y$$

If $k_x = k_y = k_z$ and $\Delta x = \Delta y = \Delta z$ this can be written as

$$\frac{3}{4}\rho C\frac{\partial T_{i,j,k}}{\partial t} = k_x\left(\frac{(T_{i-1,j,k}-T_{i,j,k})}{(\Delta x)^2}+\frac{(T_{i+1,j,k}-T_{i,j,k})}{2(\Delta x)^2}+\frac{3T_{i,j-1,k}-T_{i,j,k}}{4(\Delta x)^2}+\right.$$
$$\left.\frac{3T_{i,j+1,k}-T_{i,j,k}}{4(\Delta x)^2}+\frac{T_{i,j,k-1}-T_{i,j,k}}{(\Delta x)^2}+\frac{T_{i,j,k+1}-T_{i,j,k}}{2(\Delta x)^2}\right)+\frac{q''}{\Delta x}$$

If $\alpha = k_x/\rho C$ this becomes

$$\frac{\partial T_{i,j,k}}{\partial t} = \frac{\alpha}{3(\Delta x)^2}\left(3T_{i-1,j,k}+4T_{i,j-1,k}+4T_{i,j,k-1}-18T_{i,j,k}+3T_{i+1,j,k}+2T_{i,j+1,k}+\right.$$
$$\left.2T_{i,j,k+1}+4\frac{q''\Delta x}{k_x}\right)$$

If the derivative with respect to time is written as a foward finite difference approximation this becomes

$$T^{m+1}_{i,j,k} = \frac{1}{3}Fo\left(4T^m_{i-1,j,k}+3T^m_{i,j-1,k}+4T^m_{i,j,k-1}-18T^m_{i,j,k}+2T^m_{i+1,j,k}+3T^m_{i,j+1,k}\right.$$
$$\left.+2T^m_{i,j,k+1}+4\frac{q''\Delta x}{k_x}\right)+T^m_{i,j,k} \quad (8.3)$$

where the Fourier number is $Fo = \alpha\Delta t/(\Delta x)^2$.

External Corner/Surface Node

An external corner/surface node is shown in Figure 8.4. The volume is $5/8\Delta x\Delta y\Delta z$. The heat transfer to the adjacent internal node is the same as for the internal node:

$$q_5 = k_z\frac{T_{i,j,k-1}-T_{i,j,k}}{\Delta z}\Delta x\Delta y$$

but the heat transfer to the two surface nodes is

$$q_2 = \frac{1}{2}k_x\frac{T_{i+1,j,k}-T_{i,j,k}}{\Delta x}\Delta y\Delta z+\frac{1}{4}q''_x\Delta y\Delta z$$

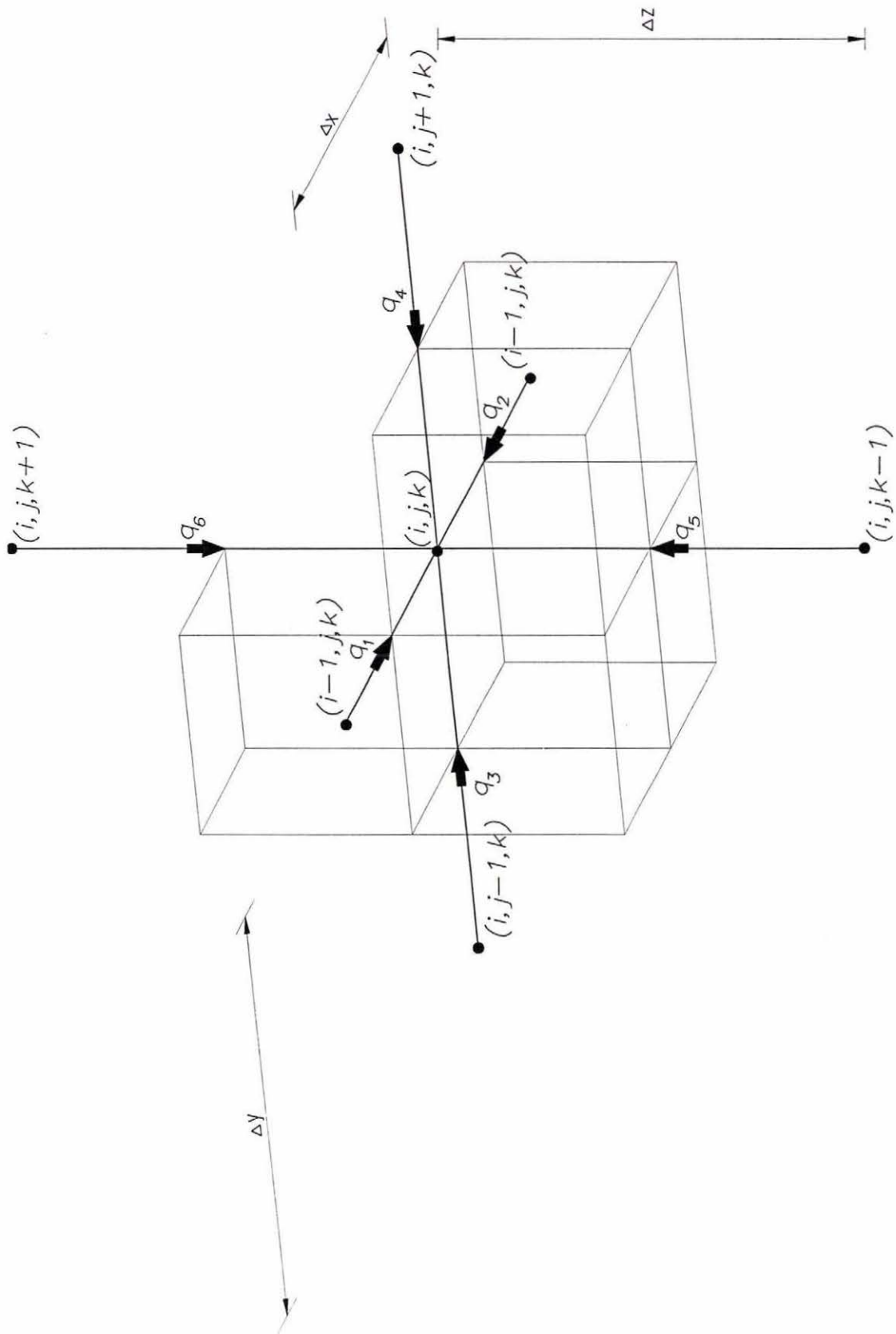

Figure 8.4: Three-dimensional external corner/surface node

and the heat transfer to the two internal edge nodes is

$$q_1 = \frac{3}{4}k_x\frac{T_{i-1,j,k} - T_{i,j,k}}{\Delta x}\Delta y\Delta z$$

The heat transfer to the edge node is

$$q_6 = \frac{1}{4}k_z\frac{T_{i,j,k+1} - T_{i,j,k}}{\Delta z}\Delta x\Delta y + \frac{3}{4}q''_z\Delta x\Delta y$$

In this case there is one adjacent node which is internal, two which are on the surface, two on internal edges and one on an external edge. This gives the following equation

$$\begin{aligned}\frac{5}{8}\rho C\Delta x\Delta y\Delta z\frac{\partial T_{i,j,k}}{\partial t} = \\ \frac{3}{4}k_x\frac{T_{i-1,j,k} - T_{i,j,k}}{\Delta x}\Delta y\Delta z + \frac{1}{2}k_x\frac{T_{i+1,j,k} - T_{i,j,k}}{\Delta x}\Delta y\Delta z + \frac{1}{4}q''_x\Delta y\Delta z \\ + \frac{3}{4}k_y\frac{T_{i,j-1,k} - T_{i,j,k}}{\Delta y}\Delta x\Delta z + \frac{1}{2}k_y\frac{T_{i,j+1,k} - T_{i,j,k}}{\Delta y}\Delta x\Delta z + \frac{1}{4}q''_y\Delta x\Delta z \\ + k_z\frac{T_{i,j,k-1} - T_{i,j,k}}{\Delta z}\Delta x\Delta y + \frac{1}{4}k_z\frac{T_{i,j,k+1} - T_{i,j,k}}{\Delta z}\Delta x\Delta y + \frac{3}{4}q''_z\Delta x\Delta y\end{aligned}$$

If $k_x = k_y = k_z$ and $\Delta x = \Delta y = \Delta z$ this can be written as

$$\begin{aligned}\frac{5}{8}\rho C\frac{\partial T_{i,j,k}}{\partial t} = k_x\left(\frac{3(T_{i-1,j,k} - T_{i,j,k})}{4(\Delta x)^2} + \frac{(T_{i+1,j,k} - T_{i,j,k})}{2(\Delta x)^2} + \frac{3T_{i,j-1,k} - T_{i,j,k}}{4(\Delta x)^2} + \right. \\ \left. \frac{T_{i,j+1,k} - T_{i,j,k}}{2(\Delta x)^2} + \frac{T_{i,j,k-1} - T_{i,j,k}}{(\Delta x)^2} + \frac{T_{i,j,k+1} - T_{i,j,k}}{4(\Delta x)^2}\right) + \frac{5q''}{4\Delta x}\end{aligned}$$

If $\alpha = k_x/\rho C$ this becomes

$$\begin{aligned}\frac{\partial T_{i,j,k}}{\partial t} = \frac{2\alpha}{5(\Delta x)^2}(3T_{i-1,j,k} + 3T_{i,j-1,k} + 4T_{i,j,k-1} - 15T_{i,j,k} + 2T_{i+1,j,k} + 2T_{i,j+1,k} + \\ T_{i,j,k+1} + \frac{q''\Delta x}{k_x}\Big)\end{aligned}$$

If the derivative with respect to time is written as a forward finite difference approximation this becomes

$$\begin{aligned}T^{m+1}_{i,j,k} = \frac{2}{5}Fo\left(3T^m_{i-1,j,k} + 3T^m_{i,j-1,k} + 4T^m_{i,j,k-1} - 15T^m_{i,j,k} + 2T^m_{i+1,j,k} + 2T^m_{i,j+1,k}\right. \\ \left. + T^m_{i,j,k+1} + \frac{q''\Delta x}{k_x}\right) + T^m_{i,j,k} \quad (8.4)\end{aligned}$$

where the Fourier number is $Fo = \alpha\Delta t/(\Delta x)^2$.

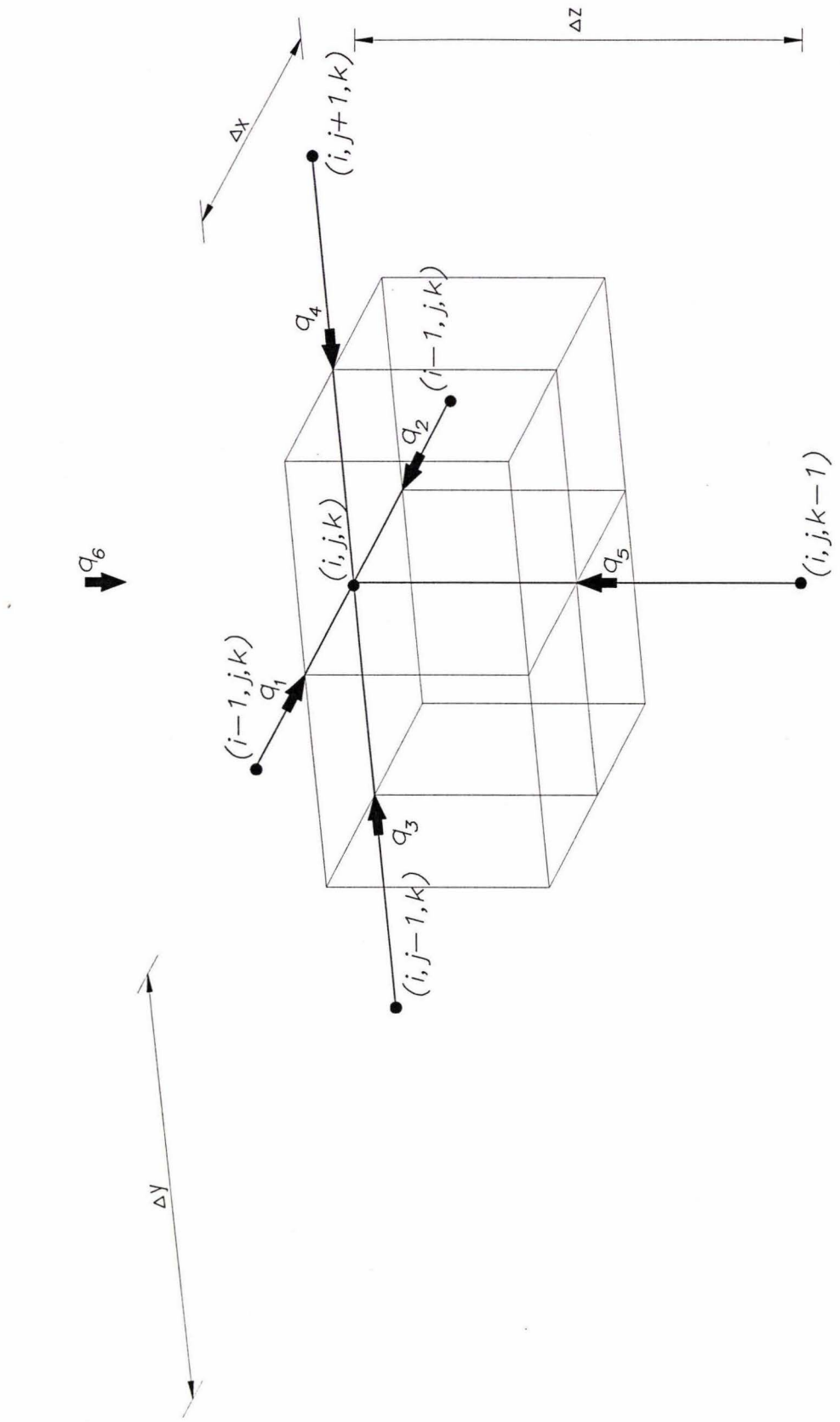

Figure 8.5: Three-dimensional surface node

Surface Node

A surface node is shown in Figure 8.5. The volume is $1/2\Delta x\Delta y\Delta z$. The heat transfer to the adjacent internal node is the same as for the internal node

$$q_5 = k_z \frac{T_{i,j,k-1} - T_{i,j,k}}{\Delta z}\Delta x\Delta y$$

but the heat transfer to the four surface nodes is

$$q_1 = \frac{1}{2}k_x \frac{T_{i+1,j,k} - T_{i,j,k}}{\Delta x}\Delta y\Delta z +$$

The heat transfer to the imaginary node out of the butt is

$$q_6 = q_z''\Delta x\Delta y$$

In this case there is one adjacent node which is internal, four which are on the surface and one out of the anode. This gives the following equation

$$\begin{aligned}\frac{1}{2}\rho C\Delta x\Delta y\Delta z\frac{\partial T_{i,j,k}}{\partial t} = \\ \frac{1}{2}k_x\frac{T_{i-1,j,k} - T_{i,j,k}}{\Delta x}\Delta y\Delta z + \frac{1}{2}k_x\frac{T_{i+1,j,k} - T_{i,j,k}}{\Delta x}\Delta y\Delta z \\ + \frac{1}{2}k_y\frac{T_{i,j-1,k} - T_{i,j,k}}{\Delta y}\Delta x\Delta z + \frac{1}{2}k_y\frac{T_{i,j+1,k} - T_{i,j,k}}{\Delta y}\Delta x\Delta z \\ + k_z\frac{T_{i,j,k-1} - T_{i,j,k}}{\Delta z}\Delta x\Delta y + q_z''\Delta x\Delta y\end{aligned}$$

If $k_x = k_y = k_z$ and $\Delta x = \Delta y = \Delta z$ this can be written as

$$\begin{aligned}\frac{1}{2}\rho C\frac{\partial T_{i,j,k}}{\partial t} = k_x\left(\frac{T_{i-1,j,k} - T_{i,j,k}}{2(\Delta x)^2} + \frac{(T_{i+1,j,k} - T_{i,j,k})}{2(\Delta x)^2} + \frac{T_{i,j-1,k} - T_{i,j,k}}{2(\Delta x)^2} + \right. \\ \left. \frac{T_{i,j+1,k} - T_{i,j,k}}{2(\Delta x)^2} + \frac{T_{i,j,k-1} - T_{i,j,k}}{(\Delta x)^2}\right) + \frac{q''}{\Delta x}\end{aligned}$$

If $\alpha = k_x/\rho C$ this becomes

$$\begin{aligned}\frac{\partial T_{i,j,k}}{\partial t} = \frac{\alpha}{(\Delta x)^2}\left(T_{i-1,j,k} + T_{i,j-1,k} + 2T_{i,j,k-1} - 6T_{i,j,k} + T_{i+1,j,k} + T_{i,j+1,k} + \right. \\ \left. 2\frac{q''\Delta x}{k_x}\right)\end{aligned}$$

If the derivative with respect to time is written as a forward finite difference approximation this becomes

$$\begin{aligned}T_{i,j,k}^{m+1} = Fo\left(T_{i-1,j,k}^m + T_{i,j-1,k}^m + 2T_{i,j,k-1}^m - 6T_{i,j,k}^m + T_{i+1,j,k}^m + T_{i,j+1,k}^m \right. \\ \left. + 2\frac{q''\Delta x}{k_x}\right) + T_{i,j,k}^m \qquad (8.5)\end{aligned}$$

where the Fourier number is $Fo = \alpha\Delta t/(\Delta x)^2$.

Internal Edge/Surface Node

An internal edge/surface node is shown in Figure 8.6. The volume is $3/8\Delta x\Delta y\Delta z$. The heat transfer to the adjacent edge node is the

$$q_5 = \frac{3}{4}k_z\frac{T_{i,j,k-1} - T_{i,j,k}}{\Delta z}\Delta x\Delta y$$

but the heat transfer to the two surface nodes is

$$q_1 = \frac{1}{2}k_x\frac{T_{i+1,j,k} - T_{i,j,k}}{\Delta x}\Delta y\Delta z$$

and the heat transfer to the two edge/surface nodes is

$$q_2 = \frac{1}{4}k_x\frac{T_{i+1,j,k} - T_{i,j,k}}{\Delta x}\Delta y\Delta z + \frac{1}{4}q''_x\Delta y\Delta z$$

The heat transfer to the imaginary node is

$$q_6 = \frac{3}{4}q''_x\Delta y\Delta z$$

In this case there are no adjacent nodes which is are internal, one which is an internal edge, two surface, two external edges and one which out of the anode. This gives the following equation

$$\begin{aligned}\frac{3}{8}\rho C\Delta x\Delta y\Delta z\frac{\partial T_{i,j,k}}{\partial t} = \\ \frac{1}{2}k_x\frac{T_{i-1,j,k} - T_{i,j,k}}{\Delta x}\Delta y\Delta z + \frac{1}{4}k_x\frac{T_{i+1,j,k} - T_{i,j,k}}{\Delta x}\Delta y\Delta z + \frac{1}{4}q''_x\Delta y\Delta z \\ + \frac{1}{2}k_y\frac{T_{i,j-1,k} - T_{i,j,k}}{\Delta y}\Delta x\Delta z + \frac{1}{4}k_y\frac{T_{i,j+1,k} - T_{i,j,k}}{\Delta y}\Delta x\Delta z + \frac{1}{4}q''_y\Delta x\Delta z \\ + \frac{3}{4}k_z\frac{T_{i,j,k-1} - T_{i,j,k}}{\Delta z}\Delta x\Delta y + \frac{3}{4}q''_z\Delta x\Delta y\end{aligned}$$

If $k_x = k_y = k_z$ and $\Delta x = \Delta y = \Delta z$ this can be written as

$$\begin{aligned}\frac{3}{8}\rho C\frac{\partial T_{i,j,k}}{\partial t} = k_x\left(\frac{T_{i-1,j,k} - T_{i,j,k}}{2(\Delta x)^2} + \frac{(T_{i+1,j,k} - T_{i,j,k})}{4(\Delta x)^2} + \frac{T_{i,j-1,k} - T_{i,j,k}}{2(\Delta x)^2} + \right. \\ \left. \frac{T_{i,j+1,k} - T_{i,j,k}}{4(\Delta x)^2} + \frac{3(T_{i,j,k-1} - T_{i,j,k})}{4(\Delta x)^2}\right) + \frac{5q''}{4\Delta x}\end{aligned}$$

If $\alpha = k_x/\rho C$ this becomes

$$\begin{aligned}\frac{\partial T_{i,j,k}}{\partial t} = \frac{2\alpha}{3(\Delta x)^2}(2T_{i-1,j,k} + 2T_{i,j-1,k} + 3T_{i,j,k-1} - 9T_{i,j,k} + T_{i+1,j,k} + T_{i,j+1,k} + \\ + 5\frac{q''\Delta x}{k_x}\Big)\end{aligned}$$

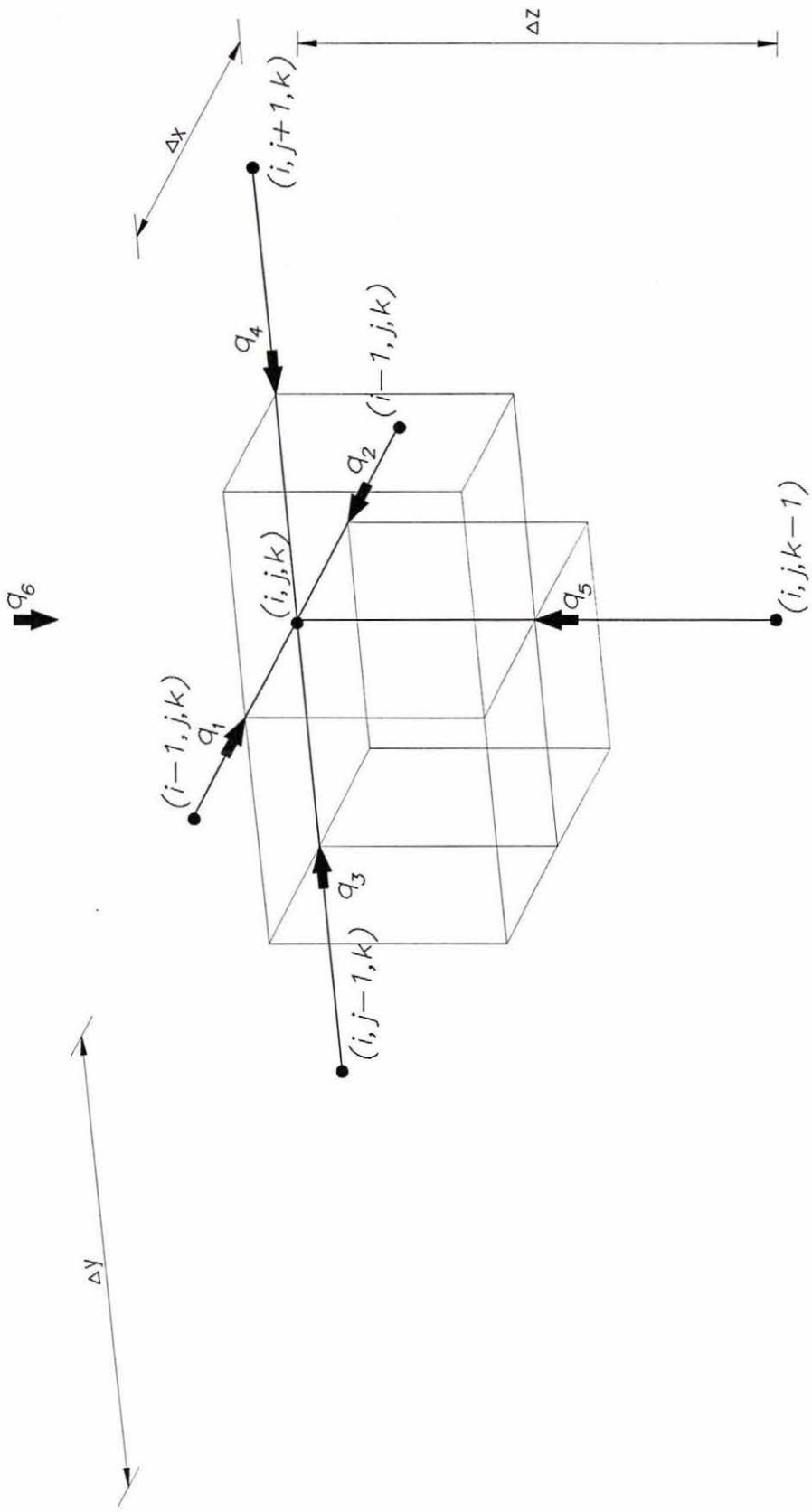

Figure 8.6: Three-dimensional internal edge/surface node

If the derivative with respect to time is written as a forward finite difference approximation this becomes

$$T_{i,j,k}^{m+1} = \frac{2}{5}Fo\left(3T_{i-1,j,k}^{m} + 3T_{i,j-1,k}^{m} + 4T_{i,j,k-1}^{m} - 15T_{i,j,k}^{m} + 2T_{i+1,j,k}^{m} + 2T_{i,j+1,k}^{m} + 1T_{i,j,k+1}^{m} + 5\frac{q''\Delta x}{k_x}\right) + T_{i,j,k}^{m} \quad (8.6)$$

where the Fourier number is $Fo = \alpha\Delta t/(\Delta x)^2$.

External Edge Node

An external edge node is shown in Figure 8.7. The volume is $1/4\Delta x\Delta y\Delta z$. The heat transfer to the adjacent edge node is

$$q_3 = \frac{1}{4}k_y\frac{T_{i,j-1,k} - T_{i,j,k}}{\Delta y}\Delta x\Delta z$$

but the heat transfer to the two surface nodes is

$$q_1 = \frac{1}{2}k_x\frac{T_{i-1,j,k} - T_{i,j,k}}{\Delta x}\Delta y\Delta z$$

The heat transfer to the imaginary nodes is

$$q_2 = \frac{1}{2}q_x''\Delta y\Delta z$$

In this case there are two adjacent nodes which are internal, two which are on the surface and two on edges. This gives the following equation

$$\begin{aligned}\frac{1}{4}\rho C\Delta x\Delta y\Delta z\frac{\partial T_{i,j,k}}{\partial t} = \\ \frac{1}{4}k_x\frac{T_{i-1,j,k} - T_{i,j,k}}{\Delta x}\Delta y\Delta z + \frac{1}{4}k_x\frac{T_{i+1,j,k} - T_{i,j,k}}{\Delta x}\Delta y\Delta z \\ + \frac{1}{2}k_y\frac{T_{i,j-1,k} - T_{i,j,k}}{\Delta y}\Delta x\Delta z + \frac{1}{2}q_x''\Delta y\Delta z \\ + \frac{1}{2}k_z\frac{T_{i,j,k-1} - T_{i,j,k}}{\Delta z}\Delta x\Delta y + \frac{1}{2}q_z''\Delta x\Delta y\end{aligned}$$

If $k_x = k_y = k_z$ and $\Delta x = \Delta y = \Delta z$ this can be written as

$$\frac{1}{4}\rho C\frac{\partial T_{i,j,k}}{\partial t} = k_x\left(\frac{3(T_{i-1,j,k} - T_{i,j,k})}{4(\Delta x)^2} + \frac{3(T_{i+1,j,k} - T_{i,j,k})}{4(\Delta x)^2} + \frac{T_{i,j-1,k} - T_{i,j,k}}{2(\Delta x)^2} + \frac{T_{i,j,k-1} - T_{i,j,k}}{2(\Delta x)^2}\right) + \frac{q''}{\Delta x}$$

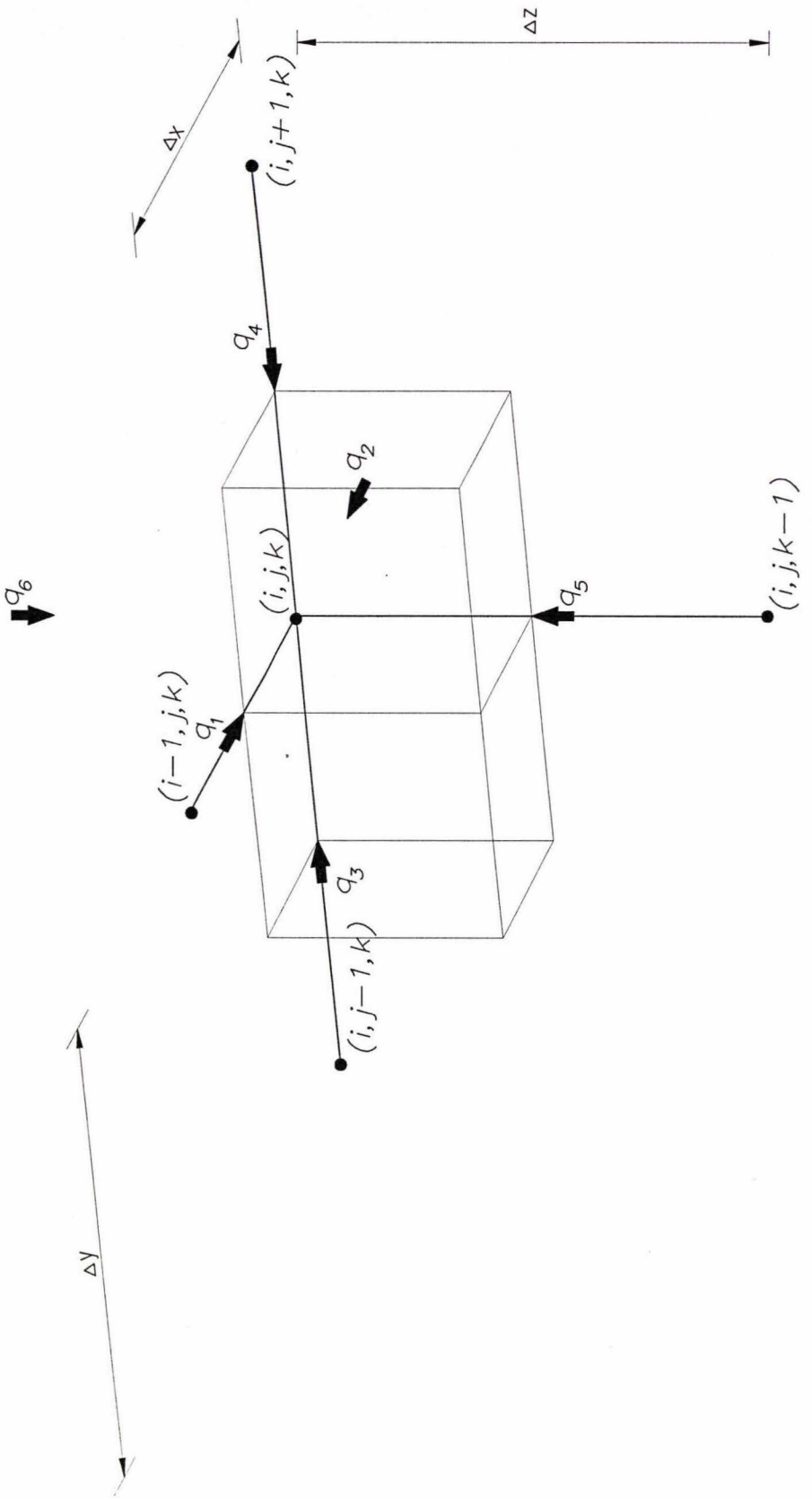

Figure 8.7: Three-dimensional external edge node

If $\alpha = k_x/\rho C$ this becomes

$$\frac{\partial T_{i,j,k}}{\partial t} = \frac{2\alpha}{5(\Delta x)^2}\left(3T_{i-1,j,k} + 3T_{i,j-1,k} + 4T_{i,j,k-1} - 15T_{i,j,k} + 2T_{i+1,j,k} + 2T_{i,j+1,k} + T_{i,j,k+1} + \frac{q''\Delta x}{k_x}\right)$$

If the derivative with respect to time is written as a forward finite difference approximation this becomes

$$T^{m+1}_{i,j,k} = \frac{2}{5}Fo\left(3T^m_{i-1,j,k} + 3T^m_{i,j-1,k} + 4T^m_{i,j,k-1} - 15T^m_{i,j,k} + 2T^m_{i+1,j,k} + 2T^m_{i,j+1,k} + 1T^m_{i,j,k+1} + \frac{q''\Delta x}{k_x}\right) + T^m_{i,j,k} \quad (8.7)$$

where the Fourier number is $Fo = \alpha\Delta t/(\Delta x)^2$.

External Corner Node

An external corner node is shown in Figure 8.8. The volume is $1/8\Delta x\Delta y\Delta z$. The heat transfer from the adjacent edge node $(i-1, j, k)$ is

$$q_1 = \frac{1}{4}k_x\frac{T_{i-1,j,k} - T_{i,j,k}}{\Delta x}\Delta y\Delta z$$

similar expressions can be found for q_3 and q_5. The heat transfer across the surface in the x-direction is

$$q_2 = \frac{1}{4}q''_x\Delta y\Delta z$$

Similar expressions can be found for q_4 and q_6. If $\Delta x = \Delta y = \Delta z$ the volume is $1/8\Delta x\Delta y\Delta z$. This gives the following energy balance equation

$$\frac{1}{8}\rho C\Delta x\Delta y\Delta z\frac{\partial T_{i,j,k}}{\partial t} = \frac{1}{4}k_x\frac{T_{i-1,j,k} - T_{i,j,k}}{\Delta x}\Delta y\Delta z + \frac{1}{4}q''_x\Delta y\Delta z + \frac{1}{4}k_y\frac{T_{i,j-1,k} - T_{i,j,k}}{\Delta y}\Delta x\Delta z + \frac{1}{4}q''_y\Delta x\Delta z + k_z\frac{T_{i,j,k-1} - T_{i,j,k}}{\Delta z}\Delta x\Delta y + \frac{1}{4}q''_z\Delta x\Delta y$$

If $k_x = k_y = k_z$ and $q''_x = q''_y = q''_z$ and since $\Delta x = \Delta y = \Delta z$ this can be written as

$$\frac{1}{8}\rho C\frac{\partial T_{i,j,k}}{\partial t} = k_x\left(\frac{T_{i-1,j,k} - T_{i,j,k}}{4(\Delta x)^2} + \frac{T_{i,j-1,k} - T_{i,j,k}}{4(\Delta x)^2} + \frac{T_{i,j,k-1} - T_{i,j,k}}{4(\Delta x)^2} + \right) + \frac{3q''}{4\Delta x}$$

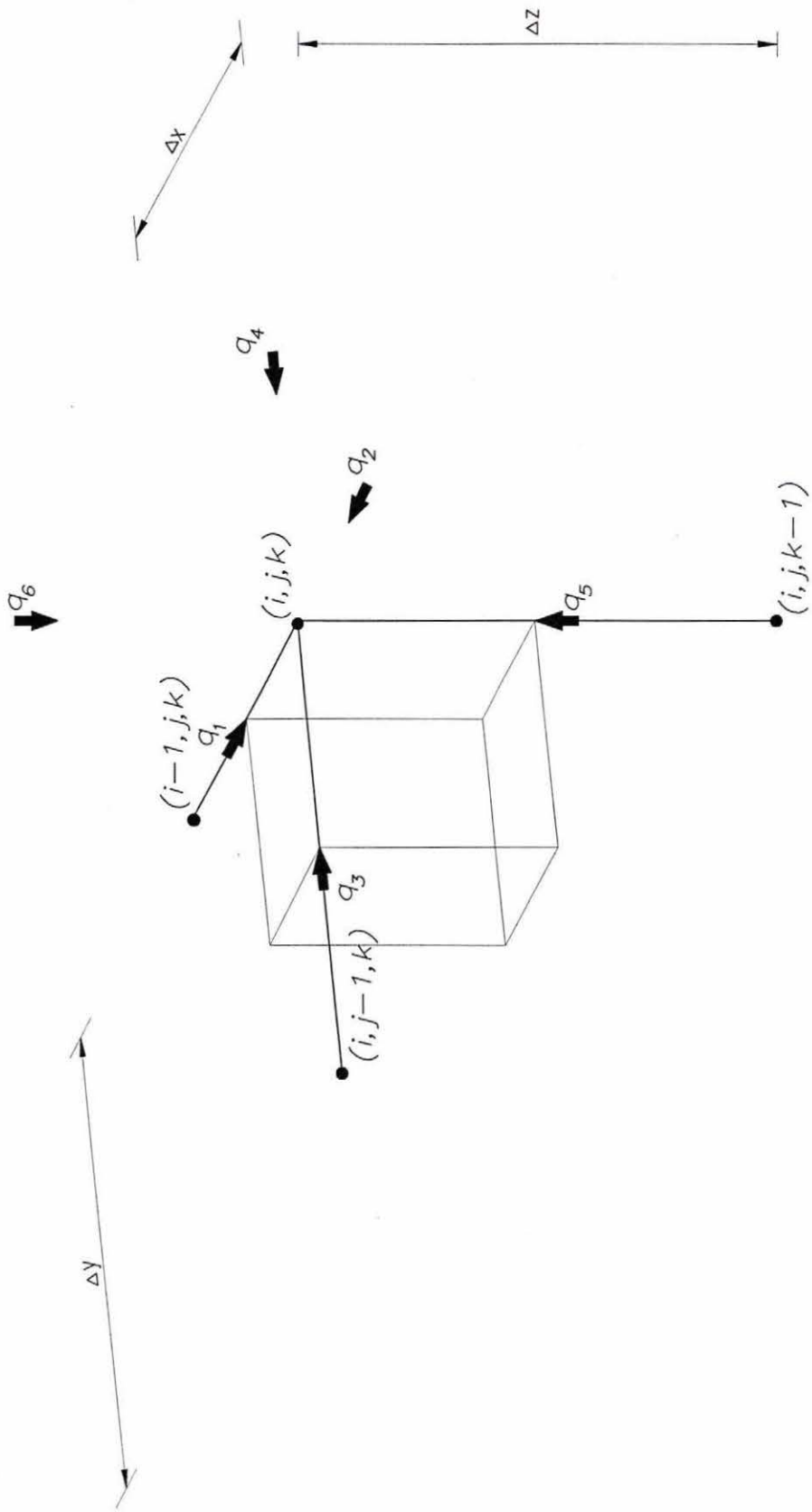

Figure 8.8: Three-dimensional external corner node

If $\alpha = k_x/\rho C$ this becomes

$$\frac{\partial T_{i,j,k}}{\partial t} = \frac{\alpha}{(\Delta x)^2}\left(2T_{i-1,j,k} + 2T_{i,j-1,k} + 2T_{i,j,k-1} - 6T_{i,j,k} + 6\frac{q''\Delta x}{k_x}\right)$$

If the derivative with respect to time is also written as a finite difference approximation this becomes

$$T^{m+1}_{i,j,k} = Fo\left(2T^m_{i-1,j,k} + 2T^m_{i,j-1,k} + 2T^m_{i,j,k-1} - 6T^m_{i,j,k} + 6\frac{q''\Delta x}{k_x}\right) + T^m_{i,j,k} \tag{8.8}$$

where the Fourier number is $Fo = \alpha\Delta t/(\Delta x)^2$. Since the heat flux is due to radiation

$$q'' = \epsilon\sigma A(T_s^4 - T_\infty^4)$$

this can be written as

$$T^{m+1}_{i,j,k} = Fo\left(2T^m_{i-1,j,k} + 2T^m_{i,j-1,k} + 2T^m_{i,j,k-1} - 6T^m_{i,j,k} + 6\frac{\epsilon\sigma\left[(T^m_{i,j,k})^4 - T_\infty^4\right]\Delta x}{k_x}\right) T^m_{i,j,k} \tag{8.9}$$

In the model considered not all of these possibilities occur, neither the internal corner nor internal side nodes are required.

8.2 Variable Physical and Thermal Properties

As in the earlier cases the different materials within the anode have different physical and thermal properties. This means the above finite difference equations must be modified to allow for this. If the same method is used as in the two dimensional case there are different types of interfaces between materials.

In the three-dimensional cases being modelled there are up to nine different types of interface. There are 5 internal interfaces, 1 external edge interface, 1 surface interface, 1 internal edge interface and 1 external corner/surface interface. The nine types of interface are shown in Figure 8.9.

Internal Node

The finite difference equation for the internal nodes can be written as

$$T^{m+1}_{i,j,k} = \delta\left(a_{i,j,k}T^m_{i-1,j,k} + b_{i,j,k}T^m_{i,j-1,k} + c_{i,j,k}T^m_{i,j,k-1} + d_{i,j,k}T^m_{i,j,k} + e_{i,j,k}T^m_{i+1,j,k} + f_{i,j,k}T^m_{i,j+1,k} + g_{i,j,k}T^m_{i,j,k+1}\right) + T^m_{i,j,k} \tag{8.10}$$

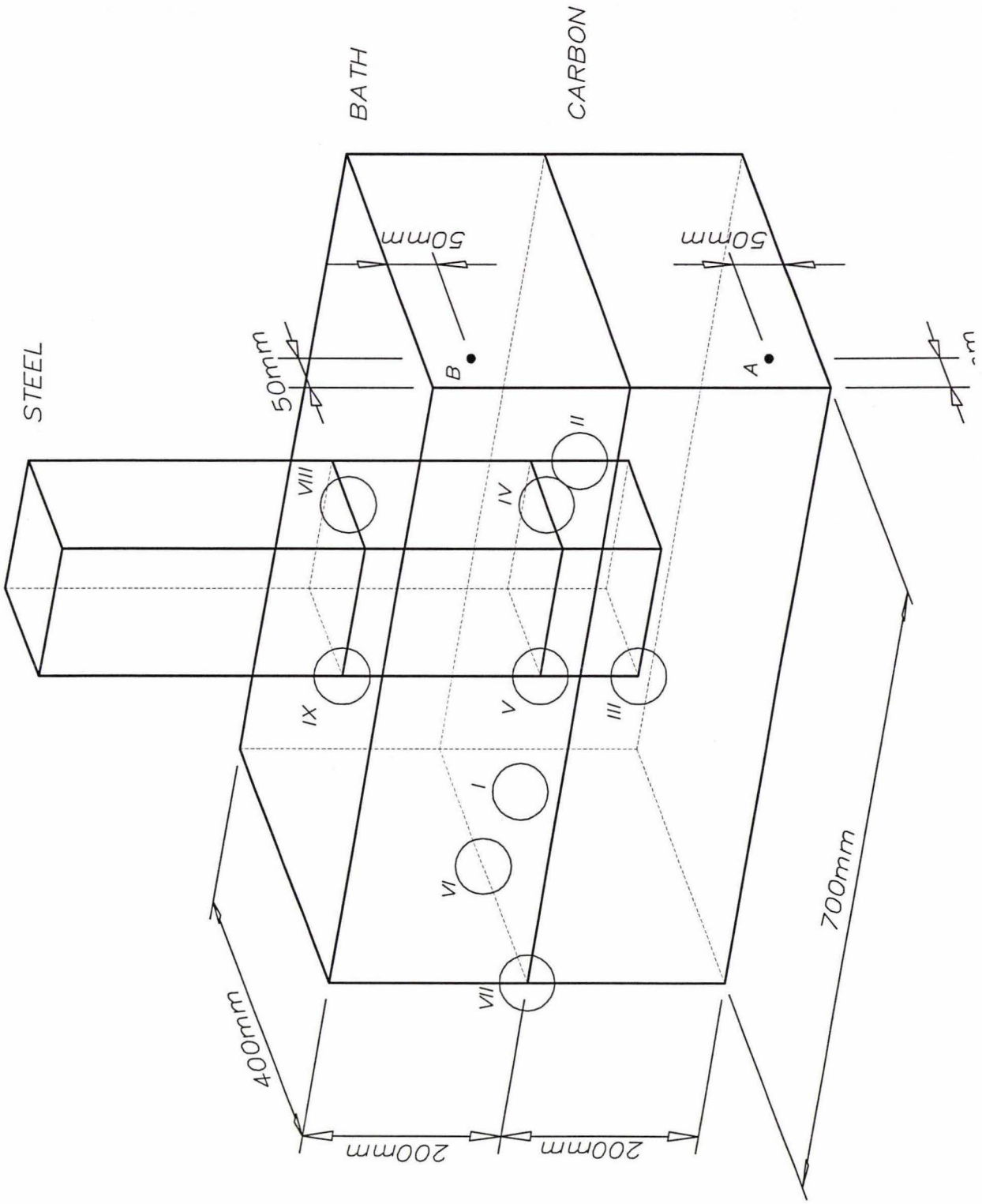

Figure 8.9: Three-dimensional approximation of a quarter anode

where $\delta = \Delta t/(\Delta x)^2$. The coefficients $a_{i,j,k}$, $b_{i,j,k}$, $c_{i,j,k}$, $e_{i,j,k}$, $f_{i,j,k}$ and $g_{i,j,k}$ are found by taking the average of the diffusivities between each node and the node $T_{i,j,k}$. The coefficient $d_{i,j,k}$ is the sum of the other six coefficients.

For the five internal node material interfaces shown in Figure 8.9 these are:

Interface Type I: The internal node shown in Figure 8.1 is on the boundary between bath and carbon so that all the material above the node is bath and all below is carbon. The coefficients for Equation (8.10) are:

$$a_{i,j,k} = \frac{\alpha_c + \alpha_b}{2}$$

$$b_{i,j,k} = \frac{\alpha_c + \alpha_b}{2}$$

$$c_{i,j,k} = \alpha_c$$

$$d_{i,j,k} = 3\alpha_c + 3\alpha_b$$

$$e_{i,j,k} = \frac{\alpha_c + \alpha_b}{2}$$

$$f_{i,j,k} = \frac{\alpha_c + \alpha_b}{2}$$

$$g_{i,j,k} = \alpha_b$$

Interface Type II: The internal node shown in Figure 8.1 is on the boundary between edge of the steel and carbon so that all the material in the quarter between node $(i-1, j, k)$ and node $(i, j, k+1)$ is steel and all the rest is carbon. The coefficients for Equation (8.10) are:

$$a_{i,j,k} = \frac{\alpha_c + \alpha_s}{2}$$

$$b_{i,j,k} = \frac{3\alpha_c + \alpha_s}{4}$$

$$c_{i,j,k} = \alpha_c$$

$$d_{i,j,k} = \frac{9\alpha_c + 3\alpha_s}{2}$$

$$e_{i,j,k} = \alpha_c$$

$$f_{i,j,k} = \frac{3\alpha_c + \alpha_s}{4}$$

$$g_{i,j,k} = \frac{\alpha_c + \alpha_s}{2}$$

Interface Type III: The internal node shown in Figure 8.1 is on the boundary between corner of the steel and carbon so that all the material in the eighth between node $(i-1,j,k)$, $(i,j-1,k)$ and node $(i,j,k+1)$ is steel and all the rest is carbon. The coefficients for Equation (8.10) are:

$$a_{i,j,k} = \frac{21\alpha_c + 3\alpha_s}{4}$$

$$b_{i,j,k} = \frac{21\alpha_c + 3\alpha_s}{4}$$

$$c_{i,j,k} = \alpha_c$$

$$d_{i,j,k} = \frac{21\alpha_c + 3\alpha_s}{4}$$

$$e_{i,j,k} = \alpha_c$$

$$f_{i,j,k} = \alpha_c$$

$$g_{i,j,k} = \frac{\alpha_c + \alpha_s}{4}$$

Interface Type IV: The internal node shown in Figure 8.1 is on the boundary between bath and carbon next to the steel. All the material in the right of the node is steel, to the left and below the node is carbon and to the left and above the node is bath. The coefficients for Equation (8.10) are:

$$a_{i,j,k} = \frac{\alpha_c + 2\alpha_s + \alpha_b}{4}$$

$$b_{i,j,k} = \frac{\alpha_c + \alpha_b}{2}$$

$$c_{i,j,k} = \frac{\alpha_b + \alpha_s}{2}$$

$$d_{i,j,k} = \frac{3\alpha_c + 6\alpha_s + 3\alpha_b}{2}$$

$$e_{i,j,k} = \frac{\alpha_c + 2\alpha_s + \alpha_b}{4}$$

$$f_{i,j,k} = \alpha_s$$

$$g_{i,j,k} = \frac{\alpha_c + \alpha_s}{2}$$

Interface Type V: The internal node shown in Figure 8.1 is on the boundary between bath and carbon next to the corner of the steel. All the material between nodes $(i-1,j,k)$ and $(i,j+1,k)$ is steel, the remaining material below the node is carbon and above the node is bath. The coefficients for Equation (8.10) are:

$$a_{i,j,k} = \frac{\alpha_c + 2\alpha_s + \alpha_b}{4}$$

$$b_{i,j,k} = \frac{\alpha_c + \alpha_b}{2}$$

$$c_{i,j,k} = \frac{3\alpha_c + \alpha_s}{4}$$

$$d_{i,j,k} = \frac{9\alpha_c + 6\alpha_s + 6\alpha_b}{4}$$

$$e_{i,j,k} = \frac{\alpha_c + \alpha_b}{2}$$

$$f_{i,j,k} = \frac{\alpha_c + 2\alpha_s + \alpha_b}{4}$$

$$g_{i,j,k} = \frac{3\alpha_b + \alpha_s}{4}$$

Surface Node

The surface node shown in Figure 8.5 must be rotated to give a vertical surface with a boundary between bath and carbon. All the material below the node is carbon and above the node is bath.

$$T^{m+1}_{i,j,k} = \frac{1}{2}\delta\left(a_{i,j,k}T^m_{i-1,j,k} + b_{i,j,k}T^m_{i,j-1,k} + c_{i,j,k}T^m_{i,j,k-1} + d_{i,j,k}T^m_{i,j,k} + 2e_{i,j,k}T^m_{i+1,j,k} + g_{i,j,k}T^m_{i,j,k+1} + \frac{q''\Delta x}{k_b} + \frac{q''\Delta x}{k_s}\right) + T^m_{i,j,k} \qquad (8.11)$$

Interface Type VI: The coefficient for Equation (8.11) are:

$$a_{i,j,k} = \frac{\alpha_c + \alpha_b}{4}$$

$$b_{i,j,k} = \frac{\alpha_c + \alpha_b}{2}$$

$$c_{i,j,k} = \frac{\alpha_c}{2}$$

$$d_{i,j,k} = \frac{3\alpha_c + 3\alpha_b}{2}$$

$$e_{i,j,k} = \frac{\alpha_c + \alpha_b}{4}$$

$$g_{i,j,k} = \frac{\alpha_b}{2}$$

External Edge Node

The external edge node shown in Figure 8.7 must be rotated to give a vertical edge on the boundary between carbon and bath. All the material above the node (i, j, k) is bath and all below is carbon.

$$T_{i,j,k}^{m+1} = 4\delta \left(a_{i,j,k} T_{i+1,j,k}^{m} + b_{i,j,k} T_{i,j+1,k}^{m} + c_{i,j,k} T_{i,j,k-1}^{m} + d_{i,j,k} T_{i,j,k}^{m} + g_{i,j,k} T_{i,j,k+1}^{m} + \frac{q''\Delta x}{k_b} + \frac{q''\Delta x}{k_c} \right) + T_{i,j,k}^{m} \tag{8.12}$$

Interface Type VII: The coefficient for Equation (8.12) are:

$$a_{i,j,k} = \frac{\alpha_c + \alpha_b}{4}$$

$$b_{i,j,k} = \frac{\alpha_c + \alpha_b}{4}$$

$$c_{i,j,k} = \frac{\alpha_c}{4}$$

$$d_{i,j,k} = \frac{\alpha_c + \alpha_b}{2}$$

$$g_{i,j,k} = \frac{\alpha_b}{4}$$

Internal Edge Node

The internal edge node shown in Figure 8.3 is on the boundary between carbon and steel. All the material between node (i, j, k) and node $(i-1, j, k)$ is steel and between node (i, j, k) and node $(i+1, j, k)$ is bath.

$$T_{i,j,k}^{m+1} = \frac{4}{3}\delta \left(a_{i,j,k} T_{i-1,j,k}^{m} + b_{i,j,k} T_{i,j-1,k}^{m} + c_{i,j,k} T_{i,j,k-1}^{m} + d_{i,j,k} T_{i,j,k}^{m} + 2e_{i,j,k} T_{i+1,j,k}^{m} + f_{i,j,k} T_{i,j+1,k}^{m} + g_{i,j,k} T_{i,j,k+1}^{m} + 2\frac{q''\Delta x}{k_b} + 2\frac{q''\Delta x}{k_s} \right) + T_{i,j,k}^{m} \tag{8.13}$$

Interface Type VIII: The coefficient for Equation (8.13) are:

$$a_{i,j,k} = \alpha_s$$

$$b_{i,j,k} = \frac{\alpha_b + 2\alpha_s}{4}$$

$$c_{i,j,k} = \frac{\alpha_b + \alpha_s}{2}$$

$$d_{i,j,k} = \frac{3\alpha_b + 6\alpha_b}{2}$$

$$e_{i,j,k} = \frac{\alpha_b}{2}$$

$$f_{i,j,k} = \frac{\alpha_b + 2\alpha_s}{4}$$

$$g_{i,j,k} = \frac{\alpha_s}{2}$$

External Corner/Surface Node

The external corner/surface node shown in Figure 8.4 is on the boundary between carbon and steel. All the material in the quarter between node $(i-1, j, k)$ and node $(i, j-1, k)$ is steel, the rest is bath.

$$T_{i,j,k}^{m+1} = \frac{5}{8}\delta \left(b_{i,j,k}T_{i,j-1,k}^{m} + c_{i,j,k}T_{i,j,k-1}^{m} + d_{i,j,k}T_{i,j,k}^{m} + 2e_{i,j,k}T_{i+1,j,k}^{m} + f_{i,j,k}T_{i,j+1,k}^{m} + g_{i,j,k}T_{i,j,k+1}^{m} + 3\frac{q''\Delta x}{k_b} + 2\frac{q''\Delta x}{k_s} \right) + T_{i,j,k}^{m} \qquad (8.14)$$

Interface Type IX: The coefficient for Equation (8.14) are:

$$a_{i,j,k} = \frac{\alpha_b + 2\alpha_s}{4}$$

$$b_{i,j,k} = \frac{\alpha_b + 2\alpha_s}{4}$$

$$c_{i,j,k} = \frac{3\alpha_b + \alpha_s}{4}$$

$$d_{i,j,k} = \frac{9\alpha_b + 6\alpha_s}{2}$$

$$e_{i,j,k} = \frac{\alpha_b}{2}$$

$$f_{i,j,k} = \frac{\alpha_b}{2}$$

$$g_{i,j,k} = \frac{\alpha_s}{4}$$

8.3 Numerical Simulation

The three-dimensional solution should give a more detailed picture of the heat flow occurring as the anodes cool than the one- and two-dimensional models. The number of nodes required increases significantly when the three-dimensional model is solved. To speed up the computation time the symmetry of the problem can be used. If the solution is found for a quarter of the problem, symmetry can be

used to find the entire solution. The physical arrangement of the butt shown in Figure 1.3 was approximated by the quarter shown in Figure 8.9.

Computation time for a grid size $\Delta x = 0.04\,m$ was approximately four minutes. If the grid size was halved, this would increase to about 45 minutes due to the increase in the number of node points.

The same physical and thermal properties were used as in the one- and two-dimensional cases. The results given are for the thermal properties given below. The thermal properties are approximations and in reality would change with the change in temperature of the materials. Each of the materials had the following properties:

Carbon:

Emissivity = 0.4	Thermal Conductivity = $k_c = 5\,W/mK$
Density = $\rho_c = 1580\,kg/m^3$	Heat Capacity = $c_c = 1670\,J/kgK$

Bath:

Emissivity = 0.4	Thermal Conductivity = $k_b = 0.4\,W/mK$
Density = $\rho_b = 2050\,kg/m^3$	Heat Capacity = $c_b = 2287\,J/kgK$

Steel:

Emissivity = 0.4	Thermal Conductivity = $k_b = 36\,W/mK$
Density = $\rho_b = 7753\,kg/m^3$	Heat Capacity = $c_b = 486\,J/kgK$

The thermal properties for carbon and bath are from [5]. The thermal properties for steel were given in [1].

8.3.1 Clean Anode

The solution was found for an anode with a thickness of $0.2\,m$, a total length of $1.4\,m$ and a depth of $0.8\,m$. The steel rods had a diameter of $0.15\,m$, a depth of $0.10\,m$ into the carbon and extended $0.8\,m$ up from the surface. The solution was

found for a quarter of this with $\Delta x = 0.05\,m$ so the number of nodes required for the carbon base was $6 \times 11 \times 19$ and for the exposed rod was $21 \times 5 \times 5$.

The temperature profile for four different times is shown in Figure 8.10. It can be seen that the temperature at the surface of the anode drops quickly and the centre more slowly. Figure 8.11 shows a cross section through the quarter, where the effect of the steel rod can be seen. The temperature over time of the point A shown in Figure 8.9[1] is given in Figure 8.14. It can be seen that the clean anode cools more quickly than the same point in a dirty anode.

8.3.2 Dirty Anode

The solution was found for the same anode as in the clean case but with a bath cover $0.2\,m$ thick on top of the carbon. This makes the base of the anode $0.4\,m$ thick. The number of nodes required for the base was $11 \times 11 \times 19$ and for the exposed rod $16 \times 5 \times 5$.

The effect of the bath cover is shown in Figure 8.12, where it can be seen that the bath stays hotter for longer and keeps the carbon hotter. The effect of the rod can be seen in the cross-sections shown in Figure 8.13.

The temperature over time of the point A shown in Figure 8.9 is given in Figure 8.14. It can be seen that the model initially predicts temperatures lower than those given by the experimental data but after about 6 hours the model starts to give temperatures higher than the experimental data. The temperature of point B in Figure 8.9 a point in the bath is given in Figure 8.15 it can be seen that the bath cools slowly compared to the carbon. This initially follows the data quite well but after 8 hours this also gives higher values than the experimental data. This could be due to convection from the anodes which becomes more significant as the temperature decreases.

8.4 Summary

The computation time required for the three-dimensional solution is significantly more than the one- or two-dimensional cases due to the extra number of nodes.

[1]The bath layer is absent in this case

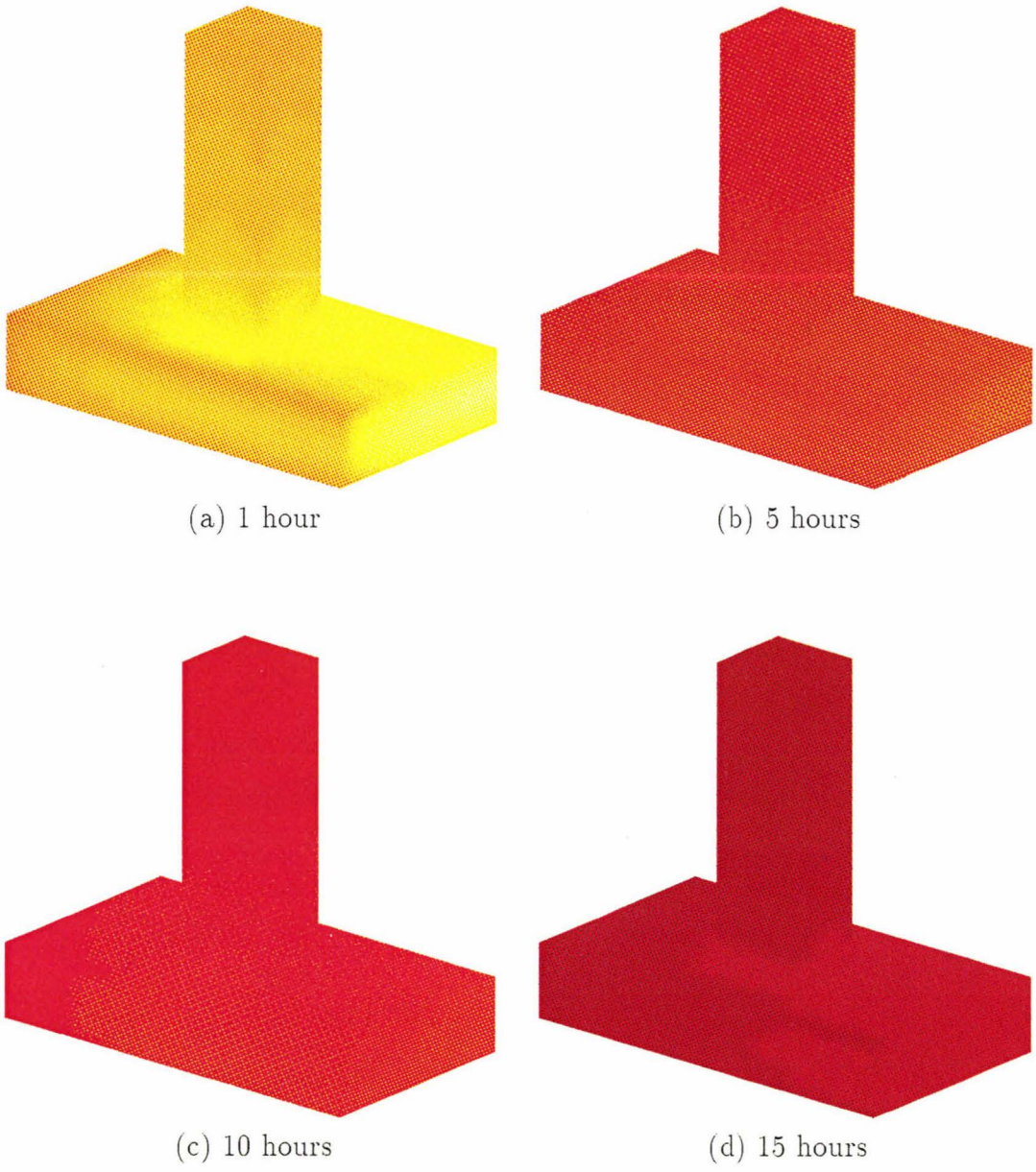

(a) 1 hour

(b) 5 hours

(c) 10 hours

(d) 15 hours

Figure 8.10: Temperature profile for a clean anode

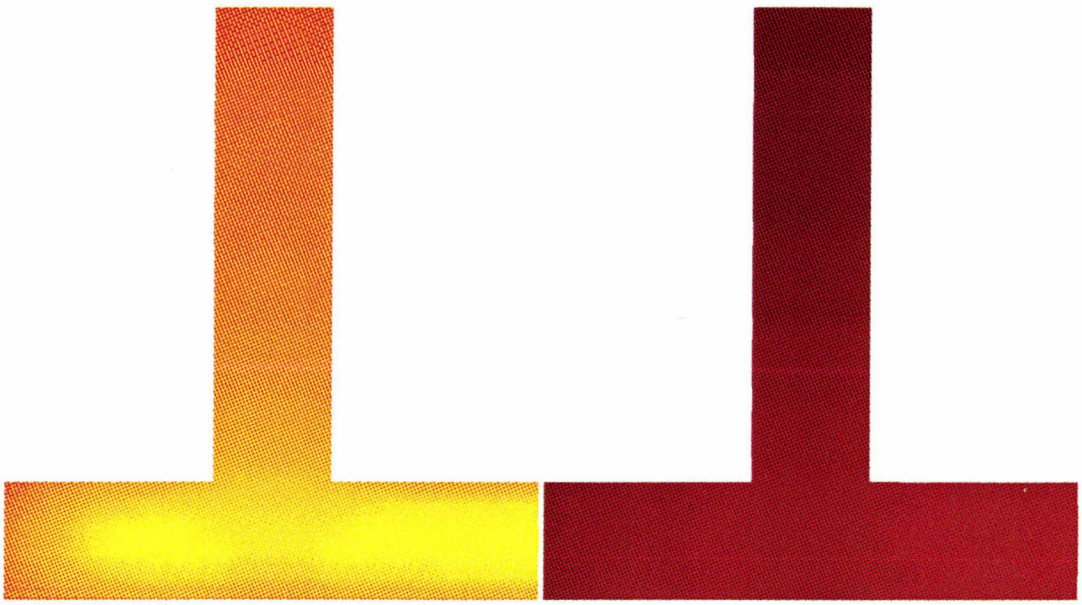

(a) 1 hour

(b) 5 hours

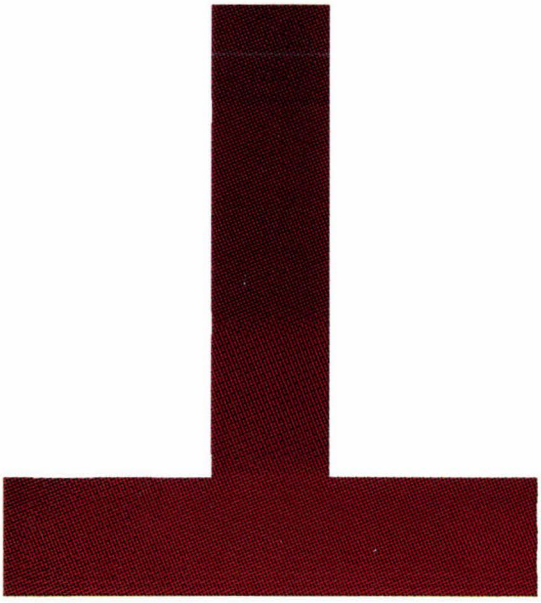

(c) 10 hours

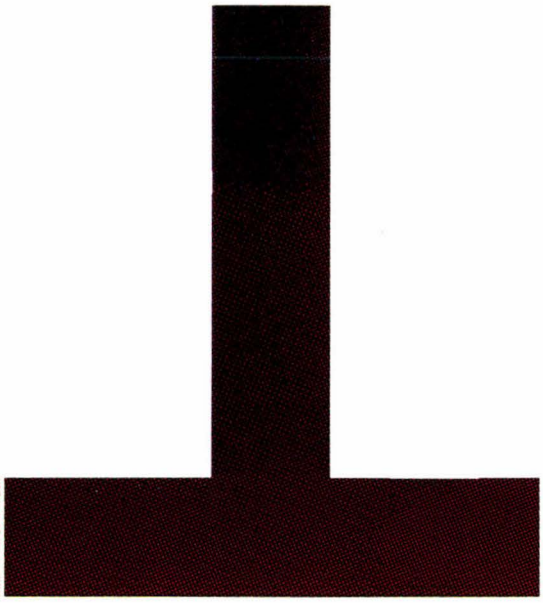

(d) 15 hours

Figure 8.11: Cross section of temperature through clean anode

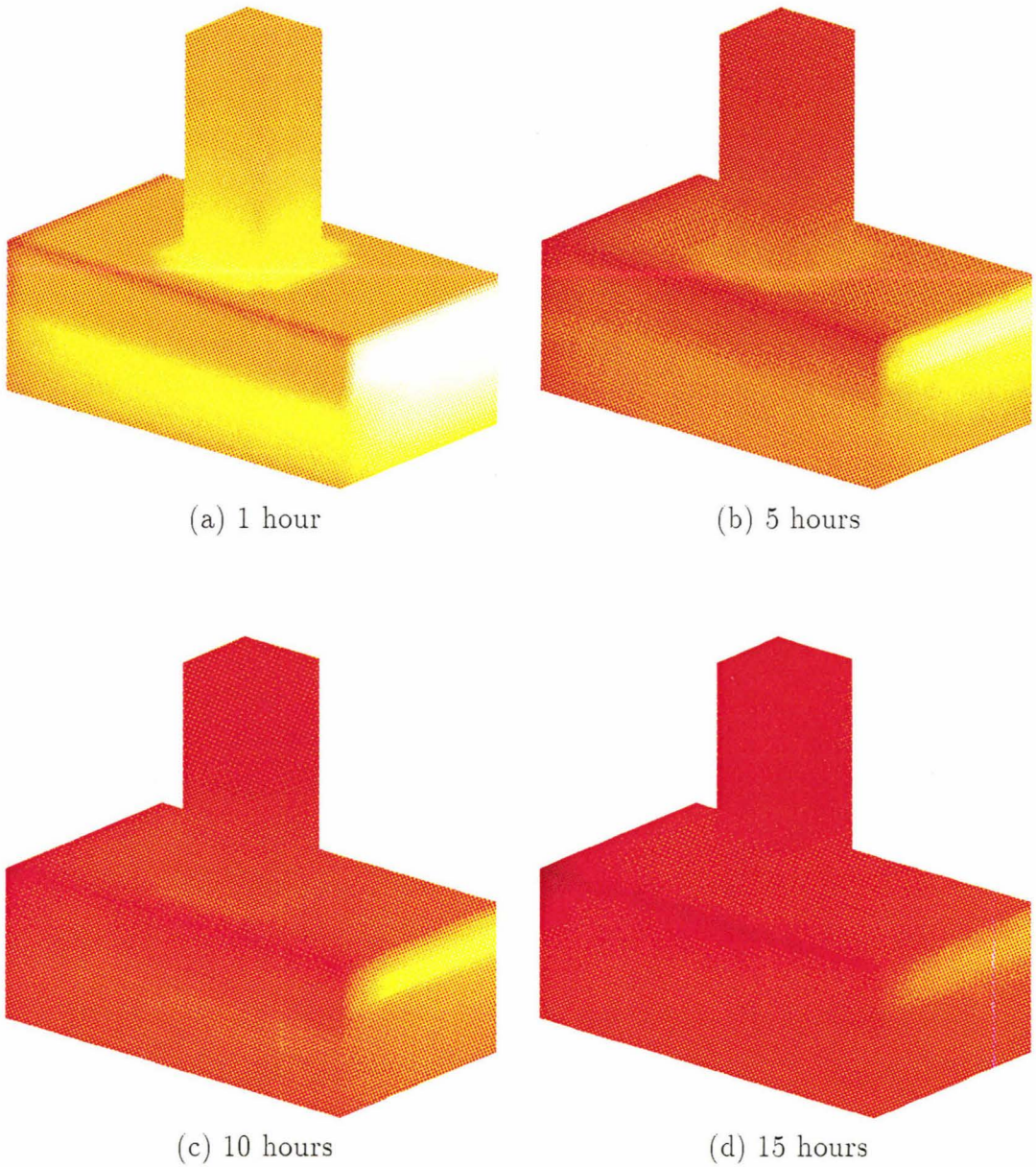

(a) 1 hour

(b) 5 hours

(c) 10 hours

(d) 15 hours

Figure 8.12: Temperature profile for a dirty anode

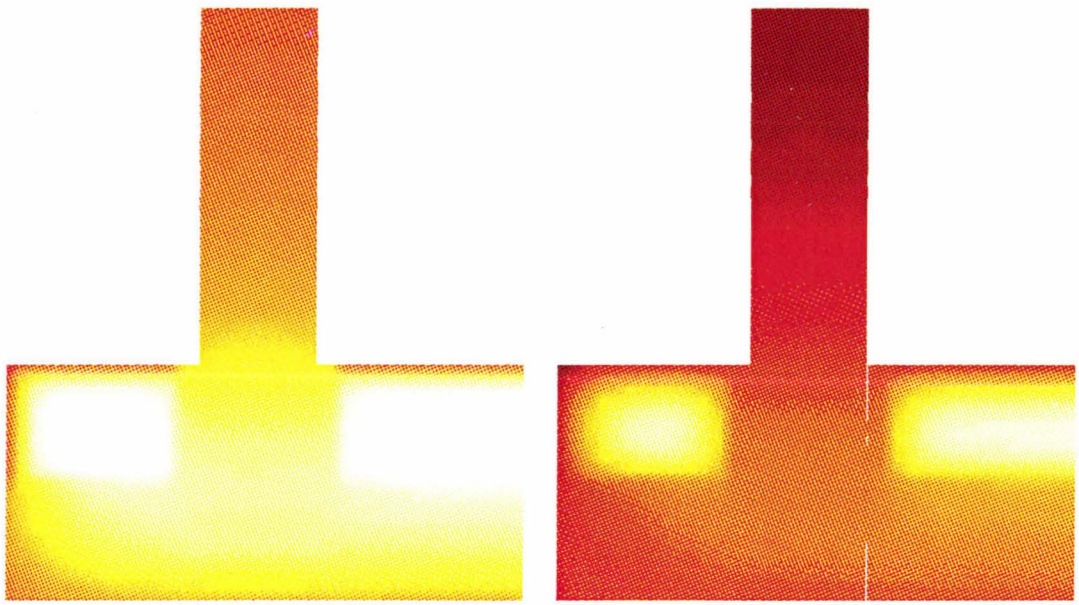

(a) 1 hour

(b) 5 hours

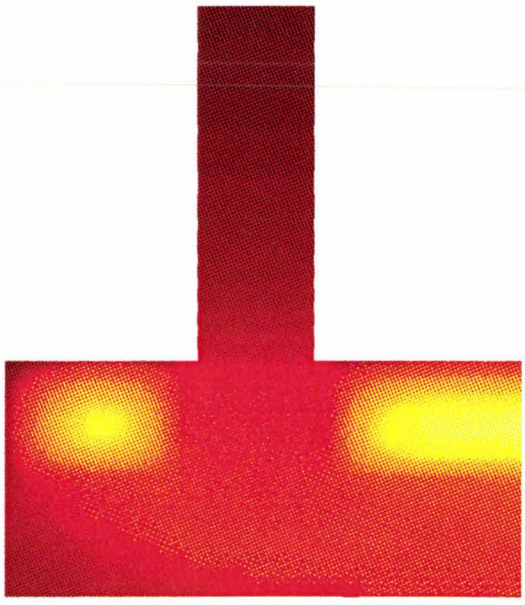

(c) 10 hours

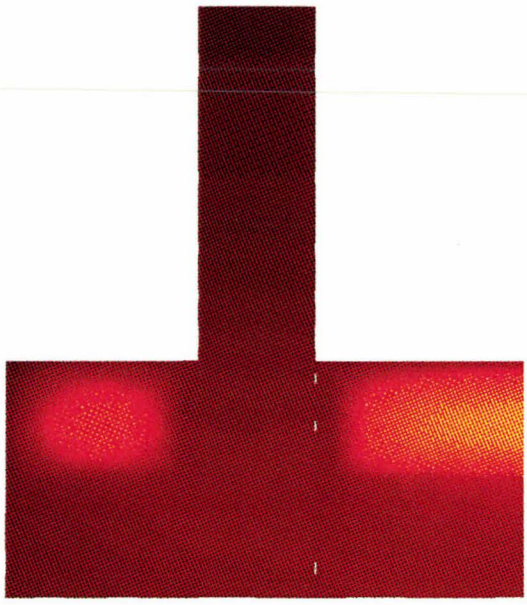

(d) 15 hours

Figure 8.13: Cross section of temperature through dirty anode

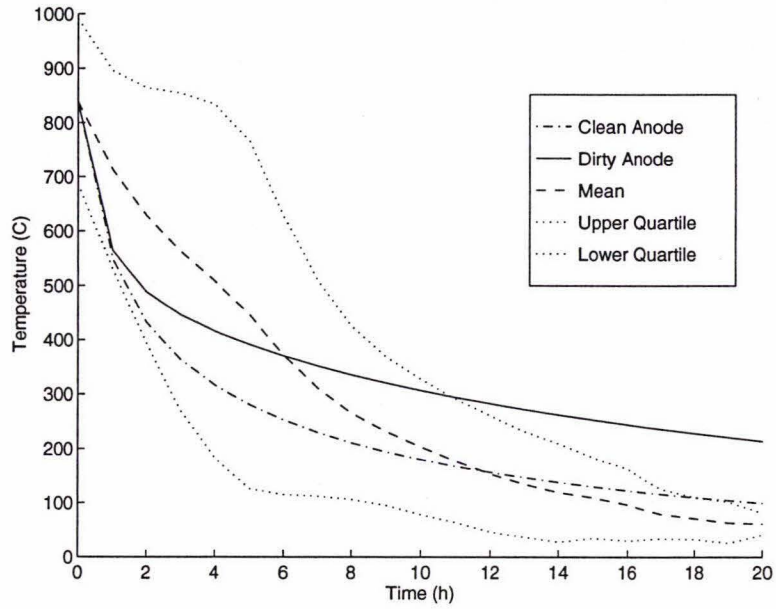

Figure 8.14: Temperature of point in carbon for clean and dirty anode

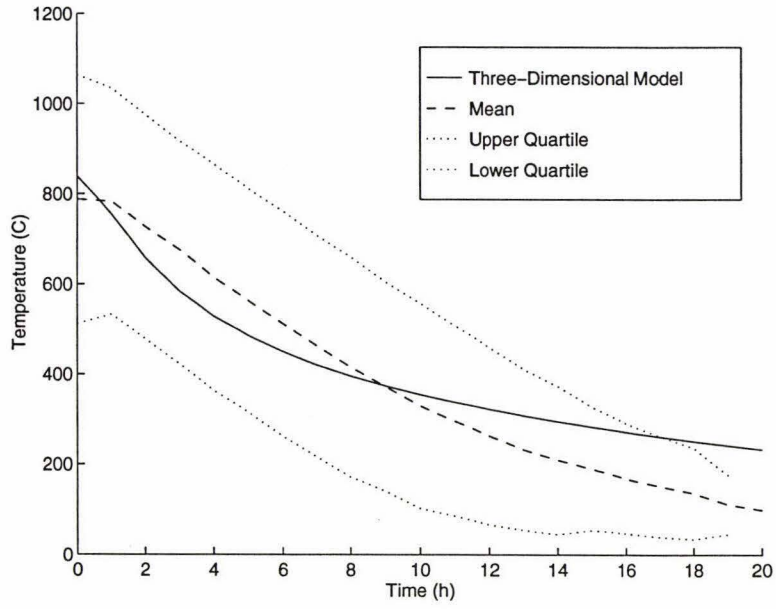

Figure 8.15: Temperature of point in bath dirty anode

By using the symmetry of the problem the number of nodes can be reduced to a quarter of the nodes required for the full problem. The computation time required for a problem with $\Delta x = 0/04\,m$ so there are $(11 \times 11 \times 19)$ nodes in the base and $(16 \times 5 \times 5)$ nodes in the rod, was approximately four minutes. If the grid size is halved to give $(21 \times 21 \times 37)$ nodes in the base and $(31 \times 9 \times 9)$ nodes in the rod, this would increase to about 45 minutes.

As can be seen the setting-up of the finite difference equations in the three-dimensional model for variable material properties is quite complicated due to all the special cases.

The visualisation of the results in three dimensions is difficult, since the temperature at all nodes can not be shown. The surface temperature for a quarter of the anode has been shown; however to see the effect of the rods, a cross-section was needed.

The three-dimensional solution gives results similar to the two-dimensional model. The major advantage is the temperature distribution is calculated for the entire anode rather than only for a cross-section of it.

Chapter 9

Conclusions

9.1 Effect of Hot Cleaning of Spent Anodes

The original question about the effect of removing the bath can now be answered. It has been seen that the bath cover has quite a major effect on the temperature of the butts.

The rate of cooling of the anodes is just one of the factors which must be considered if the bath is removed while still hot. Other considerations could be safety and cost. What will be done with the hot bath once it is removed, as it will take time to cool, is also an important consideration.

9.2 The Mathematical Model

One-, two- and three-dimensional models have been developed; all could include carbon with a bath cover. The one-dimensional model could not include the steel rods of the assembly yoke but the two- and three-dimensional models could.

The results obtained from the model show the cooling of a particular point within the spent anode quite well. It also shows the temperature profile within the anode at a given time. This can be shown on paper easily for the two-dimensional model but is more difficult for the three-dimensional model. The change of temperature with time can be shown on paper but is more effectively shown by making short animations on a computer; this has been done in MATLAB.

The computation time running on a DEC AlphaStation 200 4/233 for the one-dimensional case was less than $5\,s$, the two-dimensional case was about $24\,s$. For three-dimensions the computation time varied from 3 minutes up to about 45 minutes depending on the grid size used. Obviously as the mesh size decreases the computation time would increase. The computation times are reasonable for a even for three dimensions so it is feasible to use this model.

9.3 Future Work

There are several features which may be included in the model to give a more accurate solution. These include taking into account the heat loss due to convection especially as the temperature reduces below $350°C$. Heat loss due to forced convection would be very difficult to model but it would be possible to calculate heat loss due to natural convection.

The gap between the bath and the carbon has be assumed to be negligible but in reality it varies between about $0.01\,m$ up to $0.05\,m$. This air gap would be expected to reduce the heat transfer between the carbon and the bath. If the air between the two surfaces is moving then there would be convection from these surfaces. If the air is stationary heat would be transferred by conduction and radiation. It is unclear how this problem would be approached.

The model could be developed to take account of the rounded shape of the anodes rather than treating them as squares. However it is expected this would make little difference. The shape of the assembly yokes, including the round rods could also be included. Again it is expected this would make little difference to the overall results.

Bibliography

[1] Adrian Bejan. *Heat Transfer.* John Wiley and Sons, USA, 1993.

[2] Y. R. Gan and J. Thonstad. Heat transfer between molten and solid cryolite bath. *Light Metals*, 1990.

[3] A. V. Hassani and K. G. T. Hollands. On natural convection heat transfer from three-dimensional bodies of arbitrary shape. *Journal of Heat Transfer*, 111:363–371, may 1989.

[4] Frank P. Incropera and David P. De Witt. *Fundamentals of Heat and Mass Transfer.* John Wiley and Sons, Inc., 1985.

[5] Chen J. J. J. University of auckland. Personal Communication, 1995.

[6] Jomar Thonstad Ketil A. Rye and Xialoling Liu. Heat transfer, thermal conductivity and emissivity of hall-heroult top crust. *Light Metals*, 1995.

[7] Glen E. Myers. *Analytical Methods in Conduction Heat Transfer.* Genium Publishing Corperation, USA, 1987.

[8] Rogers and Mayhew. *Engineering Thermodynamics Work and Heat Transfer.* Longman Group UK Limited, 4th edition, 1992.

[9] W Woodworth. Butt and anode cover temperatures. Technical report, NZAS, September 1992.